2014

AN ANALYSIS OF ENERGY RESOURCES UTILIZATION FOR TWO METAL JOINING MANUFACTURING PROCESSES

Jonathan Gasser

University of Kentucky, jonathan.gasser@uky.edu

Click here to let us know how access to this document benefits you.

Recommended Citation

AN ANALYSIS OF ENERGY RESOURCES UTILIZATION FOR TWO METAL JOINING
MANUFACTURING PROCESSES

_____

THESIS

_____

A thesis submitted in partial fulfillment of the
requirements for the degree of Master of Science in
Mechanical Engineering in the College of Engineering
at the University of Kentucky

By

Jonathan Gasser

Lexington Kentucky

Director: Dr. Dusan P. Sekulic,

Professor of Mechanical Engineering

Lexington, Kentucky

2014

ABSTRACT OF THESIS

AN ANALYSIS OF ENERGY RESOURCES UTILIZATION FOR TWO METAL JOINING MANUFACTURING PROCESSES

Sustainable manufacturing involves utilizing energy resources efficiently. Currently, the state of sustainability for a given manufacturing process is described by most in a qualitative sense as opposed to using quantitative metrics. This thesis offers a segment of analysis needed to understand the state of sustainability in the context of energy resource utilization. This was accomplished by measuring the order of magnitude difference between the energy consumption of a manufacturing process vs. the theoretical minimum amount of energy required to complete the same task (aluminum T-joint bond). This analysis was completed for a TIG welding process and a controlled atmosphere brazing (CAB) process. Also, the energy Sankey diagram was constructed for the TIG welding process. The TIG welding process and CAB process consumed an average of 136.1 ± 16.5 kJ and $6,830 \pm 77$ kJ respectively to bond the same sample. The TIG welding process consumed $O(10^2$ kJ$)$ more than the theoretical minimum amount needed to complete the same bond while the CAB process consumed $O(10^4$ kJ$)$ more than the theoretical minimum. In the context of energy consumption, there are sizable margins for improvement for both metal joining processes analyzed in this study.

Keywords: Sustainable manufacturing, energy consumption, metal joining, welding, brazing

Jonathan Gasser
1/21/2014

AN ANALYSIS OF ENERGY RESOURCES UTILIZATION FOR TWO METAL JOINING
MANUFACTURING PROCESSES

By

Jonathan Gasser

_____Dr. Dusan P. Sekulic_____
(Director of Thesis)

_____Dr. James M. McDonough_____
(Director of Graduate Studies)

_____1/21/2014_____

This work is dedicated to my parents Paul and Wendy Gasser. I appreciate all of the sacrifices you have made so that I could succeed. I love you both very much.

ACKNOWLEDGEMENTS

Table of Contents

List of Figures

List of Tables

Chapter 1:   INTRODUCTION

1.1 Background and motivation

The idea of sustainability can be related to a wide variety of aspects of society including social, environmental, and economical.   Arguably the most prominent facet of society where sustainability is currently being discussed is in the realm of manufacturing. This is not surprising considering manufacturing accounts for approximately one-third of energy consumption in the United States (Branham et al, 2008).   However, many people have a turbid understanding of the idea of sustainability, and more importantly how one measures the level of sustainability of a given system.   The state of sustainability is defined as the state that, when altered by a resource interaction, does not leave a permanent change in the environment while at the same time allows for the preservation of all system functions (Bakshi et al., 2011, pp. 135). Currently, the state of sustainability for a given system is described by most in a qualitative sense using vague expressions and criteria based on biased opinion as opposed to scientific-based, quantitative metrics. There are many proponents of sustainability inspired metrics, some of the most prominent include the United Nations Commission on Sustainable Development (UNCSD) development indicators (Commission on Sustainable Development, 2001), the human development index (HDI) ((UNDP), 2013), environmental performance index (EPI) (Environmental Performance Index, 2013), and the ecological footprint (EF) (Venetoulis and Talberth, 2008, pp. 441--469). However, these current metrics contain significant shortcomings. Either single comprehensive metrics are used which are too broad to have considerable relevance, or many, less broad metrics are used which are too specific, with little consensus within the research community. The set of metrics provided by the UNCSD and EPI are examples of metrics made up of multiple indicators with low aggregation while the HDI and EF are examples of highly aggregate indicators. It would be

1

beneficial to have a consistent metric which can be used to describe the efficiency of a manufacturing process from the perspective of energy resources utilization.

The purpose of this thesis is to offer a segment of analysis needed to understand the state of sustainability for a given system in the context of energy resources. This was accomplished by measuring the order of magnitude difference between the energy resource utilization of a real manufacturing process vs. the theoretical minimum. The difference in orders of magnitudes is presented as a metric which quantifies the energy resources utilization of a given manufacturing process.

1.2 Objectives

The primary objectives of this thesis are summarized as follows:

- To describe a thermodynamic approach to considering the state of energy resources use for a given system – an assembly of aluminum parts bonded together by either brazing or welding

- To present a literature review of related topics that are of importance to the subject matter presented in this thesis as a form of background and summary of existing knowledge

- To measure the electrical energy input (energy resource use) for two metal joining processes: 1) Gas Tungsten Arc Welding (GTWA) also known as Tungsten Inert Gas (TIG) welding; 2) Controlled Atmospheric Brazing (CAB)

- To compare measured values of input energy resources use for two state-of-the-art metal joining processes to the theoretical minimum amount of energy needed to complete this task

- To quantitatively map energy and construct the Sankey diagram for the TIG welding process

- To qualitatively map exergy and construct the Grassmann diagram for the TIG welding process

1.3 Literature review

1.3.1 Thermodynamic framework

It is evident that the primary goal of any manufacturing process is to ultimately produce a high quality product. This is accomplished through a series of operations in which input materials are altered and energy resources are consumed. Thus, it is reasonable to model a manufacturing process as an open thermodynamic system having heat, work, and material flow interactions crossing the system boundary. Additionally, this enables one to consider material flows entering and leaving the system at given flow rates, temperatures, and pressures (i.e., at given thermodynamic states) as energy flows. Similar to any thermodynamic system, one must consider that the manufacturing process will incur losses due to cumulative irreversibility of all associated changes of state of the system (Bakshi et al., 2011, pp. 164).

Modeling the energy use of a manufacturing process using a thermodynamic framework allows us to utilize mass, energy, and entropy balances to better understand the magnitudes (quantity) and types of energy (quality) entering and leaving the system. Using these balances will help us to better understand the imperfections inherent within any system in terms of available energy losses and have a more lucid understanding of the efficiency of the process.
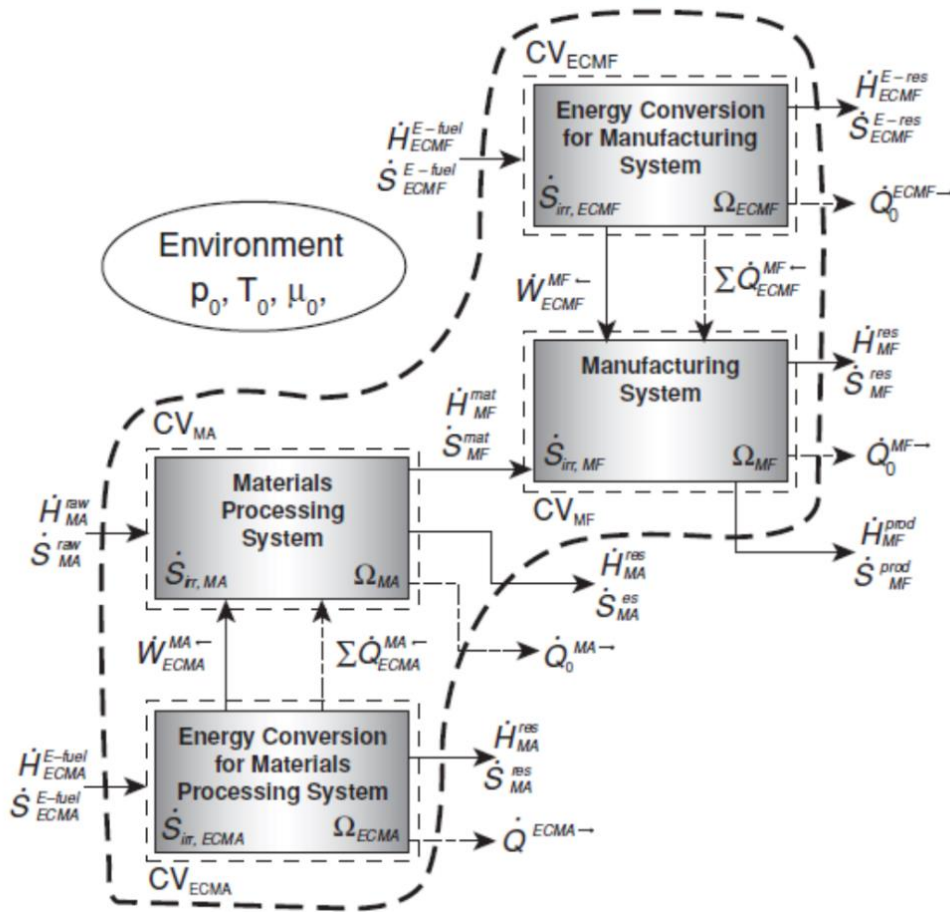
Figure 1.1: Manufacturing system block diagram (Bakshi et al., 2011, pp. 164)

Figure 1.1 is a depiction of a generic manufacturing system which displays the energy interactions the system will have with its environment. The "Manufacturing System" block (Ω_{MF}) is used to represent a given manufacturing process. It can be seen that Ω_{MF} has several interactions with other subsystems as well as with the surrounding environment. The manufacturing system may receive energy from the energy conversion subsystem in the form of work and heat as well as input energy carried by the input materials coming from the upstream materials processing subsystem. Leaving the manufacturing system, there may be energy from waste materials, heat loss to the environment, as well as the energy contained within the desired product. Ultimately, the mass, energy, and entropy balances can be used to evaluate the performance of the subsystems depicted in Figure 1.1. The subsystem of special interest in this study is the manufacturing system

4

Ω_{MF}, thus, the following three equations are used to balance changes in mass, energy, and entropy with time for Ω_{MF} (Bakshi et al., 2011, pp. 78).

Mass Balance

Equation 1.1

$$\frac{dM_{MF}}{dt} = \left(\sum_{i=1} \dot{N}_{i,in}\widetilde{M}_i\right)_{MF} - \left(\sum_{i=1} \dot{N}_{i,out}\widetilde{M}_i\right)_{MF}$$

The above equation represents the time rate change of mass of the system where $\dot{N}_i$ represents the number of moles per unit time of the ith component entering or leaving the manufacturing system and $\widetilde{M}_i$ is the molar mass of that component.

Energy Balance

Equation 1.2

$$\frac{dE_{MF}}{dt} = \sum_{k} \dot{Q}_{ECMF,k}^{MF\leftarrow} - \dot{Q}_0^{MF\rightarrow} + \dot{W}_{ECMF}^{MF\leftarrow} + \dot{H}_{MF}^{mat} - \dot{H}_{MF}^{prod} - \dot{H}_{MF}^{res}$$

The above equation represents the time rate change of the system energy. The terms $\dot{Q}_{ECMF,k}^{MF\leftarrow}$ and $\dot{W}_{ECMF}^{MF\leftarrow}$ represent the heat and work interactions respectively between the manufacturing system Ω_{MF} and the energy conversion subsystem Ω_{ECMF}. The term $\dot{Q}_0^{MF\rightarrow}$ represents the heat interaction between Ω_{MF} and the surrounding environment and is assumed to be a heat loss out of the system at the local temperature T_0. The terms $\dot{H}_{MF}^{mat}, \dot{H}_{MF}^{prod}, \dot{H}_{MF}^{res}$ represent the summed enthalpy rates of the input material flows, the output product flows, and the output residual flows.

Entropy Balance

Equation 1.3

$$\frac{dS_{MF}}{dt} = \sum_k \frac{\dot{Q}_{ECMF}^{MF\leftarrow}}{T_k} - \frac{\dot{Q}_0^{MF\rightarrow}}{T_0} + \dot{S}_{MF}^{mat} - \dot{S}_{MF}^{prod} - \dot{S}_{MF}^{res} + \dot{S}_{gen,MF}$$

Here the $\dot{Q}_{ECMF}^{MF\leftarrow}/T_k$ and $\dot{Q}_0^{MF\rightarrow}/T_0$ terms represent the entropy interactions associated with the heat transfer rates to the system Ω_{MF} and from the system to the environment respectively, at various distinct temperatures at which these exchanges take place. Additionally, the terms $\dot{S}_{MF}^{mat}$, $\dot{S}_{MF}^{prod}$, $\dot{S}_{MF}^{res}$ and represent the summed entropy rates for the material inputs, product materials, and residual waste materials. Lastly, the $\dot{S}_{gen,MF}$ term represents the entropy generation or inherent irreversibilities present in the manufacturing subsystem. This entropy generation term is paramount in that it is the basis for developing an entropy based metric for describing the state of sustainability of a given system. This will become more apparent as the exergy balance is formulated.

Exergy Balance

While energy can be defined as a change of a system property, exergy is the *available energy,* a magnitude of an energy interaction quality. Exergy has the same units as energy but is measured as the available energy to be released while the system changes the state from the given state of a system to the state of thermodynamic equilibrium with the surrounding environment (Bakshi et al., 2011, pp. 45). Moreover, exergy has both physical and chemical components which will be discussed further with the explanation of Equation 1.5.

It is understood that all processes possess inherent irreversibilities. From a thermodynamics perspective this means that each step inevitably involves losses due to an inherent departure from reversible processes and hence generates entropy, as well as (in addition) a possible

6

stream of waste materials carrying additional exergy losses, which may be also misinterpreted as energy losses (Gutowski et al, 2009, p. 1584). Thus, as the process is executed in the forward direction, there is natural decrease in the quality of energy. Additionally, any system is in contact with its surrounding environment, a thermal reservoir, in equilibrium at a given pressure, temperature, and internal energy (p_0, T_0, and μ_0). The available energy interaction of the system is constrained up to the point at which the system would reach thermodynamic equilibrium with the surroundings. Even for an ideal process which is completely reversible, the limiting energy level of the equilibrium state of the environment inhibits the ability to exploit all of a system's energy at a given state. Thus, the quality aspect of energy must be considered in addition to the quantity.

The TIG welding process studied in this thesis can be used to explain the idea of exergy and its relevance to the quality of available energy. Consider a TIG welding process which joins two pieces of aluminum into a T-shaped joint. Electric work is input into the system and causes the arc to have a temperature of $O(10^4 \text{ K})$ (Yang and Lin, 2003). This arc is used to heat the joint area until a phase change occurs and a joint is formed. During the heating and after the joint is formed heat is dissipated from the aluminum sample to the surrounding environment through natural convection and radiation until the sample eventually reaches equilibrium with the environment. It is apparent that the quantity of energy is conserved in that the same amount of electrical energy input into the sample and its immediate surroundings is eventually dissipated as thermal energy to the environment. However, the quality of the input energy is diminished in that the heat dissipated to the environment is less useful (usually useless) than the electrical energy input to the sample before it is delivered to the process. This is because the quality of energy depends not only on the manner of execution of the transformation, but on the temperature level

7

of the thermal source in comparison to the thermal reservoir (Bakshi et al., 2011, pp. 51), as a potential available for a useful work.

The energy balance and entropy balance equations can be manipulated algebraically to yield the following exergy balance equations (Bakshi et al., 2011, pp. 167).

Equation 1.4

$$\dot{E}x_{in} + \dot{E}x_{W,in} + \dot{E}x_{Q,in} = \dot{E}x_{out} + \dot{E}x_{W,out} + \dot{E}x_{Q,out} + \dot{E}x_{destruction}$$

The bulk exergy flow terms above can be separated to account for the contributions of both physical and chemical energies. Additionally it is important to note that in exergy analysis, the contributions of work and heat are not equivalent but rather the available energy of heat must be reduced by a Carnot factor of $(1 - T_0/T_k)$. Lastly, the term $\dot{E}x_{destruction}$ represents the exergy destroyed during a given process.

Equation 1.5

$$\dot{E}x_{in}^{ph} + \dot{E}x_{in}^{ch} + \dot{W}_{in} + (1 - T_0/T)\dot{Q}_{in} = \dot{E}x_{out}^{ph} + \dot{E}x_{out}^{ch} + \dot{W}_{out} + (1 - T_0/T)\dot{Q}_{out} +$$

$T_0\dot{S}_{gen}$

It can be seen that the total exergies in and out are split up into physical and chemical exergies. The physical exergy represents the difference of flow availability between the given state and the restricted dead state (the state of stable thermodynamic equilibrium with the surroundings with respect to both temperature and pressure). The chemical exergy component represents the remaining potential for extracting exergy from a system as related to the chemical potential difference between the restricted dead state and the ultimate dead state. Additionally, it should be noted that the magnitude of any work interaction corresponds exactly to the magnitude of

corresponding exergy that this energy interaction carries. This means that any work is available to be converted into a useful effect entirely (Bakshi et al., 2011, pp. 70-71), (Çengel and Boles, 2002).

Specifically for the manufacturing subsystem Ω_{MF} from Figure 1.1, this exergy balance can be reduced to the following (Bakshi et al., 2011, pp. 165):

Equation 1.6

$$\dot{W}_{ECMF}^{MF\leftarrow} = \dot{E}x_{MF}^{prod,ph} + \dot{E}x_{MF}^{res,ph} - \dot{E}x_{MF}^{mat,ph} + \dot{E}x_{MF}^{prod,ch} + \dot{E}x_{MF}^{res,ch} - \dot{E}x_{MF}^{mat,ch}$$

$$- \sum_{k>0} \left(1 - \frac{T_0}{T_k}\right) \dot{Q}_{ECMF}^{MF\leftarrow} + T_0 \dot{S}_{gen,MF}$$

It is important to note that the tern $\dot{W}_{ECMF}^{MF\leftarrow}$ is equal to the minimum amount of work necessary for input when irreversibilities are zero ($T_0 \dot{S}_{gen} = 0$). Hence, the term $T_0 \dot{S}_{gen}$ represents the difference between the theoretical minimum amount of work needed to complete a given task and the actual amount of energy resources consumed during the completion of the task.

1.3.2 Technology improvement

When attempting to improve the efficiency of a particular manufacturing process along the existing technology, the norm is to consider incremental changes which allow for only gradual improvements. This is clearly a consequence of gradual improvements to any technology as long as it is not replaced with a radically improved technology for the given task. This thesis promotes the novel idea of calculating the theoretical minimum amount of energy needed to accomplish the desired task of a manufacturing process involving metal joining and a comparison of this theoretical minimum to a present, traditional technology energy resource utilization. This comparison provides an evaluation venue that may assist us in defining a need for a novel,

transformational technology (Chu and Majumdar, 2012). Figure 1.2 taken from Bakshi et al., 2011, pp. 150 displays a generic plot which marks the margin between the industry standard energy resources needed to complete a given task and the physical minimum required to complete this task with respect to the generic timescale of past, present, and future. Also, there is a second vertical axis on the right hand side of the plot which displays how entropy generation changes with time. It is apparent that there is an asymptotic trend with regards to both the decrease of energy resources used and entropy generation for a given task with respect to time. For example, if the state-of-the-art technology used to complete a given task is T_{pr3}, it is obvious that this uses less energy than the most efficient technology of the past, T_{pa3}, but still more than a technology of the future, T_{F1}. The key point is that these improvements are incremental and their rate of improvement is decreasing with time as indicated by the formation of the horizontal asymptote. However, the horizontal axis is broken between the labels of "Future" and "∞" with a curved line attaching the path of technology evolution to represent the gap in the decrease in energy resource use which may exist and break the asymptotic trend between these two periods of time. The thermodynamics framework of this type of modeling guarantees that the margin of ΔE must be greater than zero because the second law of thermodynamics declares that entropy generation for any real process will always be greater than zero. Although a hypothetical technology which can complete a given task with the smallest margin of energy resources used may not be available now or even many years from now, it is beneficial to know the physical limit to which any future technology would be constrained with respect to energy resource usage. To sum up, a metric is needed to facilitate an assessment of a margin for improvement of energy resources use, and the rate of change, should be related to a theoretical limit of energy resources use for a given task, irrespective of technology (Nehete et al, 2013).
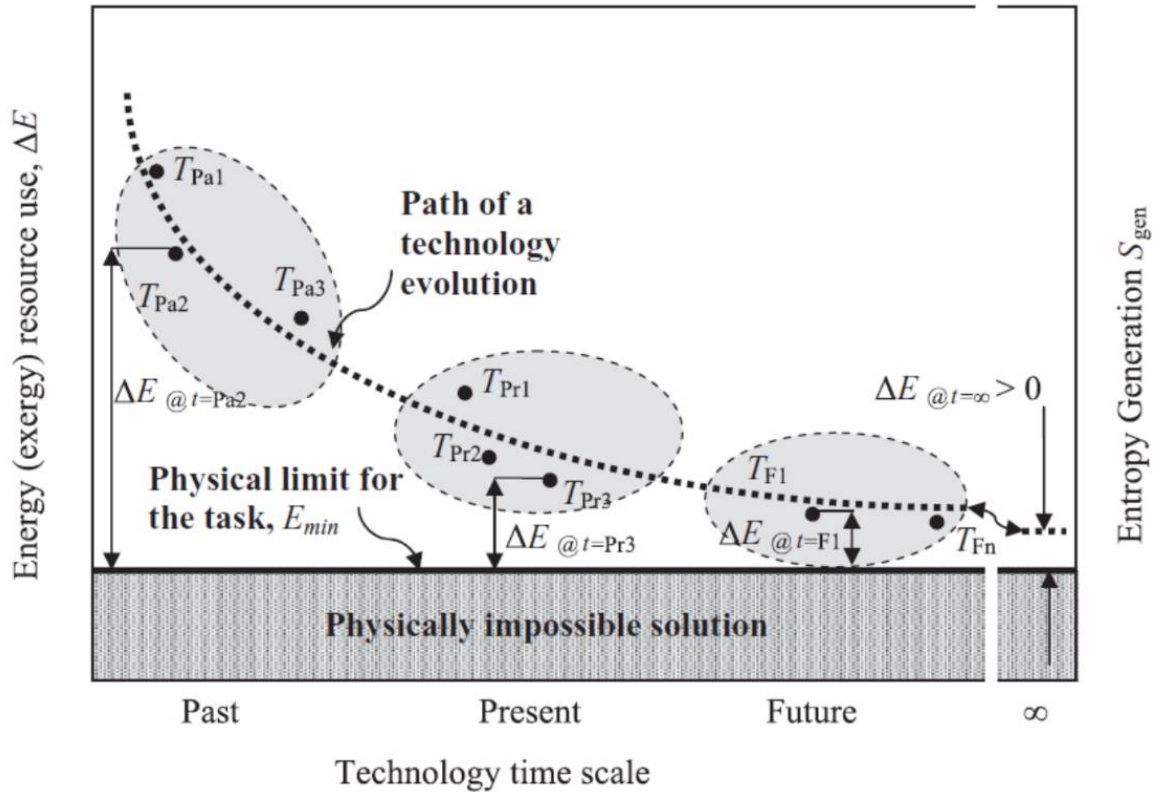
Figure 1.2: Path of a technology evolution (Bakshi et al., 2011, pp. 150)

Knowing the margin between the energy use of the state-of-the-art technology and the physical limit allows us to determine a state of energy sustainability for a given manufacturing process, in this case metal joining.

"One should keep in mind that for a full meaning of a sustainability state, the multiple domains of the given system scale must be considered. In this study, the sustainability is addressed in its quite restricted sense, related only to the energy resources use. This sustainability aspect, at the given scale of a particular manufacturing process, refers primarily to a requirement that the energy resources use must be less than the energy resources availability. In this study, this constraint is a priori satisfied but the quantification of the margin between the resources use in a real process vs. the minimum needed for the accomplishing the given task is considered," (Sekulic, 2013).

11

For example, one of the metal joining technologies studied at length in this thesis was a TIG arc welding process. This TIG welding process has an associated "path of technology evolution," and it can be inferred from Purslow, 2012 that the energy resources associated with TIG welding have decreased along a similar path as the dotted line in the Figure 1.2. In the last 100 years, several improvements in TIG welding have been implemented such as more efficient power supplies or transformers which has resulted in a decrease in energy resources needed to join metal using this technology. Based on the current trend, in the future the energy resources required would most likely decrease with further improvements, such as optimizing the electrode melt-off efficiency, using pulsed current instead of constant, or increasing the deposition efficiency of the process (Purslow, 2012, pp. 24-27). Still, each of these improvements to the existing technology makes incremental improvements in the efficiency of the process and the impact of these improvements likely decrease with time in an asymptotic trend. Thus, it is obvious that if a sizable gap exists between the theoretical physical minimum amount of energy needed to complete a task and the amount of energy currently needed to complete this task with present technologies, then only a novel revolutionary technology may bridge this gap; it is not likely to be done by small incremental improvements to the existing technology. Such a novel technology may be termed the "transformational technology" (Bakshi et al, 2011, pp. 134).

1.3.3 Specific energy analysis

One particular area of interest of energy use in manufacturing processes involves the analysis of the specific electrical work per unit of material processed. It has been observed that the electrical power requirements of many manufacturing processes are quite constrained, often in the range of 1-50 kW (Bakshi et al., 2011, pp. 177). This is displayed in Figure 1.3 which plots specific electrical energy consumption, in units of joules/kg, with respect to process rate, in units

of kg/hr. Each of the points or group of points on the plot represents specific electrical energy

usage for a particular technology from a wide range of manufacturing processes. It is interesting

to note that even though the data points represent unrelated manufacturing processes with specific

energies and process rates differing by several orders of magnitude, they can be collapsed onto a

single log-log plot. Additionally, it is apparent that the data points seem to be enclosed by four

boundaries. The diagonal boundaries represent values of 1 kW and 50 kW for the lower and upper

diagonal lines respectively.   Additionally, the lower horizontal boundary of 1 MJ/kg is

approximately equal to the specific energy needed to melt solid aluminum. Likewise, the upper

horizontal boundary of 100 MJ/kg is the approximate specific energy needed for the phase change

of aluminum from a liquid to a vapor.
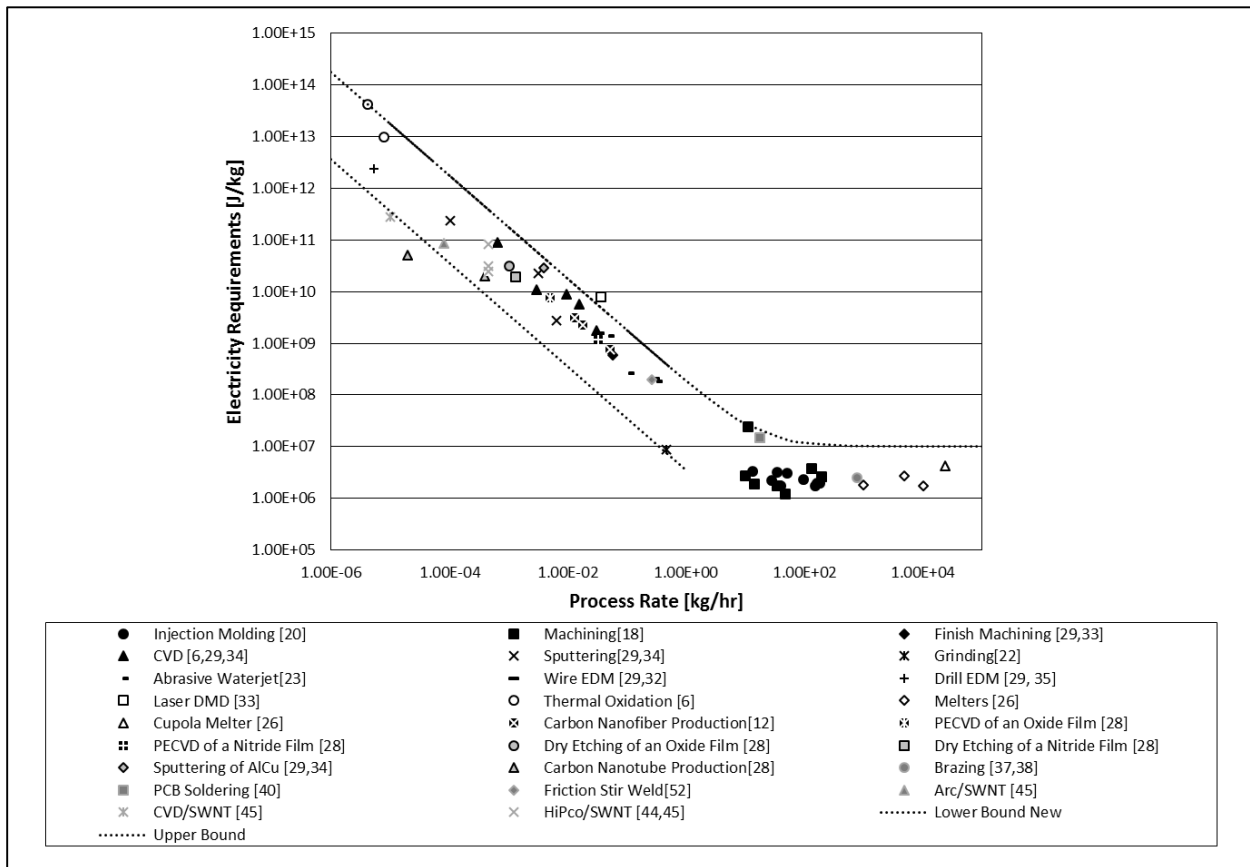
Figure 1.3: Specific energy requirements with respect to process rate adapted from Bakshi et al., 2011, pp. 178

13

The data shown in the log-log "hockey-stick" plot in Figure 1.3 inspired the specific energy analysis for different types of welding technologies. The data for this analysis was collected from literature containing energy measurements for five different welding methods. These include laser welding of titanium alloys, TIG welding of stainless steel plates, AC and DC spot welding of galvannealed low-carbon steel, and MIG welding of aluminum alloy plates. The energy measurements from each study were extracted and compiled in Table 1.1.

Table 1.1: Energy consumption and theoretical minimum of energy needed for five welding technologies

Source	Technology	Process Rate (kg/hr)	Theoretical Minimum Energy Needed (J)	Actual Energy Input (J)	Electrical Energy Use per Unit Mass (J/kg)	Theoretical Energy Use per Unit Mass (J/kg)
Zhu et al (2011)	MIG Welding	8.42E-02	1866	1.94E+05	1.11E+08	1.06E+06
		6.73E-02	1493	1.85E+05	1.32E+08	1.06E+06
		6.89E-02	1527	1.60E+05	1.11E+08	1.06E+06
		4.78E-02	1060	1.50E+05	1.50E+08	1.06E+06
Li (2004)	Spot Resistance Welding AC	4.05E-01	26	5.36E+03	2.39E+08	1.14E+06
		4.16E+00	263	5.98E+03	2.59E+07	1.14E+06
		7.19E+00	454	6.64E+03	1.66E+07	1.14E+06
		9.09E+00	574	7.34E+03	1.45E+07	1.14E+06
Li (2004)	Spot Resistance Welding DC	1.78E+00	112	4.66E+03	4.72E+07	1.14E+06
		3.37E+00	213	4.98E+03	2.66E+07	1.14E+06
		5.70E+00	360	5.50E+03	1.74E+07	1.14E+06
		9.09E+00	574	6.15E+03	1.22E+07	1.14E+06
		9.39E+00	592	6.44E+03	1.24E+07	1.14E+06
W.H. Giedt et al (1989)	TIG Welding	1.47E-01	3452	8.65E+04	2.40E+07	9.57E+05
		1.11E-01	2617	7.96E+04	2.91E+07	9.57E+05
		4.21E-01	9913	1.37E+05	1.32E+07	9.57E+05
		4.14E-01	9740	1.22E+05	1.20E+07	9.57E+05
		8.16E-01	19193	1.82E+05	9.09E+06	9.57E+05
		7.01E-01	16484	1.61E+05	9.34E+06	9.57E+05
		9.98E-01	15677	1.16E+05	7.07E+06	9.57E+05
E. Akman et al (2008)	Laser Welding	6.41E-02	0.1229	5.60E+00	6.29E+07	1.38E+06
		9.76E-02	0.1870	6.50E+00	4.79E+07	1.38E+06
		2.06E-01	0.3956	7.60E+00	2.65E+07	1.38E+06
		2.15E-01	0.4124	8.50E+00	2.84E+07	1.38E+06
		3.26E-01	0.6254	9.60E+00	2.12E+07	1.38E+06
		4.36E-01	0.8362	1.05E+01	1.73E+07	1.38E+06
		2.15E-01	0.4124	1.15E+01	3.85E+07	1.38E+06
		4.32E-01	1.1601	1.25E+01	1.49E+07	1.38E+06
		3.09E-01	1.1846	1.34E+01	1.56E+07	1.38E+06

The process rate of each sample in Table 1.1 was calculated by dividing the mass of the joint by the time it took to complete the joint. The theoretical minimum amount of energy needed to accomplish each welded sample was calculated using the following equation. The numerical values used in this equation can be found in Appendix L.

Equation 1.7

$$E_{min} = m\big[c(T_m - T_0) + L_f\big]$$

Where,

E_{min}	=	Theoretical minimum energy required to complete a certain task [kJ/kg]
m	=	Mass of the joint [kg]
c	=	Specific heat [kJ/kg K]
T_m	=	Melting temperature [K]
T_0	=	Ambient temperature [K]
L_f	=	Latent heat of fusion [kJ/kg]

It is important to note that all values of specific heat were found using the NIST database by averaging the specific heat values over temperature range from ambient to melting (NIST standard reference data, 2011). Also, the assumption was made that no metal was evaporated but only melted, thus, mass is assumed to be constant.

The actual energy input values in Table 1.1 were given by the authors for each of the data points. The specific electrical energy usage was calculated by dividing the actual energy input by the mass of the joint formed. Lastly, the specific theoretical energy was calculated by dividing the theoretical minimum values from column four by the mass of each joint.
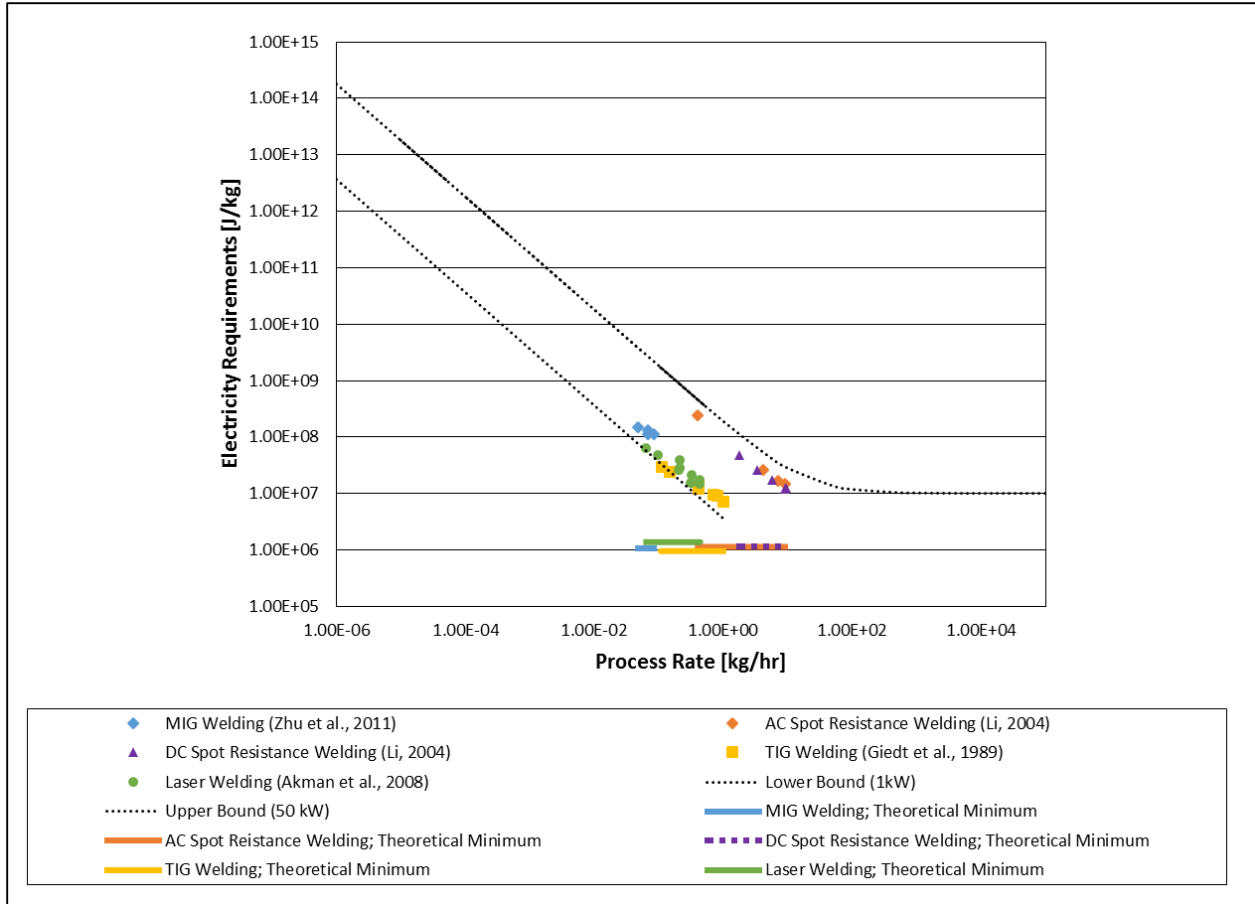
Figure 1.4: Specific energy requirements with theoretical minimums for five welding technologies

The plot in Figure 1.4 displays the values of specific electrical energy use for the five welding technologies on the same log-log plot as Figure 1.3 with the addition of specific theoretical minimums for the respective technologies. One important observation is that it seems there are two separate concentration ranges of data. The first range is closer to the lower diagonal bound and includes the MIG welding, TIG welding, and laser welding technologies. The second cluster of data is closer to the upper diagonal bound and includes the AC and DC spot resistance welding technologies. The first group of data has the common factor of all being associated with line-weld applications while the second cluster includes only spot-weld applications. The electricity requirements for both sets of data is similar, and it seems the two clusters are simply translated

16

horizontally from one another by approximately one to two orders of magnitude. This suggests that although their electricity requirements are similar, line-weld and spot-weld applications likely differ significantly with respect to process rate.

Additionally, Figure 1.4 shows that for the five different welding technologies, the theoretical minimums differ from the measured energy data by at least one order of magnitude and by as much as two orders of magnitude. This substantial gap between theoretical minimum and actual energy usage supports the idea that even state-of-the-art welding technologies have vast room for energy reduction. It is apparent that it is unlikely to bridge this sizable difference through incremental improvements of existing technologies. Rather, it is expected that only transformational improvements in technology will we have the ability to make quantum reductions in energy usage of welding applications. Likewise, understanding the immense room for improvement by comparing theoretical minimums to current technologies gives us a benchmark of the best case scenario to aim for when designing innovative energy efficient welding technologies.

1.3.4 Concluding Remarks

Every process in the realm of manufacturing can be said to have a theoretical minimum limit with respect to the resources required to accomplish the given task. This theoretical minimum is based on the physical limits of the task at hand and is completely irrespective of the technology, past, present, or future, which is used to complete the given task. In the case of metal joining, there are currently state-of-the-art technologies being used (laser welding, controlled atmospheric brazing, etc.) that require less energy resource utilization than technologies of the past. Moreover, one may hypothesize that there will be technologies in the future that will consume less energy than those of today. By knowing the current energy consumption and the theoretical physical limit

necessary to complete the task one can get a sense of the absolute margin available for improvement. Ultimately, the following metric is used to describe the margin for improvement for a given task.

Equation 1.8

$$\Delta E_{resource} = E_{in}^{actual} - E_{in}^{theoretical}$$

Where,

$\Delta E_{resource}$	=	The margin for energy resources improvement for a given task
E_{in}^{actual}	=	Measured energy consumption for a state-of-the-art technology
$E_{in}^{theoretical}$	=	Theoretical minimum amount of energy required to complete the task

Chapter 2:   EXPERIMENTAL SETUP AND PROCEDURES

The objective of this chapter is to explicitly describe the experimental setup and procedures for this study. The chapter is divided into two primary sections which highlight (1) the TIG welding experiments and (2) controlled atmosphere brazing experiments, and concludes with a summary section.

The purpose of the TIG welding experiments discussed in the first half of this chapter was to comprehensively explore the energy use of an arc welding metal joining process. This involved (i) measuring the electric energy inputs and (ii) assessment of the heat losses from the welded sample to the surrounding environment so that the energy and exergy balances could be mapped. Extensive energy and exergy balances have already been constructed for the CAB furnace used in this study (Nehete, 2013). Thus, the primary objective of the CAB metal joining experiments described in the second half of this chapter was to use them as a benchmark to compare the order of magnitude of electrical energy input to that of the TIG welding process. The thought process behind this was to compare the energy resources required for two state-of-the-art metal joining processes to complete essentially the same task (an aluminum T-joint assembly bonding).

It is understood that if we wanted to compare the two processes for optimal joint formation, an AC MIG welding process would be a more appropriate comparison to the CAB process. However, for the sake of this study we were only concerned with the energy consumption of the two processes and not necessarily optimal joint formation.   Nonetheless, the measured values of input energy for both the TIG welding process and the CAB process were ultimately compared to the theoretical physical minimum energy needed to complete respective tasks to understand the level of energy conversion performance for both processes. It should be emphasized that the objective of a manufacturing process is not to achieve the minimum energy resources use but to

19

get the desired product characterized by a desired product quality. Our analysis is not related to product quality comparison but only to the energy resources use for the same task. Moreover, we are interested in a comparison of the orders of magnitude of resources used, not necessarily exact values. Thus, the analytical and empirical tools of the analysis are adjusted accordingly.

2.1 TIG welding experiments

As previously discussed above, the objectives of the TIG welding experiments were to measure the energy resources needed to join the aluminum sample and to quantitatively map the energy balance and qualitatively map the exergy of the system. Figure 2.1 (a) displays a block diagram for a general manufacturing system and (b) a block diagram for the TIG welding process and depicts the energy inputs and outputs as well as the enthalpy flows into and out of the system that were considered in this work. The subsequent experimental procedures will describe how the data was collected to determine the magnitudes of selected energy and enthalpy flows seen in Figure 2.1(b).

(a) **(b)**
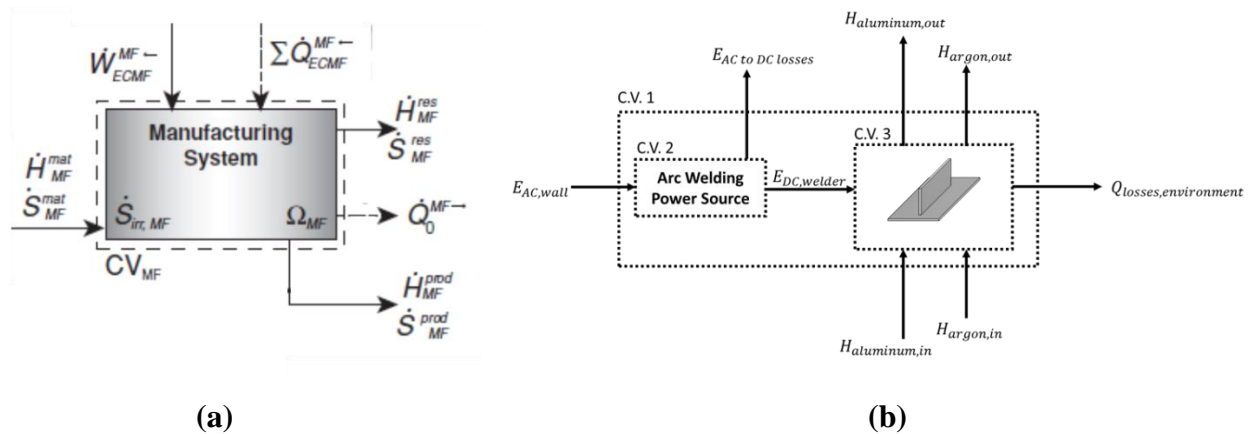
Figure 2.1 (a) A generalized manufacturing system energy interactions in terms of energy, enthalpy, and entropy flows, adapted from Bakshi et al., 2011, pp. 164; (b) Energy interactions for a TIG welding process

Figure 2.1(b) displays three control volumes relevant to the TIG welding process and are useful when presenting the energy balance in the following chapter. The boundary C.V. 1

encompasses the overall system. The system boundary is comprised of the constituents of the aluminum sample, the welding arc, and the arc welding power source. The boundary C.V. 2 is used to identify the losses that occur with the conversion of the AC electricity supplied by the wall outlet to the DC electricity of the arc (ultimately used to weld the sample). It will become more apparent how these losses are measured and accounted for in subsequent sections. Finally, C.V. 3 is the control volume which includes the aluminum sample and protective argon gas of the weld arc as material inputs. Additionally, this control volume has input DC electrical energy (work) and thermal energy which is lost to the surrounding environment. The material flows into and out of the control volume were identified as those crossing the selected system boundaries.

2.1.1 Material selection and sample preparation

The primary goal when selecting the material and sample configuration for both the TIG welding and CAB experiments was to keep them as similar as possible. This was of upmost importance because in the end, it was desired to compare the input energy for these two processes and to do so we must compare "apples with apples". There were only two distinct differences in the TIG welding samples and the CAB samples that will be introduced here and described in more detail in their respective sample preparation sections. These distinctions were imposed due to the specifics of the experimental procedures but would not impact the order of magnitude of energy flows.

1. The vertical aluminum piece was positioned in the center of the horizontal aluminum piece for the CAB samples. The position of the vertical piece was shifted to within 2 mm of the edge of the horizontal piece for the TIG welding samples.

2. The CAB samples had a segment of a 1.2 mm diameter AA 4043 filler metal wrapped tightly around the vertical aluminum piece in the joint zone. The wire segment was

21

positioned to fit snuggly into the joint where the vertical and horizontal aluminum surfaces meet. This material acted as the filler material in the brazing process. The TIG welding process did not need a filler material, but rather the joint was simply formed from the re-solidification of melted aluminum at the joint interface.

Again, it is important to emphasize that the geometry and mass of the sample components were the same except for the two idiosyncrasies described above. These differences in sample features were necessary to ensure easier joint formation for the two processes.

The following describes the sample preparation for the TIG welding experiments while the sample preparation for the CAB experiments will be described in section 2.2.1. The base metal used for all samples in this thesis was AA 3003, the chemical composition for which can be found in Appendix A. The TIG welding sample was comprised of two separate pieces of aluminum, a horizontal sheet and a vertical mating surface, the dimensions are shown in Figure 2.2. The horizontal and vertical base metal pieces were cut from a 3ft x 4ft stock AA 3003 sheet. The two aluminum pieces were fixed together by wrapping the sample assembly with two segments of 0.381mm diameter stainless steel wire in order to constrain the vertical mating surface and to keep it positioned orthogonal to the horizontal sheet. The enthalpy rate of the stainless steel wire segments was assumed negligible and thus, not included in the energy balance seen in Figure 2.1(b) because it was $O(10^4$ kJ) less than the input electrical energy of the welder.
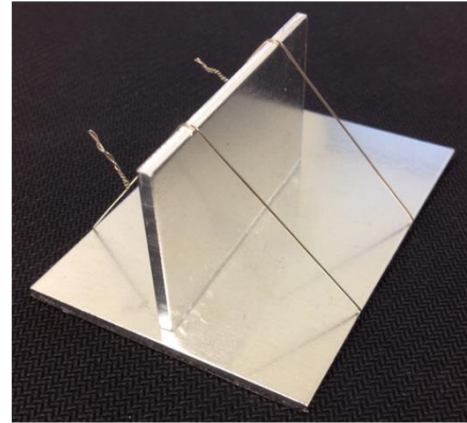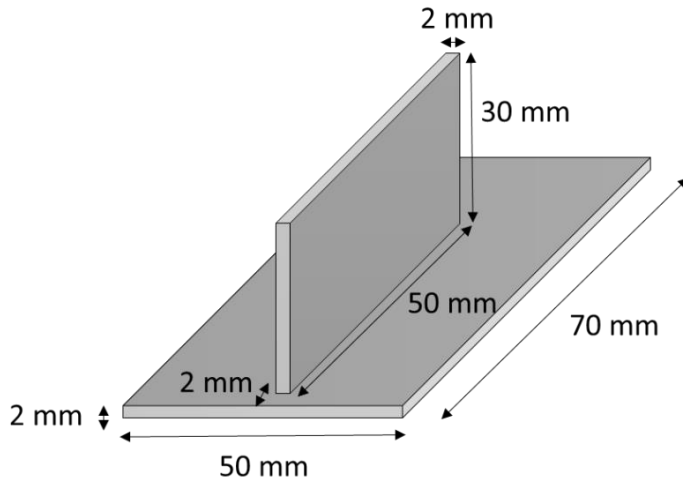
Figure 2.2: TIG welding sample with dimensions

2.1.2 Setup

The TIG welding experiments were primarily meant to provide the measurements related to four key energy components:

1. The input electrical energy from the 480 V, 3-phase Alternate Current (AC) electricity source

2. The losses associated with the arc welding power source (AWPS) converting the AC input electricity to the Direct Current (DC) electricity used for welding

3. The heat losses to the surrounding environment from the welded sample

4. The enthalpy rate of the material in and material out (argon gas and aluminum sample).

These sets of data were paramount with respect to understanding the overall energy interactions of this process.
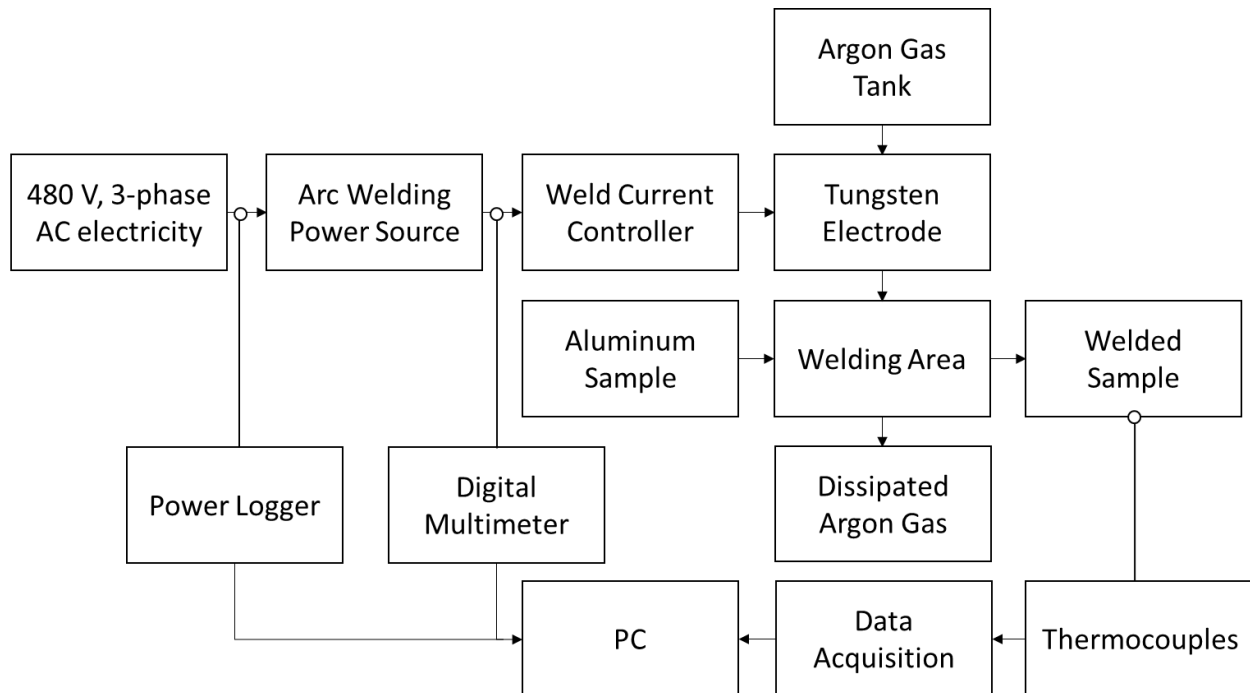
Figure 2.3: TIG welding experiments block diagram

Figure 2.3 depicts a detailed schematic block diagram for the TIG welding experiments conducted in this study and is helpful in describing the experimental procedures. First, the power logger was connected to the cables that connect the (AWPS) to the 480 V, 3-phase wall connection. The power logger used in these experiments was a Fluke 1735 which contains both voltage clamps and current probes that connect to all three legs of a 3-phase AC electricity source. The power logger was connected to the 480 V, 3-phase connection as per the instruction manual. This procedure is summarized in Appendix B and the wiring diagram is depicted in Figure 2.4 (Fluke Corporation, 2006). In this wiring diagram, the L1, L2, and L3 terms represent the three lines of the electricity connection while the N terms represent the neutral lines. The power logger allowed for accurate measurements of input power over a period of time. These power measurements were ultimately integrated with respect to time to yield the input energy needed to weld the aluminum joint. On the output side of the (AWPS), the DC electrical energy used for welding was obtained

by using a digital multimeter to measure line voltage, and the welding current controller to measure weld current.
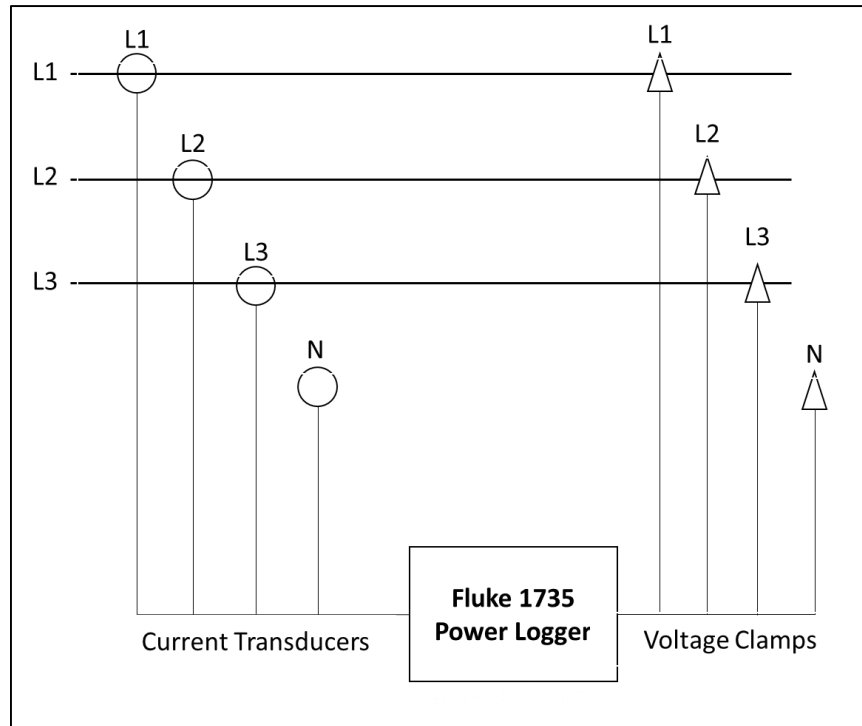
Figure 2.4: Power logger installation for a 3-phase delta connection

Lastly, two thermocouples were mounted to the aluminum sample and one thermocouple was positioned to measure ambient air temperature so that the heat loss to the surrounding environment could be evaluated. The thermocouples mounted to the sample were done so using the high temperature Pyro-Putty® 1000 paste (Aremco Products, 2013) and the locations of the thermocouples on the sample are depicted Figure 2.5. These thermocouples were connected to the computer using a National Instruments cDAQ-9192 module and a LabVIEW program was used to record the temperature values. More detailed information about the LabVIEW program can be found in Appendix B and the measured temperature data can be found in Appendix D.
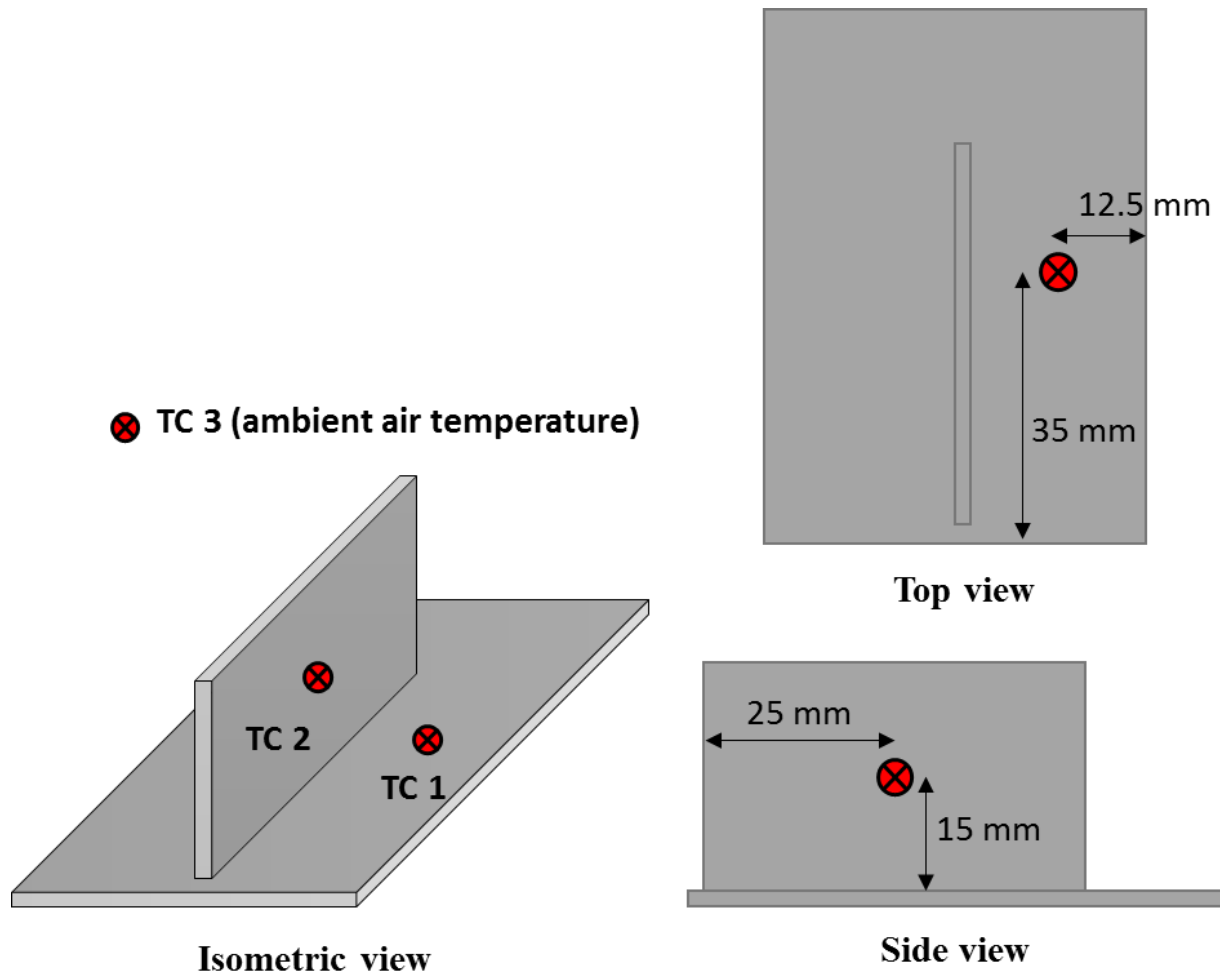
Figure 2.5: Thermocouple positions for TIG welding experiments

2.1.3 Procedures

The following explain the TIG welding procedures which were strictly followed for each of the welding experiments conducted in this study. As previously discussed, the purpose of these welding experiments was to quantify the amount of energy input needed to create a welded T-joint and to map the energy (quantitatively) and exergy (qualitatively) diagrams for the TIG welding process.

The experimental procedures began with the sample preparation as described in section 2.1.1, and then the sample was placed onto the TIG welding work area. The first step in creating

a successful welded T-joint was to spot weld the ends of the two edges of the sample as depicted in Figure 2.6. For these spot-welds, the welding current was set to 100 ± 15 A.
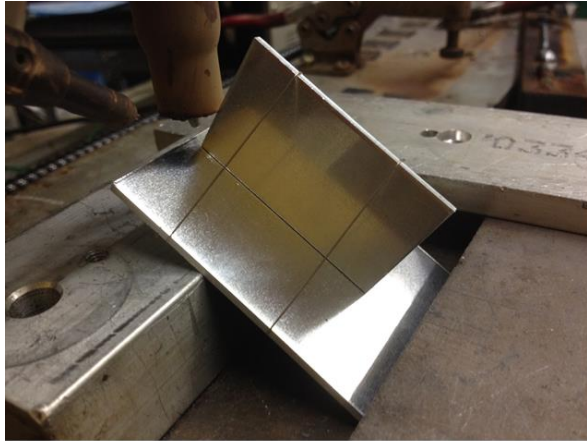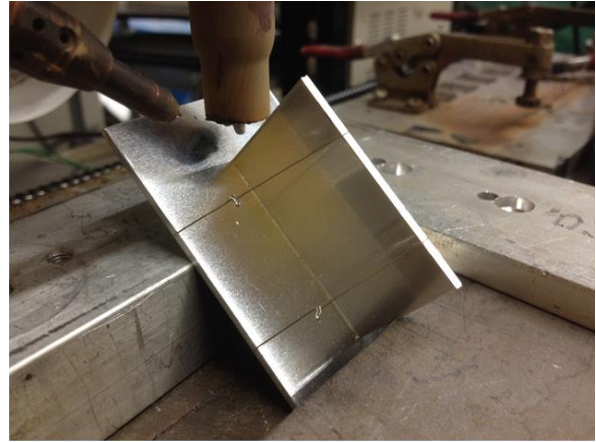
Spot-weld 1   Spot-weld 2

Figure 2.6: Sample position for spot-welds

Figure 2.7 displays an example of a sample after making the two spot-welds. The purpose of the spot-welds was simply to keep the T-joint held in position. This allowed the supporting stainless steel wires to be cut so that the line-weld could ultimately be made. It is acknowledged that this spot welding influenced the local aluminum pieces integrity. Also in principle, this additional procedure induces an additional difference when compared with the CAB samples. This difference is not considered as necessary to address except to include the energy used for these spot-welds in the total energy used for the TIG welding process. An important comment regarding the process optimization is needed. The TIG procedure and equipment was offered by the Welding Laboratory of the Institute of Sustainable Manufacturing (ISM) and no process optimization was intended. Welding aluminum is not a trivial task and requires a specific attention. So, the implemented TIG procedure was not optimized. The brazing of the sample assembly was performed by the Brazing Laboratory of the ISM and it was fully optimized and optimal process parameters have been used. The objective of the work has been to compare the two processes as

they are executed, not to optimize the quality of the bond except to achieve the same task – bonding

two Al pieces into the assembly.

Isometric view

Top view
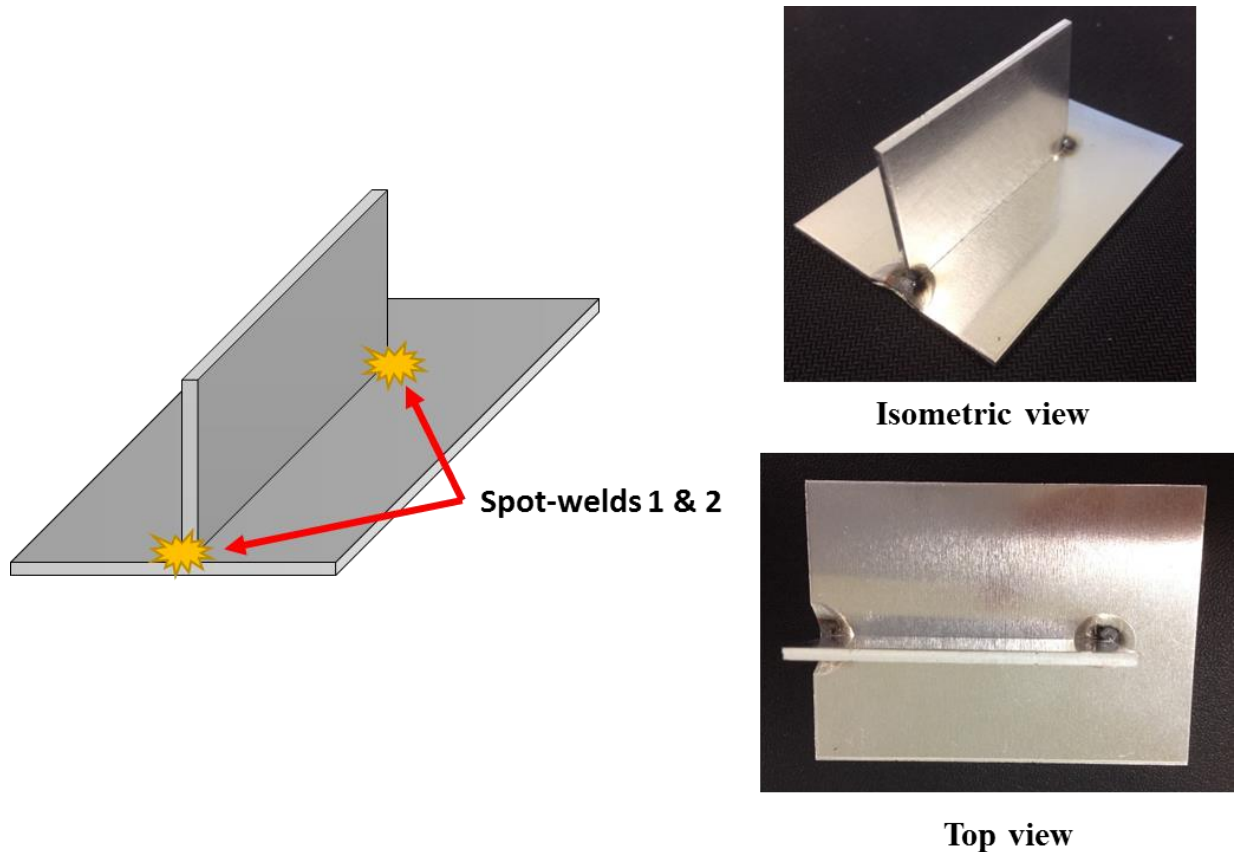
Figure 2.7: Sample after spot-weld 1 and 2

After the two spot-welds were made, the sample was rotated and set on its side as seen in

Figure 2.8 so that the electrode was positioned approximately 5 mm above the joint. The welding

current was increased to 220 ± 15 A for the line-weld. There was a short pre-heating segment

before the line-weld was made. This pre-heating segment consisted of igniting the welding arc

and holding it approximately 1 cm adjacent to the sample for approximately 23 seconds. It is

important to note that the energy consumption during this pre-heating segment was monitored and

was ultimately included in the total energy consumption for this welding process. After the pre-

heating segment, the arc was moved linearly across the joint of the sample at a rate of 66 ± 0.5

cm/min. Completing the 50 mm line weld at this rate took approximately 5 seconds. Once the arc

made a single pass across the joint area, the welding current was terminated and the sample

bonding was complete. Figure 2.9 depicts an example of a finished welded sample.

Pre-heating electrode position   Line-weld electrode position
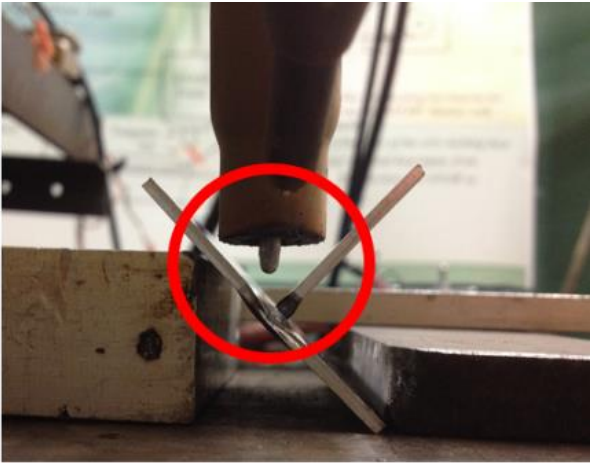
Figure 2.8: Electrode positioning during pre-heat and line-weld
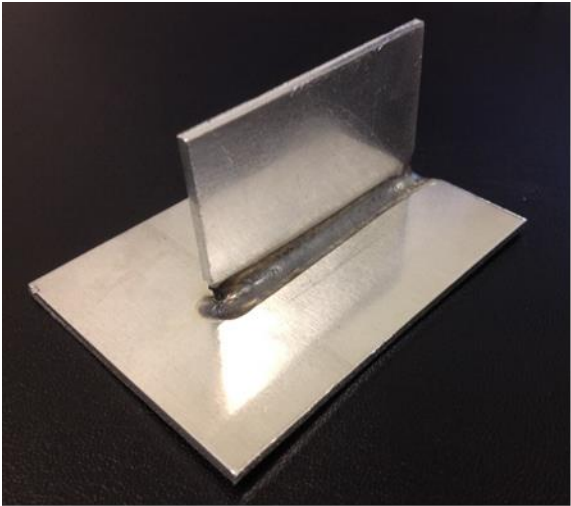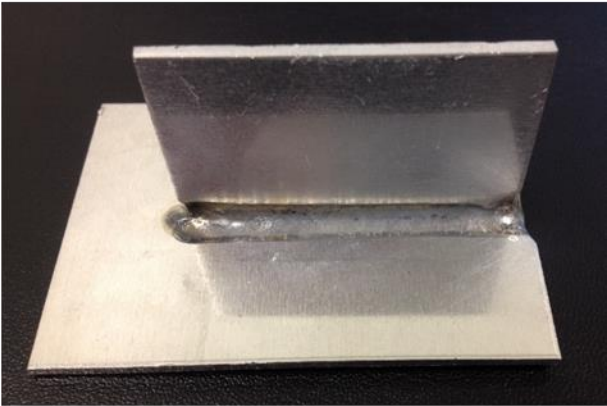
Isometric view   Side view

Figure 2.9: Finished welded sample

2.2 CAB Experiments

The controlled atmosphere brazing experiments were conducted to generate analogous bonded assemblies to compare the electrical energy input needed to that of the TIG welding experiments.

2.2.1 Sample preparation

A sample nearly identical to the one used in the TIG welding experiments previously discussed in section 2.1.1 was used again in the CAB experiments seen in Figure 2.10. Two pieces of AA 3003 were cut to the same dimensions as the TIG welding sample. For the CAB samples, a filler metal segment of 1.2 mm diameter AA 4043 was cut to a length of $130 \pm 5 \mathrm{x} 10^{-3}$ mm and wrapped tightly around the vertical aluminum piece in the corner joint zone. The wire segment was positioned to fit snuggly into the joint where the vertical and horizontal aluminum surfaces meet. This AA 4043 wire was an aluminum-silicon alloy which acted as the filler material in the brazing process (Alcotec Wire Corporation, 2013). This filler material had a lower melting point than the AA 3003 base material and thus, melted and solidified to create the brazed joint. The chemical composition for the AA 4043 can be found in Appendix A. More details about the aluminum brazing using the Controlled Atmosphere Brazing (CAB) is given in (Sekulic, 2013).
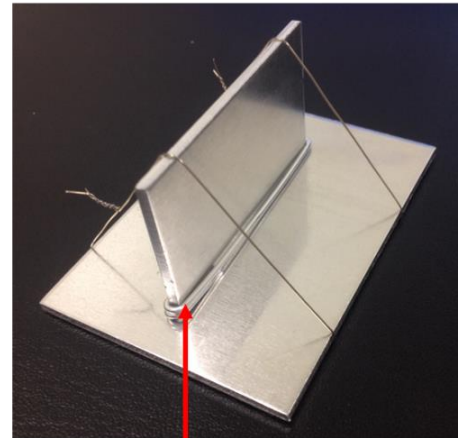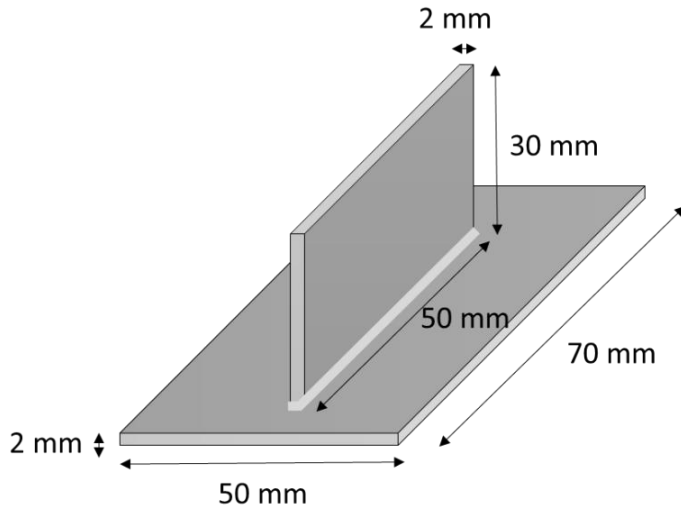
Figure 2.10: CAB experimental sample with dimensions

A strict sample preparation procedure was conducted before every sample entered the furnace to ensure an adequate joint formation. First, the horizontal and vertical AA 3003 base pieces as well as the AA 4043 wire went through the following rigorous cleaning procedure:

1. All sample components submerged in soap water in ultrasonic cleaner for 30 seconds

2. All sample components submerged in tap water in ultrasonic cleaner for 30 seconds

3. All sample components submerged in ethanol in ultrasonic cleaner for 30 seconds

The aluminum pieces were then set to dry for two minutes to complete the sample cleaning procedure. The ultrasonic cleaner was rated at 22W (L&R Ultrasonics, 2013) and was used for a total of approximately 270 seconds. This results in an energy consumption $O(10^0 \text{ kJ})$. Thus, the energy consumption of the cleaning procedure was deemed negligible as it was three orders of magnitude less than the input electrical energy of the furnace.

Before the sample was assembled, $0.05 \pm 5 \times 10^{-5}$ g of potassium aluminum fluoride flux was added to the surfaces of the three sample components (vertical and horizontal AA 3003 base metal and AA 4043 clad wire). The purpose of adding the flux to the sample was to break the oxide layer on the surfaces of the aluminum to ensure acceptable joint formation. The chemical composition of the flux can be found in Appendix A. The flux mass was measured using a high precision scale with a resolution of 1×10^{-4} g and mixed with approximately 10 small drops of ethanol. Cue tips were used to apply the flux solution to the three components of the sample. The enthalpy addition of the flux was calculated as a product of mass, specific heat, and temperature, where mass and temperature were measured and specific heat was taken from the NIST database (NIST standard reference data, 2011). The energy interaction of this added flux was calculated to be more than five orders of magnitude less than the input electrical energy of the brazing furnace and was thus neglected from the energy balance for this process. After the flux had been applied, the sample was assembled to the form seen in Figure 2.10 and was ready to be placed into the CAB furnace.

2.2.2 Setup

Figure 2.11 displays a detailed block diagram for the CAB furnace and is helpful for understanding both the experimental setup and experimental procedures described below. The components of the figure are described in more detail in Appendix B.
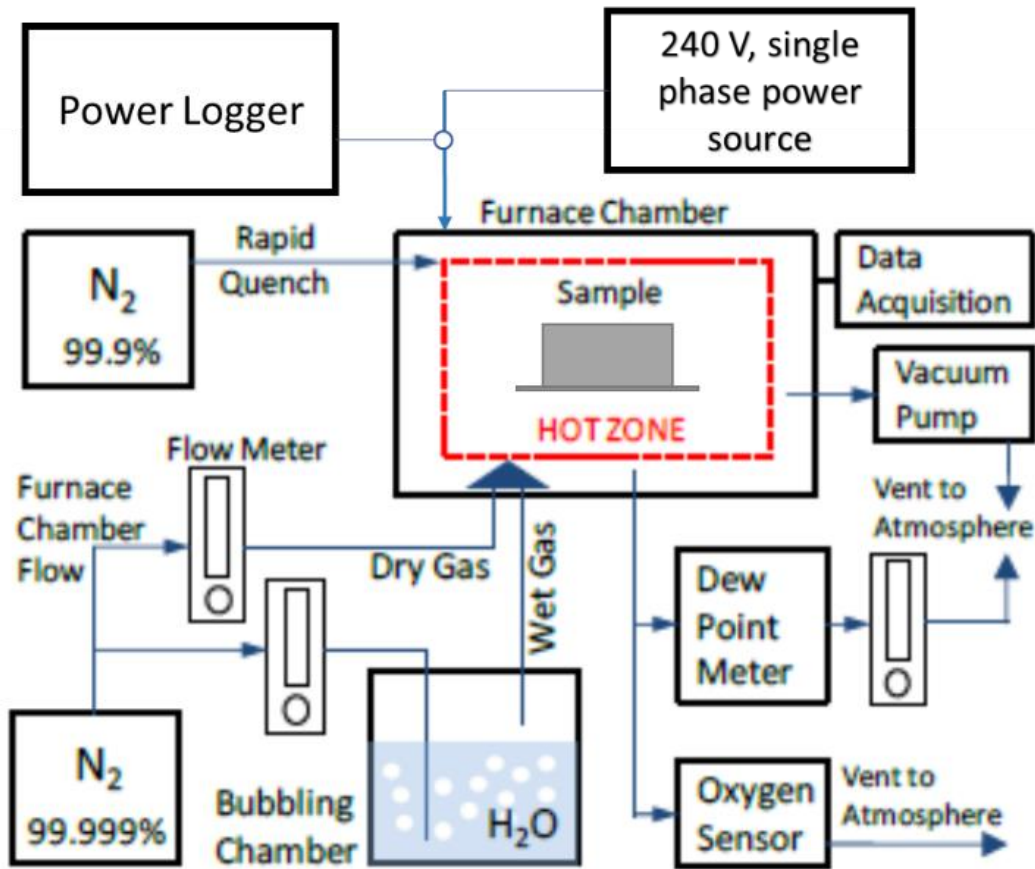
Figure 2.11: CAB experimental block diagram, adapted from Yu et al., 2012, pp. 3

The preliminary step in the experimental setup for the CAB experiments was to adequately install the power logger to the electricity input connection of the furnace (except for the compressed gas inputs, the energy resources input into the system was in form of electrical work). The CAB furnace was computer controlled, and all the relevant process parameters were independently gathered through a separate dedicated data logger system. The installation of the electrical power logger ensured that the input electrical energy required to create an aluminum brazed joint could be measured and ultimately compared to the electrical energy needed to create a TIG welded aluminum joint. The CAB furnace had a 240 V, single phase connection. The power logger was installed as per the instruction manual for a single phase connection as seen in Figure 2.12 below (Fluke Corporation, 2006).
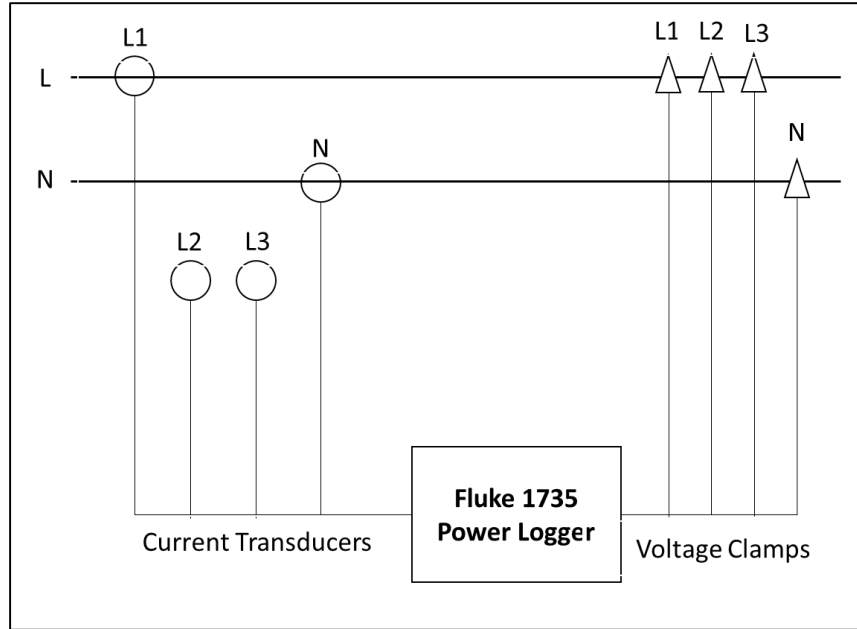
Figure 2.12: Power logger installation for a single phase connection

After the power logger was installed and the sample was prepared to the specifications discussed in section 2.2.1, the sample was placed onto the platform of the CAB furnace in the area indicated as the hot zone from Figure 2.11. The sample was positioned in the center of the platform and the work 1 and work 2 thermocouples were placed so that each was touching the horizontal piece of the sample at diagonally opposite corners as seen in Figure 2.13. The furnace was then sealed and the sample was checked to ensure that it was level and that the thermocouples were still positioned correctly. Figure 2.14 displays the orientation of the sample within the hot zone of the furnace during the experiments. Also, an infrared image of the furnace hot zone can be seen in Appendix M.
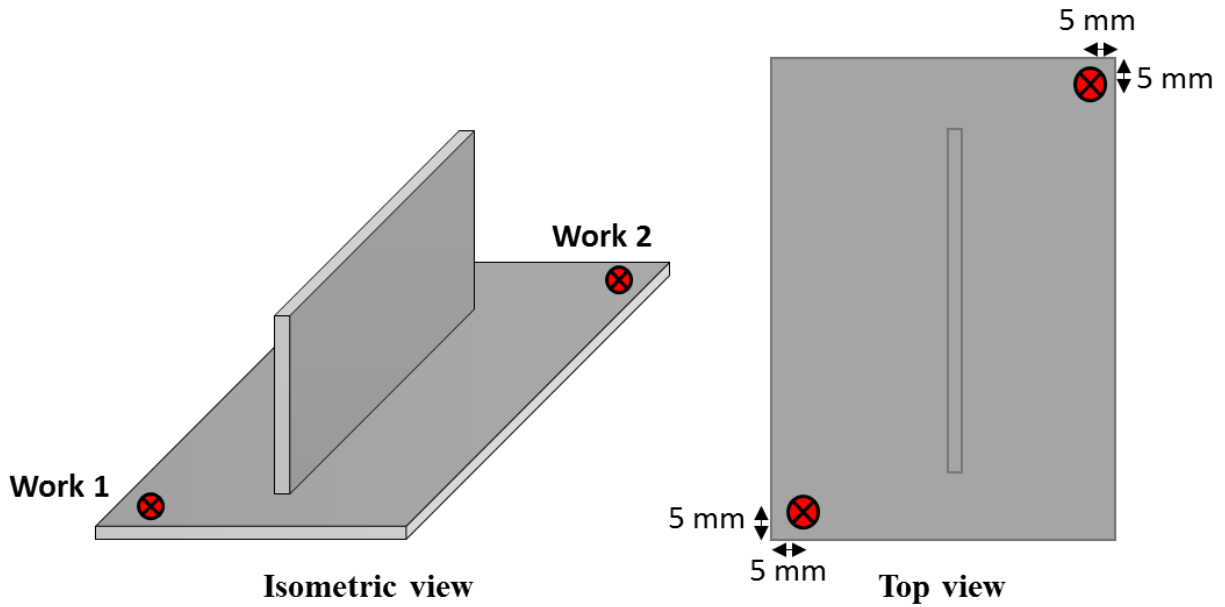
Figure 2.13: Thermocouple positions for CAB experiments
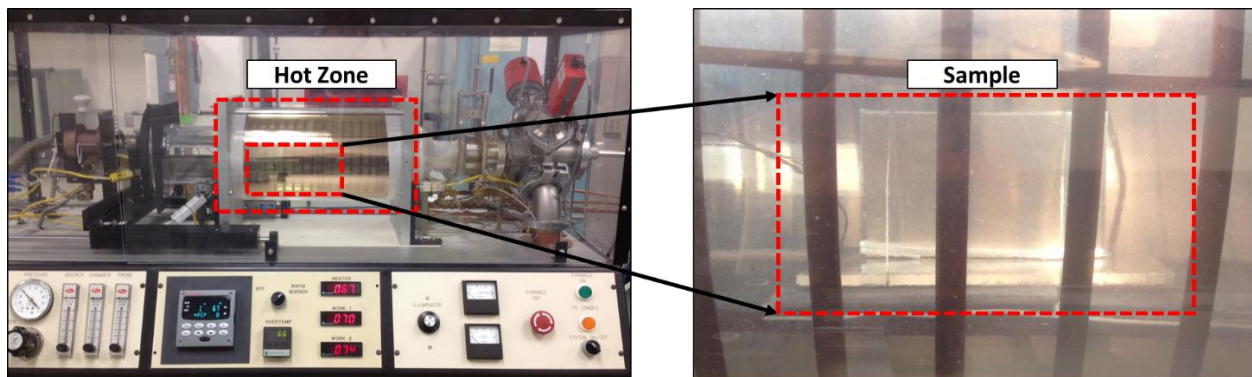
Figure 2.14: Sample position within the hot zone of the furnace for all CAB experiments

2.2.3 Procedures

The first step of the experimental procedure was the furnace purging process. The purging process creates the desired conditions inside the furnace to ensure a successful joint formation. For this study, a flow of ultra high purity nitrogen gas, specification in Appendix A, at 30 ± 2.5 psi was passed through the furnace at a flow rate of $2.0 \times 10^{-5} \pm 4.0 \times 10^{-6}$ m^3/s for approximately three hours. An oxygen sensor was used to measure the oxygen level of the furnace. After three

hours of purging, the oxygen level in the furnace was reduced to 20 ± 0.5 ppm and the furnace conditions were suitable to proceed with the brazing experimental procedures.

After the purging process, the furnace temperature profile information was entered into the furnace control software on the desktop computer. This software controlled the temperature profile for the furnace throughout the duration of the brazing process to ensure successful joint formation. The temperature profile was divided into five distinct segments as seen in Figure 2.15 and described below. A flow of ultra high purity nitrogen continuously passed through the furnace during the first four segments of the brazing procedure. During the rapid quench fifth segment an industrial grade nitrogen gas, specifications in Appendix A, was used. Note, the energy contribution of the enthalpy of the nitrogen flow into the system was calculated on the order of $O(10^2$ kJ) by finding the product of mass, specific heat and temperature. The mass is that of the nitrogen gas for both the purging process and experimental run, the value of specific heat was found using the NIST database (NIST standard reference data, 2011), and the temperature was taken to be the ambient room temperature. This energy contribution was neglected in the energy balance because it was calculated as being two orders of magnitude less than the input electrical energy to the system. A detailed energy balance for this process is presented in Nehete, 2013 and can be viewed in Appendix N.
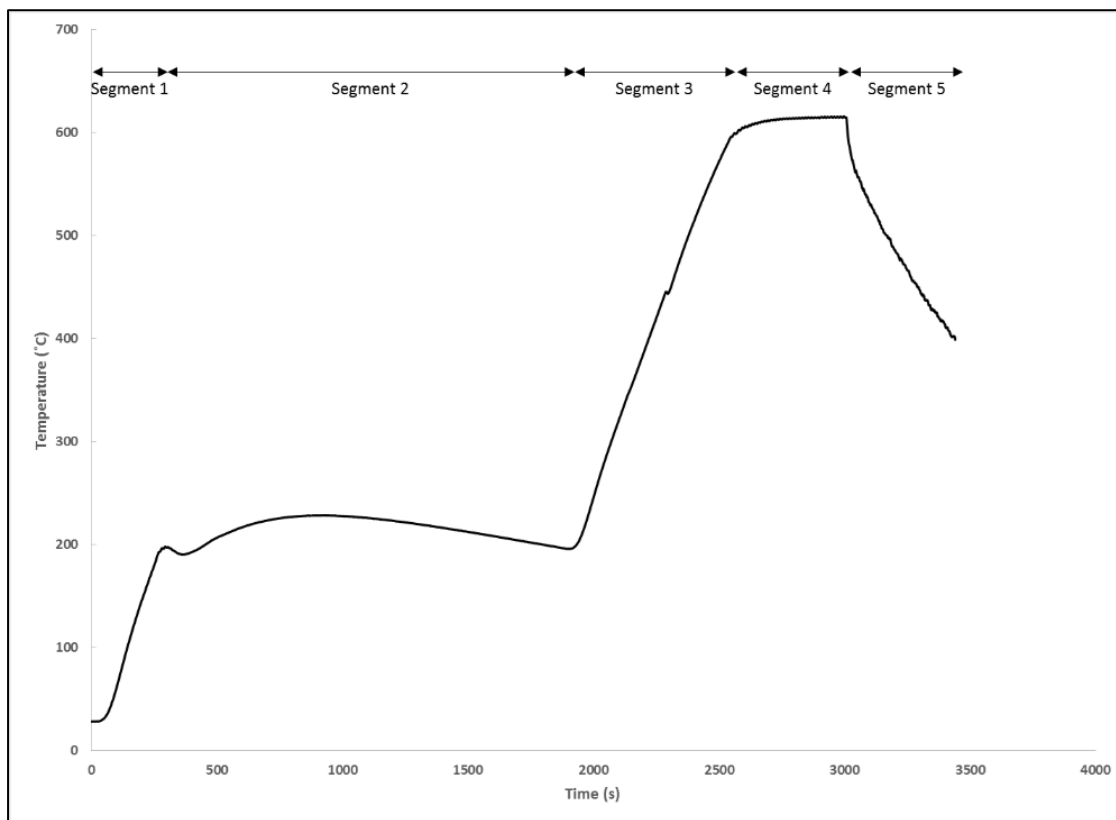
Figure 2.15: CAB experiment temperature profile

Segment 1: Pre-heat ramp-up

During the first segment, the temperature of the furnace in the controller software was set to 150 ˚C at a rate up to 100 ˚C/min. It can be seen in Figure 2.15, the furnace temperature overshot the controller setpoint and increased to approximately 200 ˚C. The power logger began collecting data at the beginning of this segment so that the input electrical energy of the process could be later calculated.

Segment 2: Pre-heat soak

The second segment was a soak period where the furnace temperature is set to pre-heat the sample for 30 minutes. This segment allows the furnace to pre-heat at a low temperature level to achieve a stable background atmosphere with the ultra high purity nitrogen forced flow through the hot zone. Again, note that the setpoint temperature of the furnace hot zone is controlled by a

controller programmed to offer the best feedback at the peak temperature (~600 °C), not at the lower temperature levels. Thus, the chamber temperature at the pre-heat soak segment reaches the setpoint but does not maintain it. This is a standard temperature history and does not sizably affect the assembly metallurgical state.

Segment 3: Ramp-up to hot stage

The third segment increased the temperature of the furnace at a rate up to 50 °C/min until both work 1 and work 2 thermocouples reached a peak temperature of 610 °C. This peak temperature of 610 °C was chosen so that the filler AA 4043 wire would melt while the base AA 3003 would not change phase. It is understood that the selected peak temperature is higher than the state-of-the-art process conditions (~605 °C), but due to a decision to offer a more conservative energy resources estimate, the temperature of 610 °C was selected.

Segment 4: Hot stage soak

The fourth segment of the temperature profile was a five minute soak at the peak temperature ~610 °C. For a state-of-the-art process this dwell time period is usually closer to two minutes. However, in an effort to obtain a conservative energy resources estimation, this dwell time was increased to five minutes. During this segment the filler wire changed from solid phase into liquid completely, and the joint was formed by a surface tension driven flow of the liquid filler metal into the joint.

Segment 5: Rapid quench cool down

The fifth and final segment of the brazing procedure was the rapid quench segment. During this segment the sample was cooled as an industrial grade nitrogen (99.9%) flow was passed through the hot zone at a flow rate of $2.0 \times 10^{-5} \pm 4.0 \times 10^{-6}$ m^3/s. This segment ended when the

heater thermocouple reached 400 ˚C. At this point the power logger was stopped concluding the experiment. The sample was left in the furnace and eventually cooled down to the room temperature in a nitrogen and air atmosphere by free convection.

2.3 Experimental setup and procedures summary

The experiments described in this chapter were designed to measure the energy resources required for two metal joining processes (TIG welding and controlled atmospheric brazing). The samples used in these experiments were made to be as identical as possible so that the energy input requirements for the two processes could be compared. There were two minor differences in the samples used for the different metal joining processes which were discussed at length in section 2.1.1. Nonetheless, these differences do not significantly affect the mass or geometry of the samples parts, and thus, it is reasonable to compare the energy resources required for their respective processes. In addition to measuring the input energy, each component of the energy balance was estimated for the TIG welding process. This allowed the energy balance to be constructed. This type of energy mapping analysis was previously been performed for the CAB process and can be seen in Appendix N (Nehete, 2013).

The next chapter will present the results for both the TIG welding and CAB experiments. For each process, the measured input energy will be presented and ultimately compared to the theoretical minimum amount of energy required to complete the respective tasks. Additionally, the quantitative energy and qualitative exergy diagrams of the TIG welding process will be presented and discussed. Lastly, the input energy resources measured for the two metal joining processes will be compared to each other and comprehensively evaluated.

Chapter 3:   **RESULTS AND DISCUSSION**

The objective of this chapter is to discuss the experimental results for both the TIG welding and CAB experiments. The first section of the chapter will focus on the TIG welding experiments. In this section, it will become evident how the input electrical energy required to complete the TIG weld was evaluated. Additionally, the experimental values of input electrical energy will be compared to the theoretical minimum amount of energy required to complete the formation of the welded joint in an effort to display the substantial difference between the two values. The final part of this section will display the (quantitative) energy and (qualitative) exergy diagrams for the TIG welding process and describe in detail how the values of these diagrams were either measured or calculated.

The second section of this chapter will highlight the results from the CAB metal joining experiments. The measured value of input electrical energy required for the CAB furnace to complete the aluminum joint will be discussed in detail and compared to the theoretical minimum amount of energy required to complete this task. Energy and exergy diagrams for this process have previously been created by Nehete (2013).

The chapter will conclude with a comparison of the input electrical energy required to complete the aluminum joint for the TIG welding process and the CAB process. Additionally, the specific energy data points from this study will be added to the "hockey stick" diagram first presented in Chapter 1.

3.1 TIG welding results

3.1.1 Magnitude of input electrical energy

One of the primary objectives of this study was to quantify the amount of electrical energy required to complete formation of an aluminum joint using a TIG welding process. This section discusses the values of power with respect to time that were measured in this study as well as how these values were used to calculate input energy. Additionally, the magnitude of electrical energy needed to make an aluminum joint using a TIG welding process will be compared to the theoretical minimum amount of energy required to complete the same task to portray the substantial margin between these two values. This difference represents the available margin for reduction in energy resources needed to complete the task of creating an aluminum joint using a TIG welding process.

In total, 11 experimental runs were performed for the TIG welding process. However, there were issues with poor bonding with four of the samples. These four samples were deemed unsuccessful bonds because each had at least one gap along the weld where the vertical and horizontal aluminum pieces were not properly joined. Although the energy data for all 11 experimental runs were measured, only the data for the seven successful welded samples are presented in this study and the data can be found in Appendix C. The uncertainty associated with these measurements was 0.2 kJ and the method for calculating this uncertainty is also presented in Appendix C. The measured values of electrical energy for the seven successful TIG welding samples are displayed in Table 3.1. It can be seen from this table that the average energy consumption for the seven samples was 136.1 ± 16.5 kJ. Taking into account (i) the mass of the assembly, the specific energy used to make the part is 4,878 kJ/kg (ii) the mass of only the welded fillet, the specific energy used to make the welded fillet is 71,260 kJ/kg.

Table 3.1: Energy consumption for TIG welding samples

Sample	Energy Consumption (kJ)				
	Spot-weld 1	Spot-weld 2	Pre-heat	Line-weld	Total
1	12.3	5.2	91.9	15.7	125.0
2	18.7	5.9	101.1	15.8	141.5
3	11.1	7.3	103.1	14.5	136.0
4	16.5	9.9	98.4	15.0	139.8
5	15.4	8.1	127.6	16.5	167.7
6	12.8	5.2	90.7	15.7	124.4
7	14.7	7.5	82.3	13.6	118.0
Average	**14.5**	**7.0**	**99.3**	**15.3**	**136.1**
Standard Deviation	**2.6**	**1.7**	**14.4**	**1.0**	**16.5**

All of the values of energy displayed in Table 3.1 were calculated by integrating the measured power data with respect to time. This trending power data was collected by the power logger during each experiment at half second intervals and integrated numerically using Microsoft Excel. The plots in Figure 3.1 display the power versus time data for each of the seven TIG welding samples and indicate the regions for spot-weld 1, spot-weld 2, pre-heat, and line-weld. In Appendix C, a selection of numerical data sets collected and used for constructing Figure 3.1 is given. The complete data set is available in digital form in the folder labeled, "Gasser Thesis Data" stored in the Brazing Laboratory (Gasser, 2013).
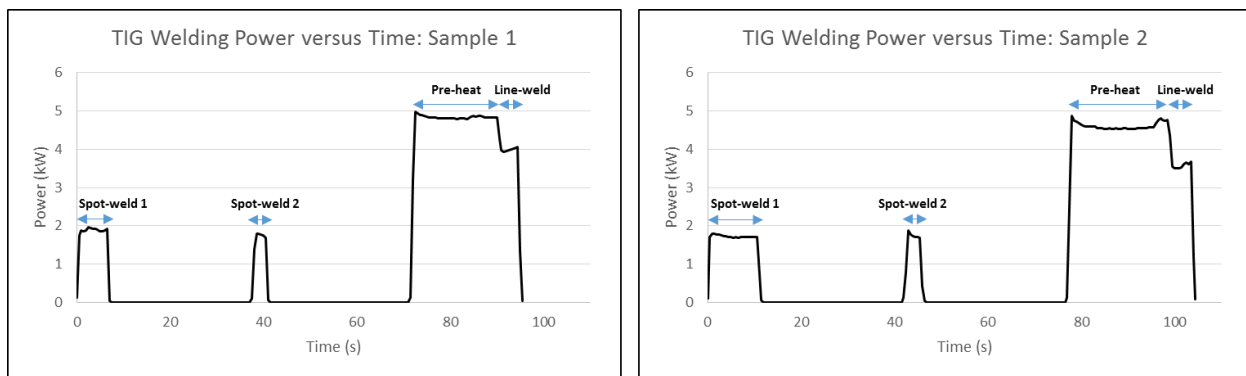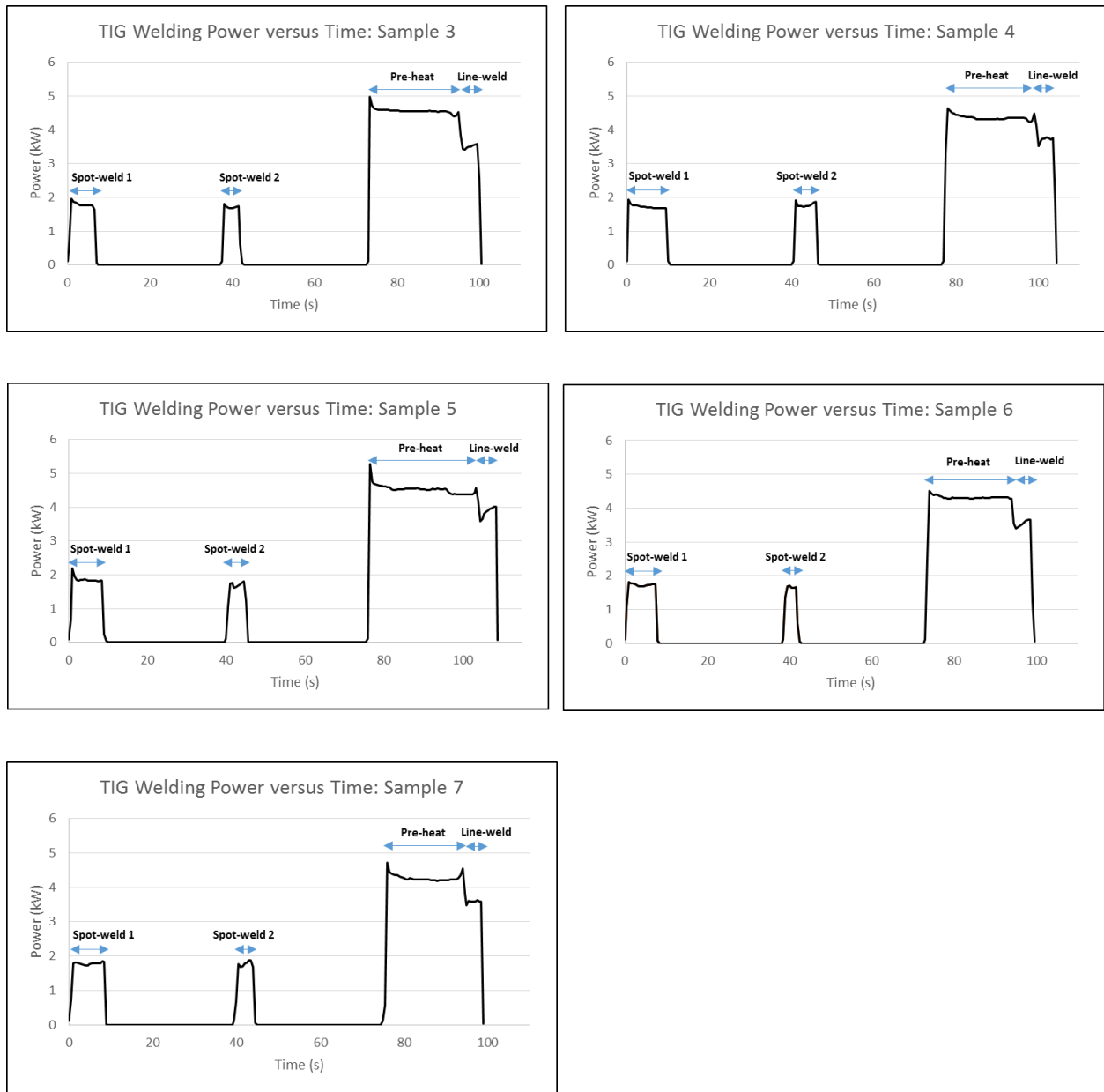
Figure 3.1: TIG welding power vs. time results for samples 1-7

It is interesting to compare the measured value of energy used during the welding process to the theoretical minimum amount of energy that would be required to complete this welded joint. In order to calculate this theoretical minimum one must first know the mass of aluminum that changed phase during the welding process. In any welding process, the microstructure of the weldment undergoes considerable changes because of the heating and cooling cycle of the weld zone (Gunaraj, 2002). The area where this microstructure changes occur is commonly referred to

43

as the heat-affected zone (HAZ). The microstructure changes are apparent when observing magnified cross-sections of the welded T-joint. From magnified cross-sections, one is able to make precise estimations of the HAZ area and ultimately calculate the mass of aluminum that experienced a phase change during the welding process. Once that mass is known, the theoretical minimum amount of energy required to complete the weld is able to be calculated. Cross-sections were made from two of the seven TIG welding samples so that the area of the HAZ could be measured. Once the HAZ was known, this value is multiplied by the length of the weld, 50mm, to find the volume of aluminum changed phases during the welding process. An assumption was adopted that the cross-section of the fillet had a two dimensional configuration. This assumption may not be satisfied for all cases, but the deviations do not impact the order of magnitude of the result. The mass of aluminum which experienced phase change during the process was calculated by multiplying the phase change volume by the density of aluminum under the assumption that the density change was negligible. Finally, the theoretical minimum amount of energy required to complete the TIG weld was calculated using Equation 1.7 with details shown in Appendix I.

Ultimately, the theoretical minimum amount of energy required to complete the TIG welded joint of the aluminum sample was estimated to be 2.0 kJ. This theoretical minimum represents the limit by which the reduction of energy resources is constrained. There is a substantial difference on the order of $O(10^2$ kJ) between the measured and theoretical minimum amount of energy required to complete the joint. Thus, it is apparent that there is sizable room for improvement with regards to the reduction in energy consumption of the arc welding process. Considering this sizable gap, it is reasonable to suggest that it is unlikely to approach this theoretical minimum through incremental improvements to the existing welding technology. In contrast, it is logical to suggest that only new revolutionary technology will be able to converge

on this theoretical minimum of required energy resources. Nonetheless, knowing the theoretical minimum by which the energy resources are constrained, no matter how advanced the technology, is of paramount importance. This theoretical minimum gives engineers and analysts a constraint with respect to reduction of energy consumption with the hope that future technologies will converge on this minimum value.

3.1.2 Process energy balance

The next of the primary objectives of this study was to map the energy and exergy interactions throughout the TIG welding manufacturing process. This mapping is usually performed by constructing the so-called Sankey (energy) and Grassmann (exergy) diagrams (Bakshi et al, 2011). The Sankey diagram includes heat and work interactions as well as enthalpy contributions. Constructing a Sankey diagram for any manufacturing process has several advantages. One benefit of this type of analysis is that the size of each branch is proportional to the magnitude of energy for that particular contribution at a given location of the system, hence intuitively depicting the magnitude of energy interactions along the process/system. This allows an analyst to quickly identify the primary energy users and areas of significant losses so that more attention can be invested in improving these energy intensive areas. For example, if there is significant losses in the conversion of AC electricity to the DC electricity used for welding, then one may consider investing in more efficient transformer in order to decrease these losses. It should be noted that for some energy/exergy interactions, the component of the flow may not be possible to present up to its scale in the context of other flow scales if being for more than one order of magnitude smaller/larger than the other. Even in these cases, the energy flow branches would be presented but with out of scale flows marked. The Sankey diagram in Figure 3.2 represents the overall energy flow for the specific TIG welding process studied in this thesis. The control volumes

45

(C.V. 1-3) are the same as indicated in Figure 2.1(b) and have previously been explained. The magnitudes of each branch are presented first in Figure 3.2 and more details regarding the determination of the magnitudes are presented in subsequent sections 3.1.2.1-3.1.2.6.
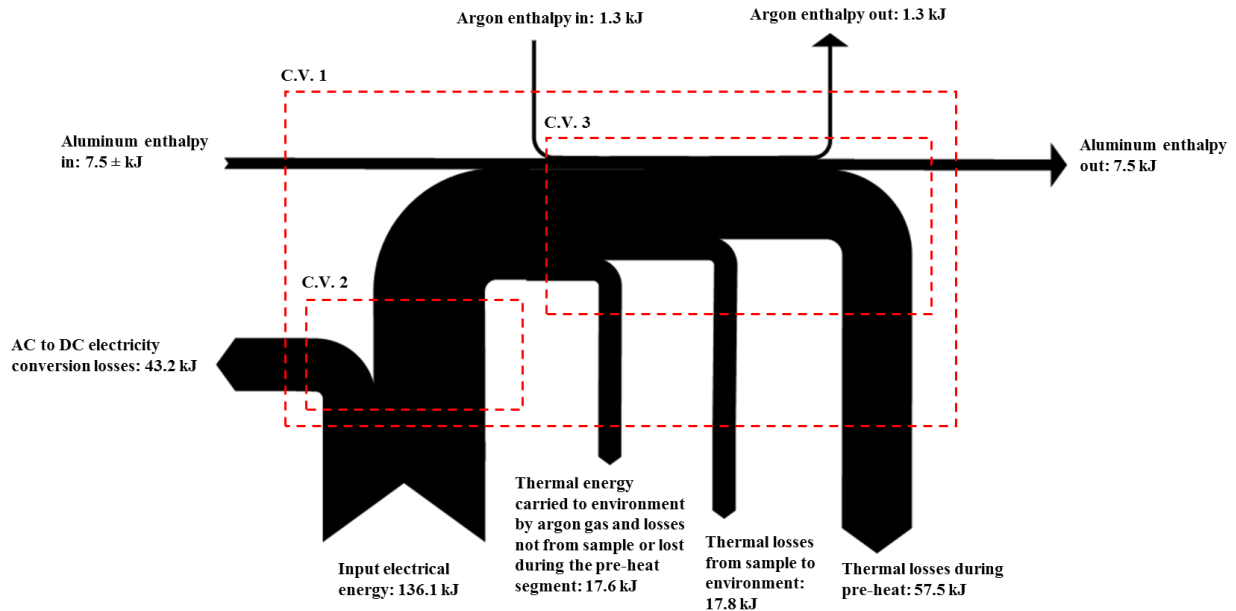
Figure 3.2: Overall TIG welding Sankey diagram

For this particular TIG welding process it is also relevant to observe the energy interactions during each step i.e. spot-weld 1, spot-weld 2, pre-heat, and line-weld segments. The following Figure 3.3 divides the overall Sankey diagram of Figure 3.2 into these four individual segments. It can be seen from this figure that the majority of the input electricity is utilized during the pre-heat segment of the welding process. It may be surprising that the welding segment has significantly smaller input energy than the pre-heating segment, however, this is a direct result of the time duration of these two segments. Observing the area under the curve for the power vs. time plots in Figure 3.1 clearly illustrates that input energy for the pre-heating segment is much larger than that for the actual welding segment.

46

It is important to note that the material stream outputs in the Sankey diagram presented in Figure 3.2 are considered at the state in equilibrium with the environment. Hence, the thermal energy carried by these streams out of the process is accounted for within the corresponding thermal losses branches of the diagram. All energy flows (in kJ) presented in Figure 3.2 are determined for the time duration of the considered process. Note also that no chemical exergy of the material streams is included.

Spot-weld 1

Argon enthalpy in: 0.2 kJ

Argon enthalpy out: 0.2 kJ

Aluminum enthalpy: 10.3 kJ

C.V. 1

C.V. 3

Aluminum enthalpy in: 7.5 kJ

AC to DC conversion losses: 3.9 kJ

C.V. 2

Thermal energy carried to environment by argon gas and thermal losses not from sample: 4.1 kJ

Thermal losses from sample: 3.7 kJ

Input electrical energy: 14.5 kJ

Spot-weld 2

Argon enthalpy in: 0.2 kJ

Argon enthalpy out: 0.2 kJ

Aluminum enthalpy: 8.4 kJ

C.V. 1

C.V. 3

AC to DC conversion losses: 1.3 kJ

C.V. 2

Thermal energy carried to environment by argon gas and thermal losses not from sample: 3.0 kJ

Thermal losses from sample: 4.6 kJ

Input electrical energy: 7.0 kJ

Pre-heat

Argon enthalpy in: 0.6 kJ

Argon enthalpy out: 0.6 kJ

Aluminum enthalpy: 13.8 kJ

C.V. 1

C.V. 3

C.V. 2

AC to DC conversion losses: 36.4 kJ

AC to DC conversion losses: 1.6 kJ

Thermal losses from pre-heat: 57.5 kJ

Input electrical energy: 99.3 kJ

Line-weld

Argon enthalpy in: 0.3 kJ

Argon enthalpy out: 0.3 kJ

C.V. 1

C.V. 3

C.V. 2

Aluminum enthalpy out: 7.5 kJ

Thermal energy carried to environment by argon gas and thermal losses not from sample: 10.6 kJ

Thermal losses from sample: 9.5 kJ

Input electrical energy: 15.3 kJ

Figure 3.3: TIG welding energy flow diagram divided into four segments; spot-weld1, spot-weld 2, pre-heat, and line-weld

48

It was described in section 3.1.1 how the magnitude of the input electrical energy of 136.1 ± 16.5 kJ was calculated. The following sub-sections 3.1.2.1-3.1.2.6 explain how each of the other magnitudes for the branches in Figure 3.2 were found.

3.1.2.1 AC to DC electricity conversion losses

During the welding process, AC electricity from a 480 V, 3-phase wall connection was input into the arc welding power source. The arc welding power source was a transformer which converted high voltage, low current input electricity to low voltage, high current DC welding electricity. It is apparent that the transformer experienced losses in the core and windings during this conversion (Heathcote, 2007, pp. 5-13). In order to quantify these losses, the DC welding electricity was measured for four experimental samples. The Fluke 1735 power logger was able to log trending data for AC electricity but did not have the capabilities to do the same for DC electricity. Therefore, the DC electricity was measured using the weld current controller to set a constant weld current while simultaneously measuring the voltage drop across arc welding power source using a digital multimeter. It is understood by the analyst that the voltage drop varied slightly with time. However, after speaking with the lead professor for the welding lab it was assured that the DC voltage does not vary significantly with time and taking spot measurements during the welding process would suffice (Zhang, 2013). Thus, the value of welding current set by the weld current controller and the voltage measurements taken across the arc welding power source were used to calculate the DC welding power. Since the DC welding power was assumed to be constant, it was multiplied by the weld time to ultimately yield values of DC welding electrical energy which are displayed in Table 3.2. The assumptions of constant voltage and current were confirmed while taking measurements during the experiments. Both parameters were monitored and observed with no significant variations which corroborated the previous

assumptions. The average TIG welding DC electrical energy delivered was found to be 92.9 ± 2.5 kJ.

Table 3.2: Input DC electrical energy for TIG welding samples

Sample	Energy (kJ)
1	95.2
2	94.4
3	92.6
4	89.6
Average	92.9
Standard Deviation	2.5

An energy balance was performed for C.V. 2 from Figure 3.4 to find the AC to DC conversion losses. This was done by finding the difference between the average input AC electrical energy (136.1 kJ) and the average welding DC electrical energy (92.9 kJ). Ultimately, it was found that the AC to DC electrical energy conversion losses were 43.2 kJ. The user manual for this transformer indicates an efficiency of 73%. We are confident the measured values of transformer losses are accurate considering they yield a transformer efficiency of 68%.

3.1.2.2 Thermal losses from sample

The thermal losses from the sample were calculated using the lumped capacitance method for transient heat transfer. This method calculates the heat transfer of a given system having spatially uniform temperature due to an assumed negligible conductive resistance. This method of analysis is commonly used in situations where a well conducting solid experiences a sudden change in its convective and radiative thermal environment. Consider the welding process where a hot aluminum sample which has just been welded is initially at a uniform temperature T_i. This sample is left to cool in its environment of lower temperature $T_\infty < T_i$. If the cooling is said to begin at time t=0, the temperature of the aluminum sample will decrease for time t>0, until it eventually

50

reaches T_∞. This reduction in temperature is due to convective and radiative heat transfer at the interface where the sample meets the surrounding air. An assumption of constant temperature within the system requires a condition of dominant resistance to convective and radiative heat transfer vs. conduction.

So, the primary assumption at the core of the lumped capacitance method is that the temperature of the solid is spatially uniform at each instant of the transient process. It is known from Fourier's law for conduction that the absence of a temperature gradient implies the existence of infinite thermal conductance. Although such a condition is physically impossible, it can be closely approximated if the resistance to conduction within the solid is small relative to the resistance to heat transfer between the solid and its surrounding environment. The Biot number (Bi) is used to compare the thermal resistance within a solid to the thermal resistance between the surface of that solid and the surroundings. If Bi<0.1, the error associated with using the lumped capacitance is small, and it is reasonable to assume that there is a uniform temperature distribution within the solid at any instant in the transient cooling process (Incropera et al., 2007, pp. 261). Equation 3.2 displays that the Biot number is the ratio of the product of the convective/radiation heat transfer coefficient and characteristic length with the thermal conductivity.

Equation 3.2

$$Bi = \frac{hL}{k}$$

The characteristic length, L, is the ratio of the sample volume over the sample surface area, in this case 9.43×10^{-3} m. The value of 237 W/mK is the thermal conductivity, k, for aluminum (Buch, 2000). The exact value of the effective heat transfer coefficient, h, was not known, however, we do know that for natural convection situations for air this value will be at the most

25 W/mK, or on the order of $O(10^1)$ (Incropera et al., 2007). For this case, a conservative value for the effective heat transfer coefficient, h, was assumed to be 25 W/m^2K. Note that with the known values for characteristic length and thermal conductivity of aluminum described above, it can be shown that a value up to 2,513 W/mK could be used for the effective heat transfer coefficient (which we know is not realistic for this situation) and still yield a Biot number less than 0.1.

Ultimately, the Biot number was calculated to be $9.9x10^{-4}$, a value far less than 0.1. Since the Biot number was less than 0.1, the error associated with using the lumped capacitance method was small. Thus, this method was used to calculate the heat transfer from the sample to the surrounding environment. The transient temperature response was determined by formulating an overall energy balance on the sample. This balance related the rate of heat loss at the surface to the rate of change of the internal energy (Incropera et al., 2007, pp. 257).

Equation 3.3

$$-\dot{Q}_{out} = \rho V c \frac{dT}{dt}$$

Where $\dot{Q}_{out}$ is the heat transfer rate from the sample to the surrounding environment, ρ is the sample mass density (Buch 2000), V is the volume of the sample, c is the specific heat of the sample (NIST standard reference data, 2011), and $\frac{dT}{dt}$ is the time rate change of the spatially independent temperature of the sample. The following plots in Figure 3.4 display the temperature profiles of four different samples with respect to time. The temperature data used to create these plots are attached in Appendix D. It can be seen that the sample temperature exhibits an asymptotic trend towards the ambient temperature of the surroundings as time increases as postulated by the

lumped capacitance method. Also, an infrared thermal image of the sample during the welding process can be viewed in Appendix M.
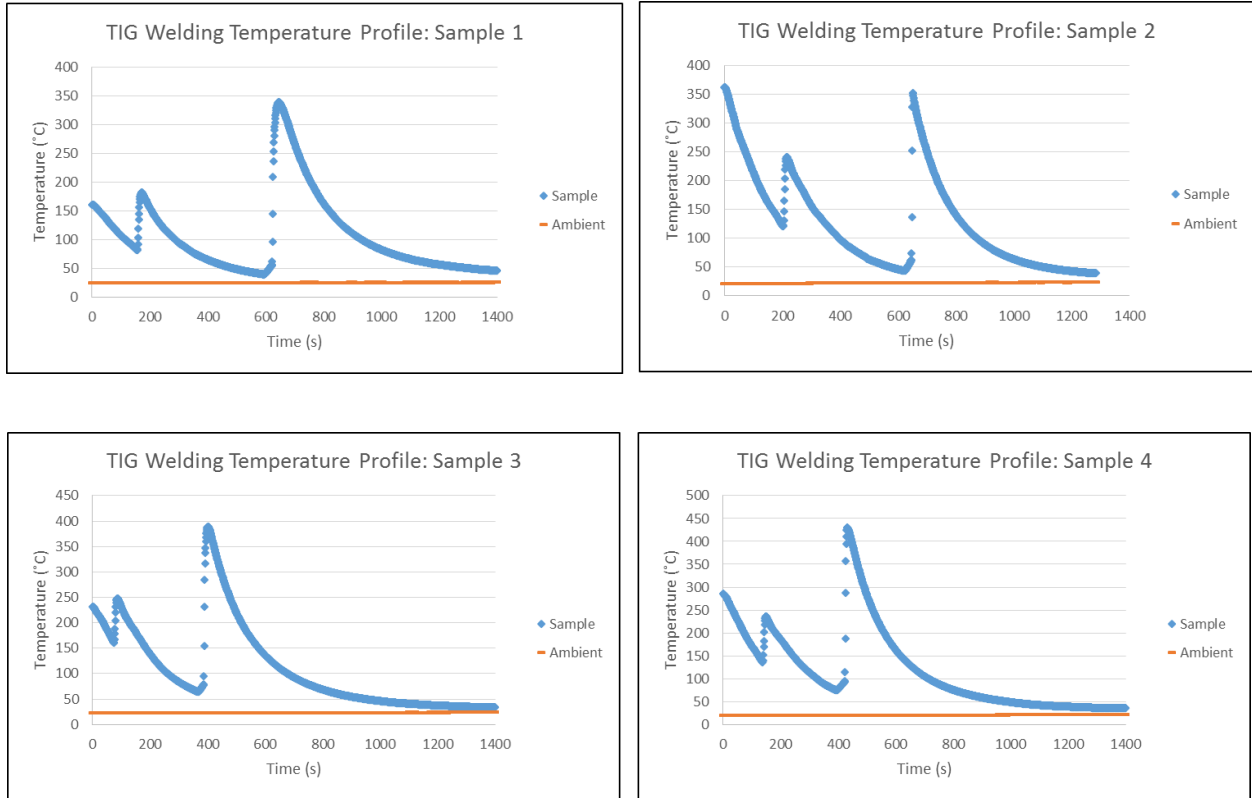
Figure 3.4: TIG welding temperature vs. time data for samples 1-4

Ultimately, Equation 3.3 was used to calculate the thermal energy losses from the sample to the surrounding environment. The volume of the sample was measured using digital calipers and the values of density and specific heat were taken from standard reference tables (NIST standard reference data, 2011). Since the $\frac{dT}{dt}$ term of the equation is not constant, it was calculated at one second intervals using the trending sample temperature data displayed in Figure 3.4. Thus, Equation 3.3 was used to calculate the heat losses at one second intervals, and these values for each sample were ultimately summed to yield the total heat loss from the sample to the surrounding environment. The uncertainty associated with measuring these values was 0.1 kJ and the method for calculating it is presented in Appendix D. The heat loss values for samples 1-4 are displayed

in Table 3.3. It is apparent that the average heat loss from the sample to the environment was 17.8 $\pm$ 2.9 kJ. This value was confirmed using two alternative methods for estimating the heat loss from the sample to the environment discussed in Appendix K.

Table 3.3: Thermal energy losses from TIG welding sample to surrounding environment

Sample	Energy (kJ)
1	14.3
2	20.6
3	16.8
4	19.6
Average	**17.8**
Standard Deviation	**2.9**

3.1.2.3 Thermal losses during pre-heat segment of welding process

The thermal losses which occurred during the pre-heat segment of the welding process were found by performing an energy balance for C.V. 1 of just the *pre-heat* segment of the Sankey diagram displayed in Figure 3.3. It was ultimately found that the thermal losses from pre-heat of the welding process were 57.5 kJ.

3.1.2.4 Aluminum sample enthalpy

The aluminum sample enters the system at an ambient room temperature of 298 K. Although the aluminum sample temperature and corresponding enthalpy was increased at times during the welding process, it eventually exited at ambient room temperature after cooling. Additionally, the sample did not enter at any significant velocity nor did it change height during the welding process. Ultimately, the enthalpy of the aluminum sample was calculated using the following equation with the actual calculations shown in Appendix J.

Equation 3.4

$$H = m\left(cT + \frac{v^2}{2} + gz\right)$$

Where,

H	=	Enthalpy [kJ]
m	=	Mass [kg]
c	=	Specific heat [kJ/kg K]
T	=	Temperature [K]
v	=	Velocity [m/s]
g	=	Acceleration due to gravity [m/s^2]
z	=	Height [m]

As seen from the calculations in Appendix J, the enthalpy of the aluminum sample was 7.5 kJ both into and out of the system boundary.

3.1.2.5 Argon enthalpy

The argon gas in the TIG welding experiments surrounded the arc to protect the weld area from oxidation and to force the molten aluminum into the joint. Equation 3.4 was again used to calculate the enthalpy of the argon gas into and out of the system and the details of these calculations can be found in Appendix J. The enthalpy of argon gas was 1.3 kJ both into and out of the TIG welding system boundary. Note that enthalpy term of the argon out of the system does not include the thermal energy carried away from the system by the argon gas and dissipated into the environment. This value was combined with the final term described next.

3.1.2.6 Thermal energy carried to environment by argon gas and losses not from sample or lost during the pre-heat segment

This branch of the Sankey diagram shown in Figure 3.2 was used to account for the thermal energy carried to the environment by the argon gas, as well as the other losses not accounted for during the pre-heat segment of the process or from the sample to the environment. The magnitude

of this branch was calculated by performing an energy balance for C.V. 1 from Figure 3.2. Each of the values in Figure 3.2 except for this one had previously been calculated or measured, thus, leaving this term as the only unknown in the equation. The energy balance yielded a value of 17.6 kJ for the magnitude of this branch.

3.1.3. Process exergy Grassmann diagram (qualitative)

In addition to mapping the energy balance for the TIG welding process, another task was to qualitatively map the exergy of the system to have a high level understanding of the exergy destruction taking place. Recalling the background discussion of exergy from chapter 1, it is important to understand that exergy is used to describe the magnitude of an energy interaction. Exergy takes into account the quality of energy in addition to the quantity and in essence can be thought of as the available energy. A strictly qualitative exergy diagram for the TIG welding process explored in this study can be seen in Figure 3.5. Also, recall that there are two components of exergy, physical and chemical as indicated in Equation 1.5. This diagram intentionally does not include the chemical exergy contribution of the aluminum sample and the argon gas because the magnitudes of these branches would be the same entering and leaving the system assuming that the outlet mass flow rates dissipate the excess thermal energy into the environment at the system boundary. The magnitudes of the branches were not measured in this thesis. Rather, the primary objective of this diagram is to illustrate (in a qualitative sense) the segments of the process where exergy is lost and to emphasize that the entire input electrical exergy is eventually lost.
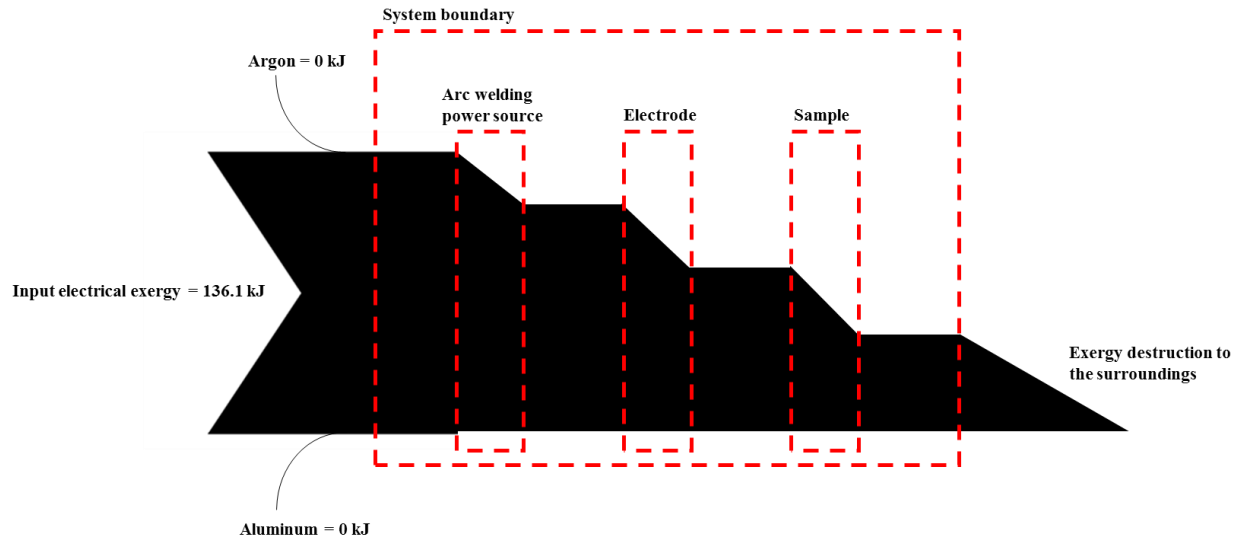
Figure 3.5: TIG welding exergy Grassmann diagram (qualitative)

As seen in Figure 3.5, the large branch of the input electrical exergy enters the system boundary and goes through the arc welding power source sub-system. Here, exergy is lost due to the inherent imperfections of transformer. The remaining electrical exergy is converted to thermal exergy in the electrode where the exergy is reduced by the Carnot factor $(1 - T_0/T_k)$ because heat and work interactions are not equivalent in exergy balance. This thermal exergy is input to the sample sub-system where losses occur as the sample temperature moves towards thermal equilibrium with its surroundings. Lastly, the magnitude of the remaining exergy is diminished to zero as thermal equilibrium with the surrounding environment is approached. As can be concluded, this manufacturing process can be characterized with total consumption of input exergy in order to perform the desired task.

3.2 CAB results

3.2.1 Magnitude of input electrical energy

Another of the primary objectives of this thesis was to compare the magnitude of input electrical energy needed to make an aluminum T-joint for both TIG welding and controlled

57

atmospheric brazing. The following results discuss the magnitude of electrical energy measured for the CAB experiments. The measured values of electrical energy for the seven successful CAB samples are displayed in Table 3.4. The uncertainty associated with these measurements was 11 kJ and the method for calculating this uncertainty is presented in Appendix C. It can be seen from this table that the average energy consumption for the seven samples was 6,830 ± 77 kJ. Taking into account (i) the mass of the assembly, the specific energy used to make the part is 244,700 kJ/kg (ii) the mass of just the welded fillet, the specific energy used to make the welded fillet is 19,290,000 kJ/kg.

Table 3.4: Energy consumption for CAB experimental samples

Sample	Energy Consumption (kJ)
1	6,830
2	6,780
3	6,740
4	6,820
5	6,790
6	6,980
7	6,850
Average	**6,830**
Standard Deviation	**77**

All of the values of energy displayed in Table 3.4 were calculated by integrating the data for power with respect to time as was done previously with the power data from the welding experiments. This trending power data was collected by the power logger at one second intervals during each experiment and integrated numerically using Microsoft Excel. The following figures display the power versus time data collected for each of the seven CAB samples. The area under the curve represents the input energy. In Appendix C, a selection of numerical data sets collected

and used for constructing Figure 3.6 is given. The complete data set is available in digital form in the folder labeled, "Gasser Thesis Data" stored in the Brazing Laboratory (Gasser, 2013).
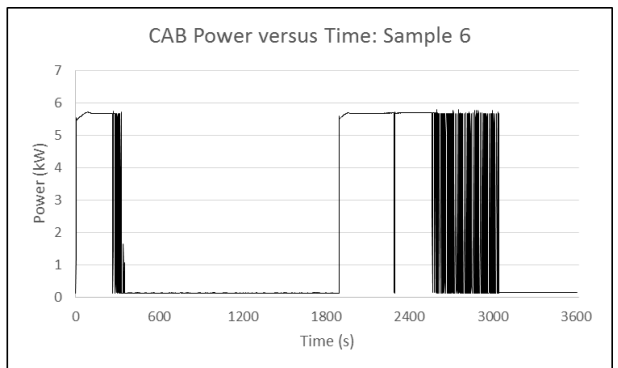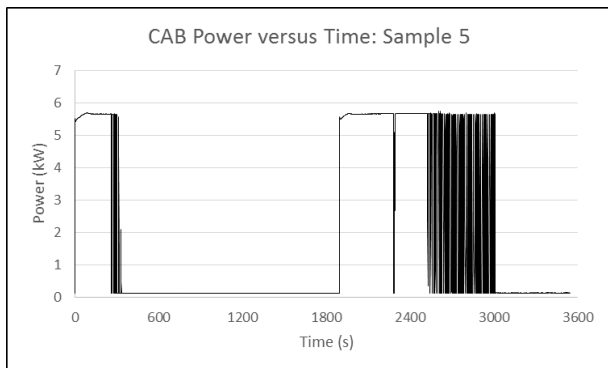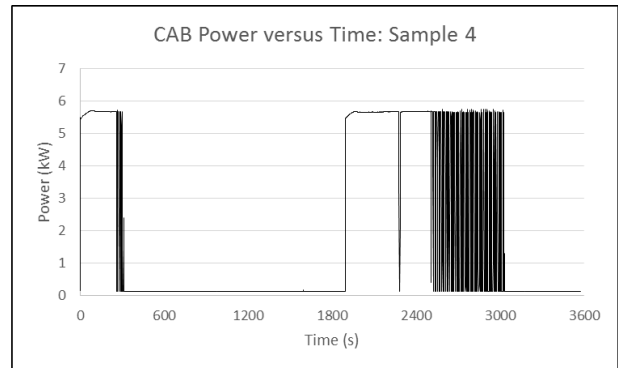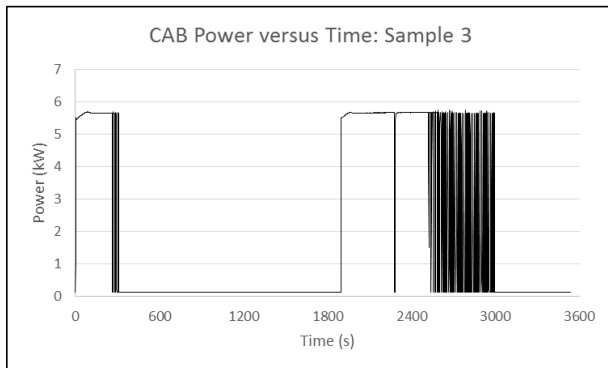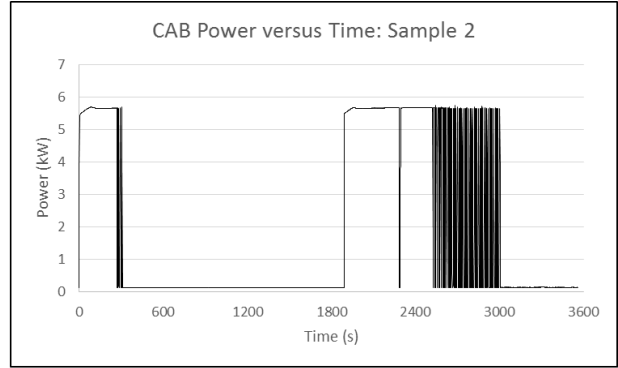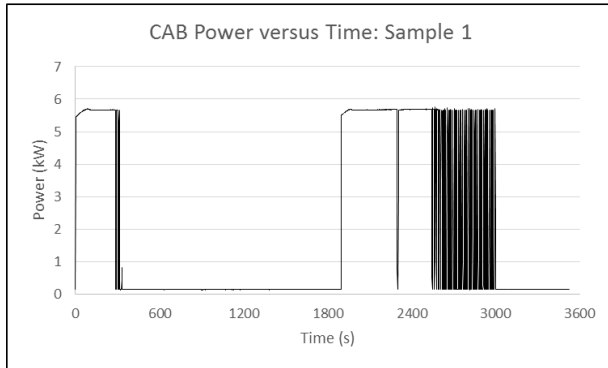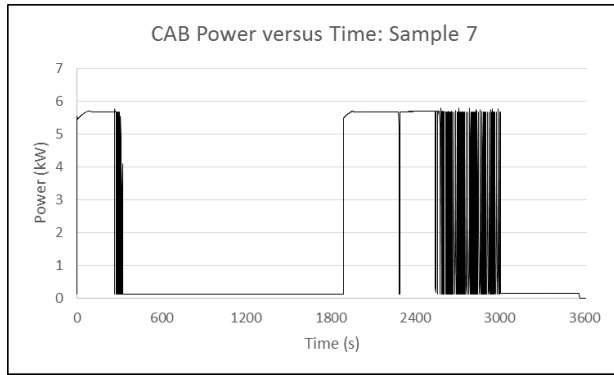
Figure 3.6: CAB power vs. time data for samples 1-7

Again, the magnitude of electrical energy required to create a T-joint for the aluminum sample using the CAB furnace was $6{,}830 \pm 77$ kJ. Similarly to what was done with the TIG welding metal joining process, it is interesting to compare the measured value with the theoretical minimum amount of energy that would be required to complete this joint. As for the TIG welding process, in order to calculate this theoretical minimum one must first know the mass of aluminum that changed phase during the brazing process. First, the volume of the brazed aluminum was identified by measuring the brazed cross-sectional area from magnified cross-sections of the CAB samples and multiplying this area by the sample length, 50 mm. This volume was then multiplied by the density of the brazed aluminum to yield the mass of brazed aluminum. Once that mass was known, the theoretical minimum amount of energy required to complete the weld was able to be calculated. Magnified cross-sections for two of the seven CAB samples are displayed in the figures below. The area of the brazed aluminum was identified to be the area within the red lines. As was done for the TIG welding samples in section 3.1.1, the theoretical minimum amount of energy required to complete the brazed aluminum joint was calculated using Equation 1.7 and these calculations are shown in Appendix I.
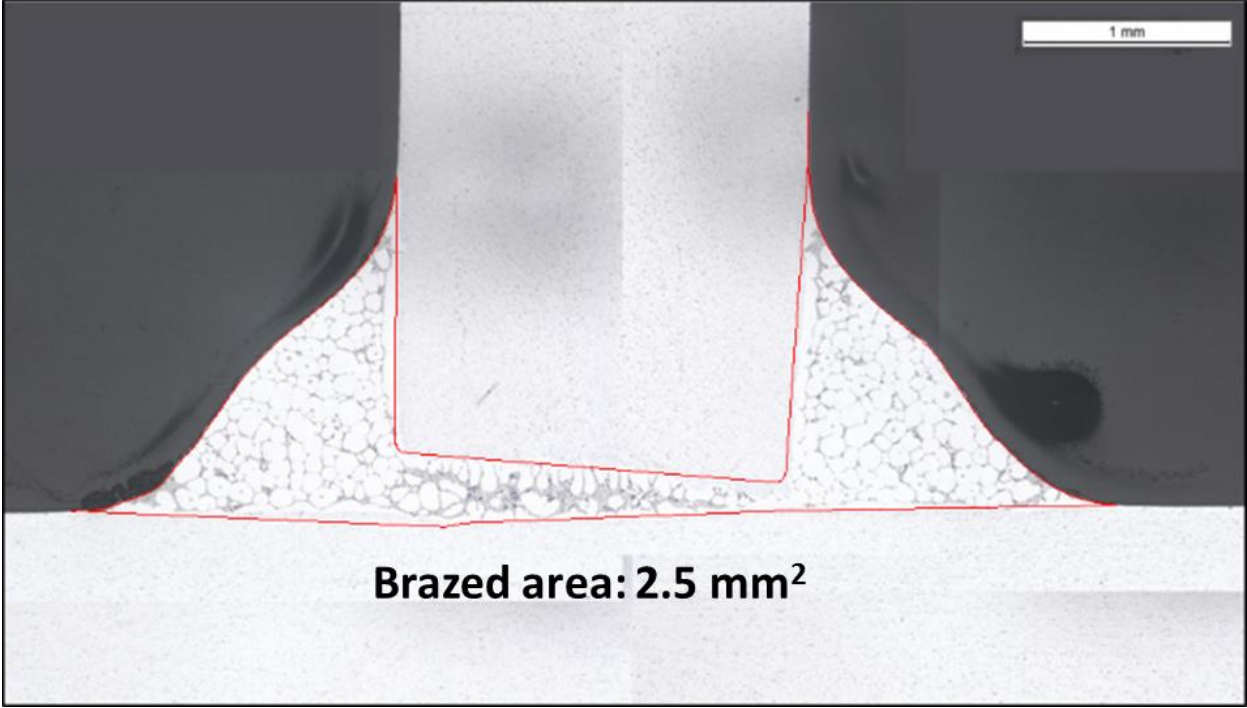
(a)
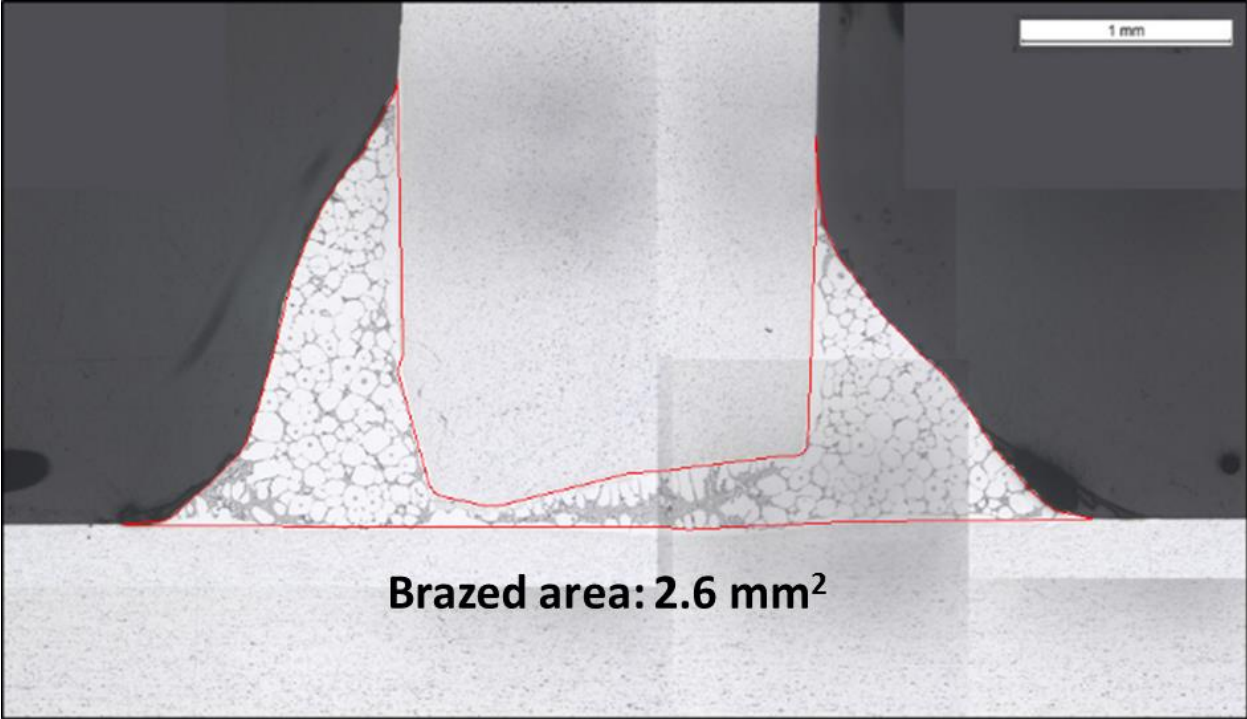
(b)

Figure 3.7 (a, b): CAB magnified cross-sections for two samples

Ultimately, the theoretical minimum amount of energy required to complete the TIG welded joint of the aluminum sample was 0.34 kJ. Compare this value to the measured value of input electricity to the CAB furnace of 6,830 ± 77 kJ and there is a difference on the order of $O(10^4$ kJ). This represents an astounding gap between the current energy resource consumption and the theoretical minimum required to complete the brazed aluminum sample. Thus, it is obvious that there is significant opportunity for reduction in energy consumption for brazing technology, at least in principle.

3.3 Discussion

The final section of this chapter is meant to summarize and discuss the findings of this study. The experiments performed in this thesis demonstrate that the energy required to form the filet of the aluminum T-joint using (1) a TIG welding process and (2) a controlled atmospheric brazing process were 136.1 ± 16.5 kJ and 6,830 ± 77 kJ respectively. From these results, it is apparent that the TIG welding process consumes over one order of magnitude less energy to complete the metal joining task. This difference can be attributed to two primary differences in the two metal joining technologies.

1. The duration it took to complete the aluminum joint for the two processes differed by more than an order of magnitude. The welding process lasted approximately $O(10^2$ seconds) while the brazing process took $O(10^3$ seconds). The longer time duration results in larger energy consumption values for the brazing process keeping the implemented energy rate.

2. The welding process utilized localized heating of the sample. In contrast, the brazing process inherently consists of heating the furnace and all of its components as well as thermal losses from each of these components to the surrounding environment.

Thus, the more localized heating technique and shorter time of the welding process made it possible to join the aluminum sample while consuming one order of magnitude less energy than with the brazing process. Nonetheless, there are positive tradeoffs to relatively high energy consumption values of brazing compared to welding. For example, brazing is able to join metals of small thickness (on the order of microns) where welding cannot. Additionally, it was observed during the experiments that the brazed samples had a better appearance than that of the welded samples as seen in Figure 3.8. Moreover, it must be noted that the mechanical integrity of the joints made by using different technologies did indeed differ. Thus, although the welding process consumed significantly less energy, there were other consequences of the two metal joining technologies unrelated to energy consumption such as joint integrity, appearance, and process rate which must be considered. Note, as indicated previously, the implemented welding process was not optimized for the best joint quality/integrity.

Welded sample   **Brazed sample**
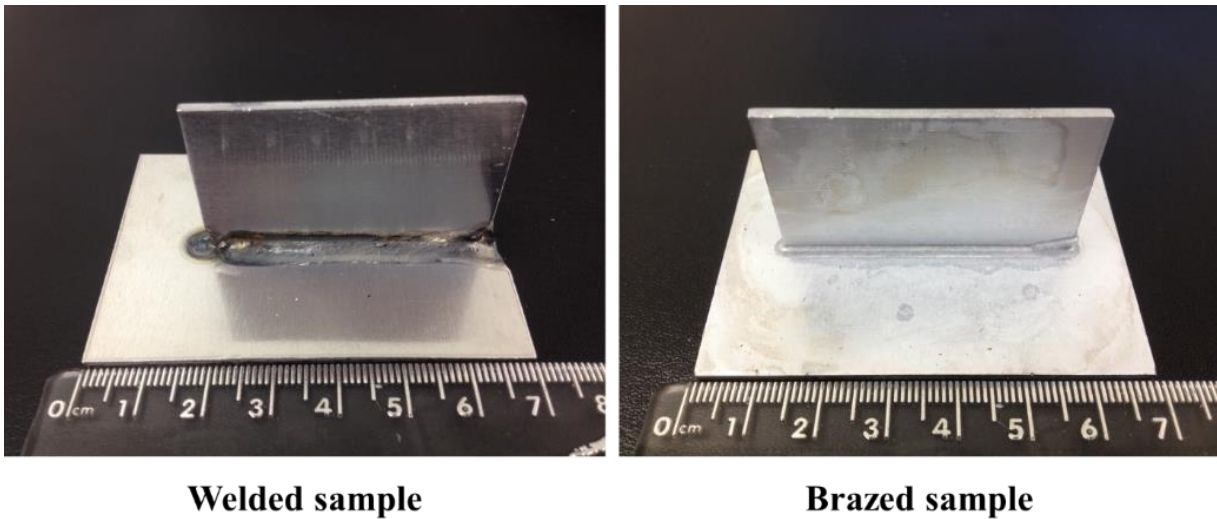
Figure 3.8: Finished samples for welding and brazing process

In addition to understanding the values of input energy resources, it is interesting to compare these values to the theoretical minimum amount of energy needed to complete the task using the two individual technologies. We are interested in exploring the maximum margins of

reduction in resource utilization for the task of metal joining, irrespective of the technology used to accomplish it. These margins are essential because they are a metric that offer an assessment of the performance of a technology in terms of its resources utilization. The metric, $\Delta E_{resource}$, presented in Equation 1.8 was previously introduced as the difference between the measured energy consumption of a state-of-the-art technology and the theoretical minimum amount of energy required to complete the given task. Table 3.5 below displays this metric for the two metal joining technologies studied in this thesis.

Table 3.5: Order of magnitude energy resource reduction

Metal Joining Technology	$O(\Delta E_{resource} \text{ kJ})$
TIG Welding	$O(10^2 \text{ kJ})$
Brazing	$O(10^4 \text{ kJ})$

The following describes how the values found in Table 3.5 were obtained. For the welded samples, we observed the magnified cross-sections to quantify the area of aluminum which changed phases during the process. From this area we were able to calculate the mass of aluminum which changed phases and eventually find a precise estimate for the theoretical minimum amount of energy needed to complete the welded joint. A similar process was used for the brazed samples as described in section 3.2.1. Note that the mass of aluminum which changed phases during the welding process was on the order $O(10^1 \text{ kg})$ more than during the brazing process which contributes to the discrepancy in theoretical minimum energy values given below. Ultimately for the welding process, it was found that the theoretical minimum amount of energy required to complete the welded joint was 2.0 kJ. Compared to the input energy of 136.1 ± 16.5 kJ for the welding process, there is a two orders of magnitude difference. Likewise for the brazing process, it was found that the theoretical minimum amount of energy required to complete the brazed joint

was 0.34 kJ. Compared to the input energy of $6,830 \pm 77$ kJ, there is a difference of four orders of magnitude. Thus, it is obvious that a sizable margin of improvement in resource utilization exists for the two metal joining processes. The margins of two and four orders of magnitude for TIG welding and controlled atmosphere brazing respectively are metrics which appropriately evaluate the performance of their respective technology in terms of resource utilization.

The measured results for electrical energy requirements of the TIG welding and CAB processes were also added to the previously discussed "hockey-stick" diagram seen in Figure 3.9. Again, this diagram plots specific energy requirements with respect to process rate on a log-log graph for a wide range of manufacturing processes. In this particular version of the plot, the data points shown in green represent the points added from information found in the literature review discussed in chapter 1. These processes include MIG welding, TIG welding, AC spot resistance welding, DC spot resistance welding, and laser welding. Additionally, the values from the TIG welding and CAB experiments conducted in this study were added and can be seen in red. It is interesting from this plot that the TIG welding results from this study closely follow the results from the TIG, MIG, and laser welding processes from the literature review. This correspondence supports the accuracy of the results from these TIG welding experiments. In contrast, the CAB brazing data point from these experiments does not closely match the brazing point labeled "Brazing [37, 38]" which has a significantly higher process rate and lower specific energy requirement. It is postulated that the discrepancy stems from the fact that the "Brazing [37, 38]" data point is from a large scale industrial process. In contrast, the CAB experiments in this study focused on a small scale furnace used primarily for academic research. Nonetheless, both the TIG welding and controlled atmosphere brazing points formulated from the data collected from this study are positioned fittingly within the upper and lower bounds of the grouped data points.
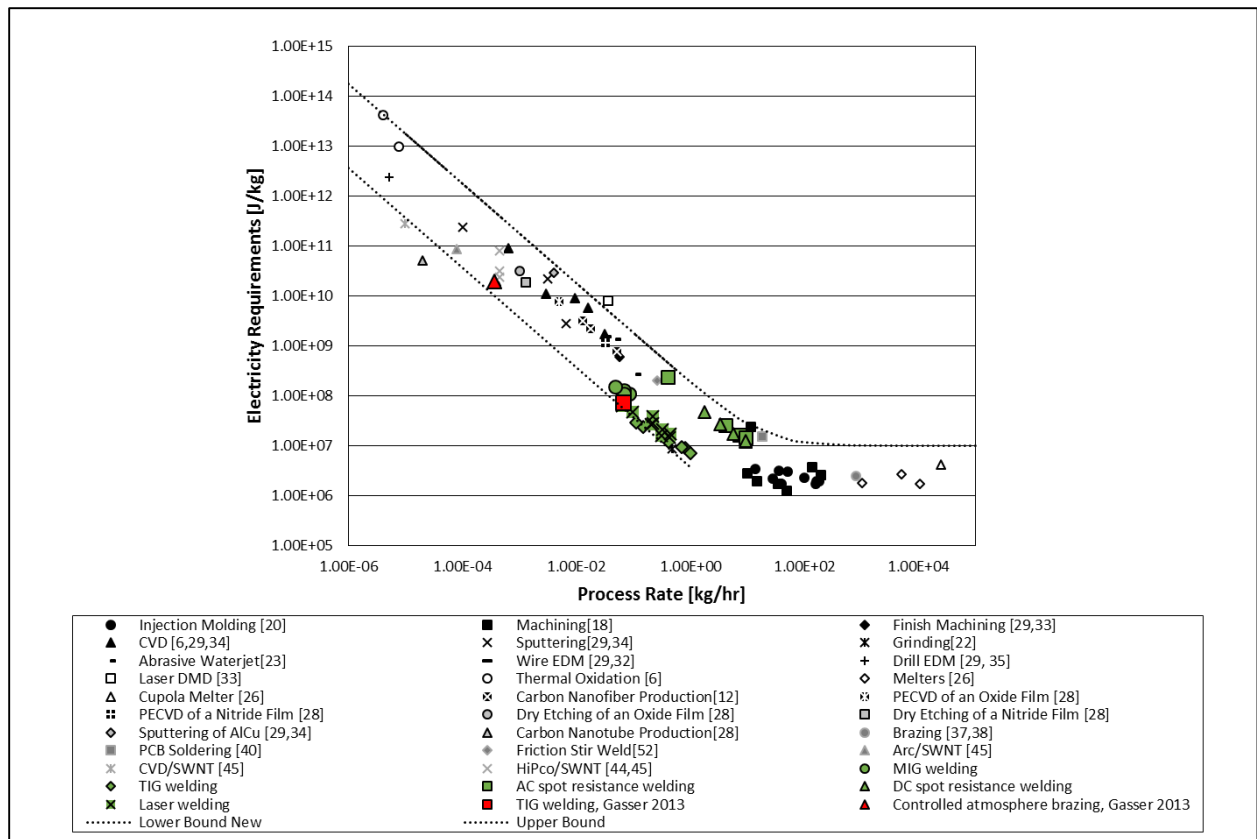
Figure 3.9: Specific electrical energy vs. process rate with added points from literature review (green) and from original TIG welding and CAB experiments (red), adapted from Bakshi et al., 2011, pp. 178

Chapter 4:   CONCLUSIONS AND FUTURE STUDY

4.1 Conclusions summary

It is apparent that energy resource reduction in manufacturing is a necessary strategy to be applied to more sustainable processes in the future (for the purpose of this study we consider here the sustainability in its narrow sense without considering further social and environmental aspects of it). This involves decreasing energy consumption and using the required energy for any manufacturing task more efficiently. For any process, there can be calculated a theoretical minimum amount of energy required to complete the desired task regardless of the technology used to accomplish is. Presently, the considered manufacturing technologies consume several orders of magnitude more energy than the theoretical minimum. It is unlikely to bridge this sizable gap through incremental improvements to existing technologies. Rather it is necessary to develop new, revolutionary means of manufacturing which attempt to reduce energy resource utilization to the theoretical minimum.

Specifically, this thesis evaluated the input energy required to complete an aluminum T-joint using two state-of-the-art metal joining processes (TIG welding and controlled atmosphere brazing). The TIG welding technology required an average of 136.1 ± 16.5 kJ to complete the T-joint as compared to the theoretical minimum amount of energy calculated to complete the joint of 2.0 kJ. The difference between the two values is a sizable two orders of magnitude. The CAB furnace consumed an average of $6,830 \pm 77$ kJ input energy to join the aluminum sample. The theoretical minimum amount of energy required to complete the brazed joint was calculated to be 0.34 kJ. Thus, there was an astonishing four orders of magnitude difference between the energy consumed and the theoretical minimum amount of energy needed to braze the sample. A detailed study of both processes indicates a substantial gap between current and theoretical minimum of

energy use for both the TIG welding and CAB experiments which suggests significant opportunities for energy utilization reduction. Considering the margin is several orders of magnitude for both processes, it is not likely to merge this gap with small, incremental improvements to the existing technologies.

4.2 Future study

The material presented in this thesis analyzes the energy resource utilization for two state-of-the-art metal joining processes. Further additions to this thesis work would be to explore the energy consumption of more metal joining technologies. Although, there were energy consumption data values for other welding technologies presented in the literature review, this data was accumulated from secondary sources. It would be beneficial to perform firsthand experiments to measure the energy consumption of these technologies.

Additionally, the CAB furnace used in the brazing experiments of this study is primarily meant for research purposes and not for industrial mass production of brazed material. In an industrial setting, a CAB furnace will braze multiple samples at once and often in a continuous not a batch process, and is thus expected to consume less energy per sample than the furnace used in this study. Consequently, it would be beneficial to extensively study the energy consumption of CAB furnaces used in a full scale industrial applications and ultimately, compare the energy usage with the values found in this study.

Lastly, this thesis produced an exergy Grassman diagram for the TIG welding process in a limited qualitative sense. As previously indicated, this type of detailed exergy analysis has been completed for the controlled atmosphere brazing process (Nehete, 2013), and it would be beneficial to compare these results with the welding technology. Further work related to this thesis will measure the necessary parameters to produce an extensive and quantitative analysis of the

exergy destruction throughout this process. A more in depth exergy diagram will aide in the understanding of internal exergy destruction within the components of the system as well as external losses to the surrounding environment.

Appendix A: CHEMICAL COMPOSITIONS AND NITROGEN GAS PROPERTIES

CHEMICAL COMPOSITIONS

Composition in weight percent maximum unless shown as a range.

AA 3003, (The Aluminum Association, 2009)

Si	Fe	Cu	Mn	Zn	Al
0.6	0.7	0.05-0.20	1.0-1.5	0.10	Rem.

AA 4043, (The Aluminum Association, 2009)

Si	Fe	Cu	Mn	Mg	Zn	Ti	Al
4.5-6.0	0.80	0.30	0.05	0.05	0.10	0.20	Rem.

Aluminum potassium fluoride (NOCOLOK® Flux, 2003)

K	Al	F
19	53.5	27.5

NITROGEN GAS PROPERTIES (Purity Plus, 2013)

Grade	Impurity	Specification
PurityPlus Extra Dry (Industrial Grade)	Moisture Oxygen	< 8 ppm 19.5% to 23.5%
PurityPlus 5.0 (Ultra High Purity)	Oxygen Moisture Total Hydrocarbons	< 2 ppm < 3 ppm < 0.5 ppm

Appendix B: EXPERIMENTAL EQUIPMENT AND SOFTWARE

The following gives detailed descriptions of the equipment and software used in the experiments and analysis of this thesis.

EQUIPMENT

- Autoline® PM 200 Arc Welding Power Source: This arc welding power source was used to convert the three phase AC electricity input to DC electricity needed for arc welding. This power source is designed for TIG welding processes with the following specifications (Autoline® PM 200 Arc Welding Power Source Technical Manual).

  Welding Amperage Range: 1-200 A
  Max. Open-Circuit Voltage: 80 V
  Average power consumption: 4 kW

- Fluke 1735 Power Logger: This logger measures and records voltage, current, and power data for AC powered equipment. The power logger has both voltage clamps and current probes which attach to all three legs of the connection. For the TIG welding experiments the logger measured the input power from of a 480V, 3-phase delta connection. For the CAB experiments the logger measured the input power from 240V, single phase connection (Fluke Corporation, 2006).

  Voltage range: 100-830 V AC

  > Intrinsic error: ±(0.2% of measured value + (5 x resolution))

  > Operating error: ±(0.5% of measured value + (10 x resolution))

  > Resolution: 0.1 V

  Current range: 0-3000 A

  > Intrinsic error: ±(0.5% of measured value + (10 x resolution))

Operating error: ±(1% of measured value + (10 x resolution))

Flexi set measuring error: ±(2% of measured value + (10 x resolution))

Position influence: ±(3% of measured value + (10 x resolution))

Power errors are calculated by adding the errors of voltage and current.

- Super OMEGACLAD® Thermocouple Probes: These type K thermocouples are used for high temperature measurement. The positive side of the thermocouple is nickel-chromium wire while the negative side is made of nickel-aluminum wire. They have a maximum range of -200 to 1250 C. The standard error is 2.2 C or 0.75% (whichever is greater) above 0 C and 2.2 C or 2% whichever is greater for temperatures below 0 C (Omega, 2013).

- Fluke Model 115 true-rms multimeter: This multimeter was used to measure the DC voltage of the TIG arc welder during the welding process. The measured range of this application was 60 V. In this range, the multimeter has a resolution of 0.01 V with an accuracy of ± 0.5% [% of reading] + 2 [resolution] (Fluke Corporation, 2006).

- National Instruments NI cDAQ-9172: This is an eight-slot USB chassis designed for use with C Series I/O modules. It is capable of measuring a broad range of analog and digital I/O signals and sensors using a Hi-Speed USB 2.0 interface. This hardware was used in tandem with the NI 9211 to record temperature data with time for the welded aluminum sample (National Instruments Corporation, 2008).

Analog Input

Maximum sample rate: 3.2 MS/s

Timing accuracy: 50 ppm of sample rate

Timing resolution: 50 ns

Analog Output

Maximum update rate: 1.6 MS/s

Timing accuracy: 50 ppm of sample rate

Timing resolution: 50 ns

- National Instruments NI 9211: This thermocouple input module is for use with the NI cDAQ-9172 for high-accuracy temperature measurements (National Instruments Corporation, 2010).

- CA2091 controlled atmosphere brazing furnace: This furnace is a resistively heated, hot-wall tub furnace which was used for the brazing of aluminum 3003 samples. Figure 2.11 displays a block diagram of the furnace and the components used in conjunction with the furnace for the CAB process. The process chamber is fabricated from thick-wall fused quartz and contains an advanced coating which reflects heat back into the hot zone while simultaneously allowing visible light to pass through. The hot zone is comprised of a spirally would electric heater inside concentric quartz tubes and is supported by end caps with ceramic inserts. A flow of the 99.9% N2 gas is input into the hot zone during the rapid quench segment of the process. The ultra-high purity (99.999%) N2 gas tank is used for the other four segments of the process as well as the three hour purging process completed before the experiments and is controlled using a flow meter. The dew point meter and oxygen sensor are used to monitor and collect data for the exiting stream of nitrogen gas. Three Type K thermocouples were used (1) control the heater, (2) measure temperature of the sample. Temperature control of the CAB is accomplished using the program FOCUS (Furnace Optimal Control User-Friendly Software).

- General Eastern 1311DR dew point analyzer: This sensor was used to measure and record the dew point of the furnace chamber. The sensor has an accuracy of ±0.2ºC with a range from -80ºC to +85ºC (General Eastern, 2006). The dew point data for the seven samples from this study can be found in Appendix G.

- Teledyne 316RA oxygen analyzer: This oxygen sensor measures the concentration of oxygen in the brazing furnace chamber. The sensor has an operating range of 0-10,000 ppm with an accuracy of ±5% (Teledyne Analytical Instruments, 1993). The oxygen concentration measurements for the seven samples from this study can be found in Appendix H.

SOFTWARE

- Fluke Power Log Software Version 2.9.2: This PC software is used to transfer logged data from the Fluke 1735 Power Logger to a PC for graphical and tabular evaluation. The software was used in this thesis to view active power measurements with time for both the TIG welder and controlled atmospheric brazing furnace. The power data was exported to Excel to be integrated with respect to time to yield energy consumption.

- LabVIEW Version 12.0: A LabVIEW program was designed to measure and record temperature measurements with respect to time of the aluminum sample as it was being welded. This data was used to measure the thermal energy losses from the sample to the surrounding environment. The following screen shots display the front panel and block diagram of the program respectively.
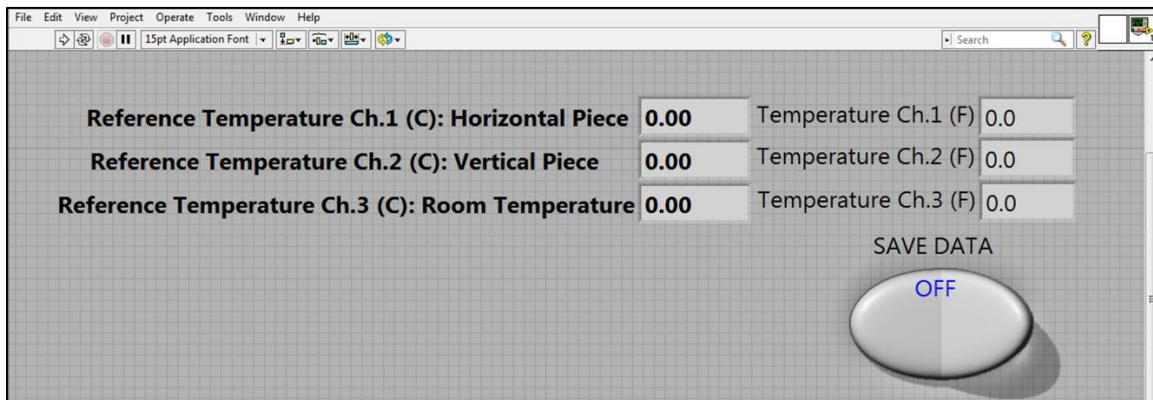
Front panel of temperature measurement LabVIEW program
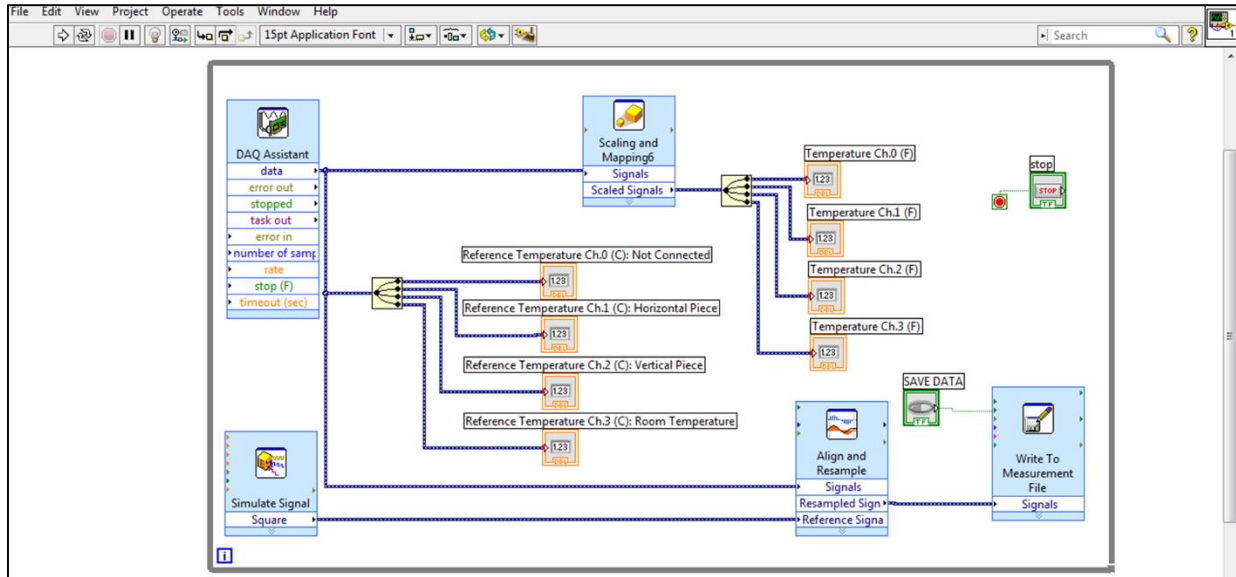
Block diagram of temperature measurement LabVIEW program

- E!sankey Version 3.2.0.424: This software was used to map the energy and exergy flows.

Appendix C: TIG WELDING POWER MEASUREMENTS AND UNCERTAINTY ANALYSIS

POWER MEASUREMENTS:

The power data in this table corresponds to the plots displayed in Figure 3.1. Note that for the compactness of this narrative, only every 5th data point is displayed in the following table. The complete data set is stored in the electronic data archive in the data folder titled "Gasser Thesis Data" in the Brazing Laboratory.

The zeroes in the data below represent the times where the arc welding power source was turned off for safety reasons while the sample re-positioned. The sample was re-positioned after spot-weld 1 and after spot-weld 2 as described is section 2.1.3.

Time (s)	Average Active Power (kW)						
	Sample 1	Sample 2	Sample 3	Sample 4	Sample 5	Sample 6	Sample 7
0	0.1	0.1	0.1	0.1	0.1	0.1	0.1
2.5	2.0	1.8	1.8	1.8	1.8	1.7	1.8
5	1.9	1.7	1.8	1.7	1.8	1.7	1.8
7.5	0.0	1.7	0.0	1.7	1.8	1.8	1.8
10	0.0	1.7	0.0	0.1	0.0	0.0	0.0
12.5	0.0	0.0	0.0	0.0	0.0	0.0	0.0
15	0.0	0.0	0.0	0.0	0.0	0.0	0.0
17.5	0.0	0.0	0.0	0.0	0.0	0.0	0.0
20	0.0	0.0	0.0	0.0	0.0	0.0	0.0
22.5	0.0	0.0	0.0	0.0	0.0	0.0	0.0
25	0.0	0.0	0.0	0.0	0.0	0.0	0.0
27.5	0.0	0.0	0.0	0.0	0.0	0.0	0.0
30	0.0	0.0	0.0	0.0	0.0	0.0	0.0
32.5	0.0	0.0	0.0	0.0	0.0	0.0	0.0
35	0.0	0.0	0.0	0.0	0.0	0.0	0.0
37.5	0.1	0.0	0.1	0.0	0.0	0.0	0.0
40	1.8	0.0	1.7	0.0	0.1	1.7	0.7
42.5	0.0	0.8	0.1	1.7	1.6	0.1	1.8
45	0.0	1.7	0.0	1.8	1.2	0.0	0.0
47.5	0.0	0.0	0.0	0.0	0.0	0.0	0.0
50	0.0	0.0	0.0	0.0	0.0	0.0	0.0
52.5	0.0	0.0	0.0	0.0	0.0	0.0	0.0
55	0.0	0.0	0.0	0.0	0.0	0.0	0.0

57.5	0.0	0.0	0.0	0.0	0.0	0.0	0.0
60	0.0	0.0	0.0	0.0	0.0	0.0	0.0
62.5	0.0	0.0	0.0	0.0	0.0	0.0	0.0
65	0.0	0.0	0.0	0.0	0.0	0.0	0.0
67.5	0.0	0.0	0.0	0.0	0.0	0.0	0.0
70	0.0	0.0	0.0	0.0	0.0	0.0	0.0
72.5	5.0	0.0	0.0	0.0	0.0	0.0	0.0
75	4.8	0.0	4.6	0.0	0.0	4.4	0.1
77.5	4.8	2.5	4.6	3.3	4.7	4.3	4.4
80	4.8	4.6	4.6	4.4	4.6	4.3	4.3
82.5	4.8	4.6	4.6	4.4	4.5	4.3	4.2
85	4.9	4.5	4.5	4.3	4.5	4.3	4.2
87.5	4.8	4.5	4.5	4.3	4.6	4.3	4.2
90	4.8	4.5	4.5	4.3	4.5	4.3	4.2
92.5	4.0	4.5	4.5	4.4	4.5	4.3	4.2
95	1.3	4.6	4.5	4.4	4.5	3.4	3.5
97.5	0.0	4.8	3.5	4.3	4.4	3.6	3.6
100	0.0	3.5	2.6	3.5	4.4	0.0	0.0
102.5	0.0	3.7	0.0	3.8	4.4	0.0	0.0
105	0.0	0.0	0.0	0.0	3.6	0.0	0.0
107.5	0.0	0.0	0.0	0.0	4.0	0.0	0.0

UNCERTAINTY ANALYSIS:

The uncertainty analysis for the power measurements were performed exactly as per the Fluke 1735 power logger user manual. The total uncertainty value calculated using the methods below is given in section 3.1.1.

Power uncertainties are calculated by adding the uncertainties of voltage and current. There were four types of uncertainties associated with the current measurements indicated below.

Current uncertainties

- Intrinsic uncertainty: $\pm$(0.5% of measured value + (10 x resolution))
- Operating uncertainty: $\pm$(1% of measured value + (10 x resolution))
- Flexi set measuring uncertainty: $\pm$(2% of measured value + (10 x resolution))
- Position influence: $\pm$(3% of measured value + (10 x resolution))

With a current resolution of 0.01 A.

The total current uncertainty was obtained using the sum of squares rule seen below.

$$u_c = \sqrt{u_i^2 + u_{op}^2 + u_m^2 + u_{pi}^2}$$

Where,

u_c =   Total uncertainty associated with current measurements
u_i =   Intrinsic uncertainty
u_{op} =   Operating uncertainty
u_m =   Flexi set measuring uncertainty
u_{pi} =   Uncertainty associated with position influence

There were two types of uncertainty associated with voltage measurements.

Voltage uncertainties

- Intrinsic uncertainty: ±(0.2% of measured value + (5 x resolution))
- Operating uncertainty: ±(0.5% of measured value + (10 x resolution))

With a voltage resolution of 0.1 V.

The total voltage uncertainty was obtained using the sum of squares rule.

$$u_v = \sqrt{u_i^2 + u_{op}^2}$$

Where,

u_v =   Total uncertainty associated with current measurements
u_i =   Intrinsic uncertainty
u_{op} =   Operating uncertainty

Ultimately, the total uncertainty associated with the power measurements was calculated by adding the current and voltage uncertainties as indicated by the user manual.

$$u_{tot} = u_c + u_v$$

Where,

u_{tot} =   Total uncertainty associated with power measurements

Appendix D: TIG WELDING TEMPERATURE MEASUREMENTS AND UNCERTAINTY ANALYSIS

TEMPERATURE MEASUREMENTS:

The first table displays temperature measurements for samples 1 and 2 while the second table displays temperature measurements for samples 3 and 4. This temperature data corresponds to the plots in Figure 3.4. Note that for the compactness of this narrative, only every 10th data point is displayed in the following tables. The complete data set is stored in the electronic data archive in the data folder titled "Gasser Thesis Data" in the Brazing Laboratory.

Samples 1 & 2:

	Temperature (ºC)					
	Sample 1			Sample 2		
Time (s)	TC 1: Horizontal Plate	TC 2: Vertical Plate	TC 3: Ambient	TC 1: Horizontal Plate	TC 2: Vertical Plate	TC 3: Ambient
0	163.2	158.8	24.8	393.9	331.9	21.2
10	158.7	157.1	24.8	364.1	340.0	21.5
20	153.3	150.7	24.8	336.7	329.2	21.4
30	147.7	145.9	24.8	314.4	314.1	21.3
40	142.2	140.5	24.8	299.9	289.7	21.3
50	137.2	132.9	24.8	283.6	275.4	21.3
60	131.4	126.5	24.8	268.5	264.5	21.4
70	124.6	121.6	24.8	254.2	252.6	21.4
80	119.1	116.2	24.8	241.4	240.7	21.4
90	113.1	111.1	24.8	226.4	228.4	21.4
100	107.8	106.4	24.8	213.1	216.4	21.5
110	102.9	101.6	24.7	200.9	204.5	21.4
120	98.4	97.4	24.7	189.8	193.1	21.4
130	94.5	93.3	24.8	179.3	182.1	21.5
140	89.2	89.2	24.8	169.9	172.9	21.5
150	84.0	85.2	24.9	161.1	163.5	21.6
160	106.4	131.6	24.9	153.1	155.3	21.6
170	174.5	187.9	24.8	146.0	147.9	21.6
180	171.0	178.7	24.8	138.6	140.8	21.6
190	163.2	165.4	24.7	129.5	132.8	21.6
200	154.2	155.3	24.8	121.2	124.3	21.7
210	145.4	146.0	24.9	206.5	231.7	21.7
220	137.6	137.9	24.8	231.0	243.8	21.7

230	130.7	130.6	24.8	220.3	226.5	21.8
240	124.3	124.3	24.9	211.8	209.8	21.8
250	119.2	117.0	24.8	202.2	201.4	21.9
260	114.4	112.3	24.7	192.0	192.4	21.8
270	108.8	107.9	24.8	184.2	183.8	21.8
280	103.6	103.4	24.6	174.4	174.0	21.8
290	98.3	99.2	24.7	165.4	165.6	21.9
300	94.0	94.6	24.8	156.5	157.3	22.0
310	91.1	90.6	24.8	149.1	150.0	22.0
320	88.0	87.3	24.8	143.1	143.0	22.0
330	84.0	83.7	24.7	137.7	137.3	22.0
340	80.3	80.0	24.7	131.1	131.3	22.0
350	77.2	76.8	24.8	125.2	125.3	22.0
360	74.6	73.8	24.8	119.6	119.8	22.1
370	72.2	71.5	24.8	113.9	114.3	22.1
380	69.7	69.3	24.8	108.9	109.3	22.1
390	67.4	66.9	24.9	102.3	104.3	22.2
400	65.2	64.8	24.9	96.2	99.0	22.1
410	63.1	62.8	24.8	93.8	94.3	22.2
420	61.2	60.8	24.9	88.8	90.1	22.2
430	59.3	59.1	24.9	85.4	86.1	22.2
440	57.4	57.3	25.1	82.8	82.7	22.2
450	55.5	55.7	24.9	79.1	79.5	22.3
460	54.0	54.1	24.9	75.7	76.1	22.3
470	52.5	52.6	24.9	72.6	73.0	22.3
480	51.1	51.0	24.9	69.5	70.1	22.3
490	49.8	49.8	24.9	66.7	67.2	22.3
500	48.7	48.5	24.9	63.1	63.3	22.5
510	47.3	47.4	24.9	61.2	61.2	22.7
520	46.2	46.2	25.0	59.5	59.3	22.5
530	45.3	45.1	25.0	57.6	57.4	22.5
540	44.3	44.2	25.1	55.6	55.7	22.6
550	43.4	43.2	25.1	53.6	53.8	22.6
560	42.5	42.3	25.0	51.9	52.1	22.6
570	41.7	41.3	25.0	50.6	50.5	22.6
580	40.8	40.5	25.1	49.0	49.0	22.7
590	40.0	39.7	25.0	47.6	47.5	22.6
600	41.8	42.5	25.2	46.3	46.2	22.6
610	48.4	48.0	25.1	45.1	44.9	22.7

620	55.3	55.5	25.1	43.8	43.6	22.7
630	310.3	271.0	25.0	48.8	47.7	22.8
640	340.1	329.6	24.9	57.3	55.7	22.7
650	335.0	337.5	25.0	366.8	290.0	22.7
660	324.1	328.1	25.0	323.5	330.2	22.8
670	310.2	313.4	25.0	301.3	308.5	22.9
680	295.5	298.1	25.1	283.6	288.6	22.9
690	279.5	282.5	25.1	265.5	269.5	23.0
700	265.2	267.7	25.0	249.0	252.5	22.9
710	250.5	254.0	25.1	234.1	237.1	22.9
720	238.1	240.9	25.0	220.0	222.6	22.9
730	226.9	228.5	25.4	207.0	209.2	22.9
740	215.1	217.0	25.6	193.9	196.1	23.1
750	204.9	206.7	25.3	183.3	185.3	23.1
760	195.4	196.5	25.6	173.2	174.9	23.1
770	187.4	187.0	25.5	164.1	165.3	23.2
780	178.6	178.3	25.3	155.9	156.7	23.1
790	170.1	170.3	25.3	148.1	148.5	23.0
800	163.5	163.1	25.4	140.8	141.3	23.0
810	156.6	155.4	25.5	133.7	134.1	23.0
820	150.9	149.5	25.3	127.5	127.8	23.0
830	144.8	143.2	25.0	121.4	121.6	23.1
840	138.0	137.4	25.4	115.8	115.9	23.2
850	132.5	132.4	25.4	110.9	110.8	23.1
860	127.4	127.6	25.2	105.9	106.0	23.1
870	123.1	122.8	25.2	101.5	101.6	23.1
880	119.3	118.4	25.3	97.2	97.2	23.1
890	115.5	114.5	25.4	93.5	93.3	23.2
900	110.9	110.4	25.6	89.8	89.5	23.2
910	107.3	106.6	25.3	86.3	86.1	23.2
920	104.7	102.9	25.3	83.1	82.9	23.4
930	100.8	99.8	25.1	79.9	79.6	23.5
940	97.7	97.1	25.2	77.1	76.9	23.2
950	95.1	94.1	25.4	74.7	74.2	23.2
960	91.9	91.6	25.7	72.3	71.9	23.1
970	90.1	88.9	25.6	70.1	69.6	23.1
980	87.4	86.4	25.5	67.9	67.4	23.2
990	85.4	84.1	25.4	66.0	65.4	23.2
1000	82.9	81.7	25.6	64.0	63.5	23.1

1010	80.9	79.8	25.3	62.4	61.9	23.0
1020	79.1	78.0	25.3	60.7	60.1	23.2
1030	77.1	76.2	25.1	59.2	58.6	23.3
1040	75.4	74.3	25.0	57.7	57.1	23.2
1050	73.5	72.8	25.0	56.3	55.7	23.3
1060	72.1	71.2	25.2	55.1	54.5	23.3
1070	70.5	69.7	25.4	53.8	53.1	23.4
1080	69.0	68.3	25.5	52.7	52.0	23.4
1090	68.1	67.1	25.7	51.7	51.0	23.3
1100	66.9	65.7	25.8	50.7	50.0	23.4
1110	65.2	64.4	25.4	49.8	49.0	23.5
1120	63.9	63.2	25.4	48.9	48.0	23.4
1130	63.2	62.2	25.5	48.0	47.2	23.5
1140	62.5	61.2	25.5	47.2	46.5	23.5
1150	61.3	60.2	25.5	46.5	45.6	23.5
1160	60.6	59.2	25.6	45.7	44.9	23.4
1170	59.4	58.3	25.3	45.1	44.3	23.4
1180	58.7	57.5	25.6	44.5	43.6	23.3
1190	57.9	56.7	25.7	43.9	43.1	23.4
1200	57.2	55.8	25.5	43.4	42.5	23.5
1210	56.6	55.1	25.6	42.8	41.9	23.5
1220	55.9	54.4	25.4	42.4	41.4	23.4
1230	55.2	53.7	25.4	41.8	41.0	23.6
1240	54.6	53.0	25.6	41.3	40.5	23.6
1250	54.0	52.5	25.5	40.9	40.0	23.7
1260	53.5	51.7	25.3	40.5	39.6	23.7
1270	52.6	51.2	25.4	40.1	39.2	23.6
1280	52.1	50.7	25.4	39.7	38.8	23.7
1290	51.5	50.1	25.6			
1300	51.0	49.5	25.5			
1310	50.6	49.0	25.5			
1320	49.6	48.3	25.7			
1330	49.4	47.9	25.7			
1340	49.1	47.4	25.6			
1350	48.5	46.8	25.6			
1360	48.2	46.5	25.7			
1370	48.0	46.1	25.6			
1380	47.6	45.8	25.5			
1390	47.3	45.4	25.6			

Time (s)	1400	46.8	45.0	25.8			

Samples 3 & 4

	Sample 3			Sample 4		
Time (s)	TC 1: Horizontal Plate	TC 2: Vertical Plate	TC 3: Ambient	TC 1: Horizontal Plate	TC 2: Vertical Plate	TC 3: Ambient
0	251.4	211.5	22.7	306.0	264.2	19.5
10	236.2	213.2	22.6	287.5	270.0	19.6
20	221.7	209.6	22.6	274.0	258.2	19.5
30	209.6	205.9	22.7	259.0	248.3	19.4
40	196.2	198.1	22.7	242.4	239.6	19.4
50	184.3	189.0	22.6	228.3	228.9	19.5
60	173.1	178.8	22.7	215.3	217.4	19.5
70	160.7	168.1	22.7	201.7	205.5	19.8
80	201.0	238.8	22.7	190.1	194.2	19.7
90	238.6	251.5	22.8	179.4	183.0	19.5
100	227.5	236.4	22.8	169.9	173.3	19.6
110	215.3	221.5	22.7	161.0	164.3	19.5
120	205.7	210.0	22.8	150.7	154.7	19.5
130	196.9	199.6	22.8	140.7	145.0	19.4
140	189.2	191.5	22.7	140.8	163.2	19.5
150	180.5	183.7	22.7	229.3	242.8	19.6
160	170.3	174.8	22.7	217.6	227.2	19.5
170	162.2	166.7	22.8	208.7	213.3	19.6
180	152.6	157.8	22.8	200.9	203.0	19.7
190	144.5	149.4	22.9	192.9	194.1	19.7
200	136.6	141.2	22.9	185.9	186.5	19.6
210	129.3	133.5	22.9	178.0	178.5	19.6
220	122.0	126.7	22.9	168.7	170.5	19.6
230	115.3	120.1	22.8	160.0	162.0	19.8
240	109.2	113.9	22.8	152.3	154.2	19.7
250	103.7	107.9	22.9	144.8	146.6	19.7
260	99.0	102.6	22.9	136.7	139.2	19.8
270	94.4	97.7	22.9	130.3	132.4	19.9
280	90.0	93.1	23.0	124.1	125.8	19.7

290	86.2	89.0	23.0	118.5	120.1	19.7
300	82.4	85.0	23.0	113.0	114.4	19.9
310	79.0	81.4	23.1	107.9	109.3	19.9
320	75.7	78.0	23.1	102.5	104.1	19.9
330	72.9	74.9	23.1	97.2	98.9	19.7
340	69.9	72.0	23.0	92.5	94.2	19.9
350	67.4	69.1	23.0	88.3	89.6	19.9
360	64.9	66.5	23.0	84.8	85.8	20.0
370	64.6	66.5	23.2	81.4	82.3	20.0
380	72.4	73.7	23.2	78.4	79.2	20.1
390	254.0	316.6	23.2	75.3	76.1	19.9
400	386.5	388.5	23.3	77.8	77.9	20.0
410	375.1	381.2	23.2	85.0	84.2	19.9
420	347.7	361.3	23.3	92.0	91.1	20.1
430	326.2	340.1	23.1	445.3	404.0	20.0
440	305.2	318.8	23.4	418.8	414.2	20.1
450	287.9	299.8	23.2	390.7	395.2	20.2
460	271.4	282.1	23.3	364.2	371.3	20.2
470	257.0	266.2	23.4	339.5	347.0	20.1
480	242.1	250.9	23.4	318.0	325.0	20.2
490	228.4	237.0	23.4	297.8	304.4	20.2
500	216.1	224.2	23.0	280.2	286.2	20.1
510	205.0	212.1	23.0	263.5	268.8	20.1
520	195.0	201.6	23.0	248.8	253.6	20.0
530	184.0	191.5	23.0	234.6	239.1	20.0
540	176.1	182.1	22.9	221.5	225.6	20.0
550	168.2	173.3	22.8	209.8	213.6	20.0
560	161.3	165.2	22.8	198.8	202.3	20.0
570	152.9	158.0	22.8	188.5	191.9	20.0
580	146.2	150.9	22.8	178.9	182.1	20.0
590	140.0	144.4	22.9	170.3	173.4	20.1
600	134.0	138.2	22.9	161.8	164.9	20.1
610	129.2	132.5	22.9	154.1	156.8	20.0
620	124.0	127.1	23.0	147.1	149.7	20.1
630	118.6	121.9	23.0	140.5	143.1	20.1
640	113.8	117.3	22.9	134.6	137.0	20.2
650	109.2	112.6	22.9	128.7	131.0	20.2
660	105.4	108.5	22.9	123.6	125.7	20.1
670	101.7	104.4	22.9	118.2	120.2	20.1

680	98.5	100.8	22.9	113.2	115.1	20.3
690	94.9	97.3	23.0	108.9	110.6	20.2
700	91.6	93.9	23.1	104.7	106.4	20.5
710	88.5	90.9	23.0	100.9	102.5	20.6
720	85.6	87.9	23.4	97.1	98.7	20.5
730	82.9	85.2	23.2	93.7	95.3	20.3
740	80.3	82.5	23.0	90.5	92.1	20.2
750	78.0	80.1	23.1	87.5	88.9	20.5
760	76.1	77.7	23.2	84.9	86.2	20.4
770	73.9	75.4	23.1	82.3	83.5	20.4
780	71.6	73.4	23.1	79.6	81.0	20.3
790	69.8	71.3	23.0	77.2	78.6	20.3
800	68.1	69.5	23.1	75.0	76.3	20.4
810	66.3	67.6	23.0	72.9	74.2	20.4
820	64.5	66.0	23.0	70.9	72.2	20.4
830	62.8	64.3	23.1	69.0	70.3	20.4
840	61.4	62.8	23.3	67.3	68.6	20.5
850	60.2	61.4	23.4	65.7	66.9	20.5
860	58.8	59.9	23.2	63.9	65.2	20.6
870	57.4	58.6	23.2	62.4	63.7	20.5
880	56.2	57.3	23.1	60.9	62.3	20.6
890	55.3	56.2	23.2	59.6	60.9	20.7
900	54.0	55.0	23.2	58.3	59.6	20.6
910	53.2	53.9	23.2	57.0	58.4	20.7
920	52.3	52.9	23.3	55.7	57.2	20.6
930	51.2	52.0	23.3	54.6	56.0	20.7
940	50.4	51.1	23.3	53.6	54.9	20.7
950	49.6	50.1	23.3	52.7	54.0	20.7
960	48.7	49.3	23.3	51.8	53.0	20.8
970	47.9	48.5	23.3	50.8	52.2	20.7
980	47.3	47.7	23.2	49.8	51.2	20.7
990	46.7	47.1	23.1	49.0	50.4	20.8
1000	46.1	46.4	23.2	48.1	49.5	20.9
1010	45.2	45.8	23.3	47.2	48.6	20.8
1020	44.6	45.1	23.3	46.5	47.9	20.9
1030	43.9	44.5	23.2	45.8	47.1	21.1
1040	43.4	43.9	23.3	45.1	46.5	20.9
1050	42.8	43.3	23.3	44.4	45.7	20.9
1060	42.5	42.7	23.3	43.8	45.1	21.0

1070	41.9	42.2	23.2	43.2	44.5	21.0
1080	41.5	41.7	23.2	42.7	44.0	21.1
1090	41.2	41.3	23.3	42.1	43.5	21.1
1100	40.7	40.9	23.5	41.7	43.0	21.0
1110	40.3	40.4	23.6	41.3	42.5	21.1
1120	40.0	40.0	23.6	40.9	42.1	21.0
1130	39.6	39.7	23.4	40.4	41.7	21.1
1140	39.4	39.3	23.3	40.0	41.3	21.0
1150	39.0	38.9	23.4	39.7	41.0	21.0
1160	38.4	38.6	23.5	39.4	40.6	21.0
1170	38.2	38.2	23.5	39.0	40.3	21.0
1180	37.8	37.9	23.5	38.8	39.9	21.1
1190	37.6	37.5	23.5	38.5	39.6	21.0
1200	37.4	37.3	23.5	38.3	39.4	21.0
1210	37.2	37.0	23.5	38.0	39.1	21.1
1220	36.8	36.8	23.5	37.7	38.9	21.1
1230	36.7	36.5	23.5	37.5	38.6	21.1
1240	36.4	36.3	23.8	37.1	38.3	21.1
1250	36.2	36.0	23.8	36.9	38.1	21.2
1260	35.9	35.8	23.7	36.8	37.9	21.2
1270	35.6	35.5	23.9	36.6	37.7	21.2
1280	35.4	35.2	23.8	36.3	37.5	21.2
1290	35.3	35.0	23.7	36.1	37.3	21.2
1300	35.1	34.8	23.6	36.0	37.1	21.2
1310	34.9	34.6	23.6	35.8	37.0	21.2
1320	34.7	34.4	23.6	35.7	36.8	21.2
1330	34.5	34.2	23.7	35.6	36.7	21.3
1340	34.3	34.0	23.6	35.4	36.5	21.3
1350	34.2	33.8	23.7	35.3	36.4	21.3
1360	34.2	33.7	23.7	35.2	36.3	21.3
1370	34.0	33.5	23.8	35.0	36.1	21.4
1380	33.9	33.4	23.8	34.8	35.9	21.4
1390	33.8	33.2	23.7	34.7	35.8	21.4
1400	33.6	33.1	23.6	34.6	35.7	21.4

UNCERTAINTY ANALYSIS:

The Super OMEGACLAD® Thermocouple Probes used to take temperature measurements in these experiments have a standard uncertainty of 2.2 C or 0.75% (whichever is greater) above 0 C (Omega 2013).

Appendix E: CAB POWER MEASUREMENTS AND UNCERTAINTY ANALYSIS

POWER MEASUREMENTS:

The power data in this table corresponds to the plots displayed in Figure 3.6. Note that for the compactness of this narrative, only every 25th data point is displayed in the following table. The complete data set is stored in the electronic data archive in the data folder titled "Gasser Thesis Data" in the Brazing Laboratory.

Time (s)	Average Active Power (kW)						
	Sample 1	Sample 2	Sample 3	Sample 4	Sample 5	Sample 6	Sample 7
0	0.1	0.1	0.1	0.2	0.1	0.1	0.1
25	5.5	5.5	5.5	5.6	5.5	5.5	5.5
50	5.6	5.6	5.6	5.6	5.6	5.6	5.6
75	5.7	5.7	5.7	5.7	5.7	5.7	5.7
100	5.7	5.7	5.7	5.7	5.7	5.7	5.7
125	5.7	5.7	5.7	5.7	5.7	5.7	5.7
150	5.7	5.7	5.7	5.7	5.7	5.7	5.7
175	5.7	5.7	5.7	5.7	5.7	5.7	5.7
200	5.7	5.7	5.7	5.7	5.7	5.7	5.7
225	5.7	5.7	5.7	5.7	5.7	5.7	5.7
250	5.7	5.7	5.7	5.7	5.7	5.7	5.7
275	5.7	5.7	5.7	5.7	5.7	5.7	5.7
300	5.7	0.1	0.1	4.9	5.7	0.1	5.7
325	0.1	0.1	0.1	0.1	0.1	1.1	0.5
350	0.1	0.1	0.1	0.1	0.1	0.2	0.1
375	0.1	0.1	0.1	0.1	0.1	0.1	0.1
400	0.1	0.1	0.1	0.1	0.1	0.1	0.1
425	0.1	0.1	0.1	0.1	0.1	0.1	0.1
450	0.1	0.1	0.1	0.1	0.1	0.1	0.1
475	0.1	0.1	0.1	0.1	0.1	0.1	0.1
500	0.1	0.1	0.1	0.1	0.1	0.1	0.1
525	0.1	0.1	0.1	0.1	0.1	0.1	0.1
550	0.1	0.1	0.1	0.1	0.1	0.1	0.1
575	0.1	0.1	0.1	0.1	0.1	0.1	0.1
600	0.1	0.1	0.1	0.1	0.1	0.1	0.1
625	0.1	0.1	0.1	0.1	0.1	0.1	0.1
650	0.1	0.1	0.1	0.1	0.1	0.1	0.1
675	0.1	0.1	0.1	0.1	0.1	0.1	0.1

700	0.1	0.1	0.1	0.1	0.1	0.1	0.1
725	0.1	0.1	0.1	0.1	0.1	0.1	0.1
750	0.1	0.1	0.1	0.1	0.1	0.1	0.1
775	0.1	0.1	0.1	0.1	0.1	0.1	0.1
800	0.1	0.1	0.1	0.1	0.1	0.1	0.1
825	0.1	0.1	0.1	0.1	0.1	0.1	0.1
850	0.1	0.1	0.1	0.1	0.1	0.1	0.1
875	0.1	0.1	0.1	0.1	0.1	0.1	0.1
900	0.1	0.1	0.1	0.1	0.1	0.1	0.1
925	0.1	0.1	0.1	0.1	0.1	0.1	0.1
950	0.1	0.1	0.1	0.1	0.1	0.1	0.1
975	0.1	0.1	0.1	0.1	0.1	0.1	0.1
1000	0.1	0.1	0.1	0.1	0.1	0.1	0.1
1025	0.1	0.1	0.1	0.1	0.1	0.1	0.1
1050	0.1	0.1	0.1	0.1	0.1	0.1	0.1
1075	0.1	0.1	0.1	0.1	0.1	0.1	0.1
1100	0.1	0.1	0.1	0.1	0.1	0.1	0.1
1125	0.1	0.1	0.1	0.1	0.1	0.1	0.1
1150	0.1	0.1	0.1	0.1	0.1	0.1	0.1
1175	0.1	0.1	0.1	0.1	0.1	0.1	0.1
1200	0.1	0.1	0.1	0.1	0.1	0.1	0.1
1225	0.1	0.1	0.1	0.1	0.1	0.1	0.1
1250	0.1	0.1	0.1	0.1	0.1	0.1	0.1
1275	0.1	0.1	0.1	0.1	0.1	0.1	0.1
1300	0.1	0.1	0.1	0.1	0.1	0.1	0.1
1325	0.1	0.1	0.1	0.1	0.1	0.1	0.1
1350	0.1	0.1	0.1	0.1	0.1	0.1	0.1
1375	0.1	0.1	0.1	0.1	0.1	0.1	0.1
1400	0.1	0.1	0.1	0.1	0.1	0.1	0.1
1425	0.1	0.1	0.1	0.1	0.1	0.1	0.1
1450	0.1	0.1	0.1	0.1	0.1	0.1	0.1
1475	0.1	0.1	0.1	0.1	0.1	0.1	0.1
1500	0.1	0.1	0.1	0.1	0.1	0.1	0.1
1525	0.1	0.1	0.1	0.1	0.1	0.1	0.1
1550	0.1	0.1	0.1	0.1	0.1	0.1	0.1
1575	0.1	0.1	0.1	0.1	0.1	0.1	0.1
1600	0.1	0.1	0.1	0.1	0.1	0.1	0.1
1625	0.1	0.1	0.1	0.1	0.1	0.1	0.1
1650	0.1	0.1	0.1	0.1	0.1	0.1	0.1

1675	0.1	0.1	0.1	0.1	0.1	0.1	0.1
1700	0.1	0.1	0.1	0.1	0.1	0.1	0.1
1725	0.1	0.1	0.1	0.1	0.1	0.1	0.1
1750	0.1	0.1	0.1	0.1	0.1	0.1	0.1
1775	0.1	0.1	0.1	0.1	0.1	0.1	0.1
1800	0.1	0.1	0.1	0.1	0.1	0.1	0.1
1825	0.1	0.1	0.1	0.1	0.1	0.1	0.1
1850	0.1	0.1	0.1	0.1	0.1	0.1	0.1
1875	0.1	0.1	0.1	0.1	0.1	0.1	0.1
1900	5.5	5.5	5.5	5.5	5.5	5.5	5.5
1925	5.6	5.6	5.6	5.6	5.6	5.6	5.6
1950	5.7	5.7	5.7	5.7	5.7	5.7	5.7
1975	5.7	5.7	5.7	5.7	5.7	5.7	5.7
2000	5.7	5.7	5.7	5.7	5.7	5.7	5.7
2025	5.7	5.7	5.7	5.7	5.7	5.7	5.7
2050	5.7	5.7	5.7	5.7	5.7	5.7	5.7
2075	5.7	5.7	5.7	5.7	5.7	5.7	5.7
2100	5.7	5.7	5.7	5.7	5.7	5.7	5.7
2125	5.7	5.7	5.7	5.7	5.7	5.7	5.7
2150	5.7	5.7	5.7	5.7	5.7	5.7	5.7
2175	5.7	5.7	5.7	5.7	5.7	5.7	5.7
2200	5.7	5.7	5.7	5.7	5.7	5.7	5.7
2225	5.7	5.7	5.7	5.7	5.7	5.7	5.7
2250	5.7	5.7	5.7	5.7	5.7	5.7	5.7
2275	5.7	5.7	5.7	5.7	5.7	5.7	5.7
2300	0.1	5.7	5.7	5.7	5.7	5.7	5.7
2325	5.7	5.7	5.7	5.7	5.7	5.7	5.7
2350	5.7	5.7	5.7	5.7	5.7	5.7	5.7
2375	5.7	5.7	5.7	5.7	5.7	5.7	5.7
2400	5.7	5.7	5.7	5.7	5.7	5.7	5.7
2425	5.7	5.7	5.7	5.7	5.7	5.7	5.7
2450	5.7	5.7	5.7	5.7	5.7	5.7	5.7
2475	5.7	5.7	5.7	5.7	5.7	5.7	5.7
2500	5.7	5.7	5.7	5.7	5.7	5.7	5.7
2525	5.7	1.5	1.5	4.4	5.5	5.7	5.7
2550	5.7	5.7	5.7	5.7	5.7	5.7	5.7
2575	3.4	5.7	5.7	5.7	5.7	5.7	5.7
2600	5.7	0.1	0.1	5.5	0.1	5.7	5.7
2625	5.7	0.1	0.1	0.1	0.1	0.1	5.7

2650	0.1	0.1	0.8	0.4	0.1	0.1	5.7
2675	0.1	5.7	5.1	5.7	0.2	0.1	5.7
2700	0.1	5.7	5.7	5.7	5.6	0.1	5.7
2725	0.8	5.7	5.7	0.8	5.7	0.1	5.7
2750	5.7	0.1	5.7	0.1	5.7	0.1	5.7
2775	5.7	0.1	5.7	0.1	5.7	0.1	5.7
2800	0.1	0.1	5.7	5.7	5.7	0.1	5.7
2825	0.1	5.7	5.7	5.7	5.7	0.4	5.7
2850	0.1	5.7	5.7	0.1	5.2	5.4	5.7
2875	5.6	1.0	5.3	0.1	2.2	5.7	5.7
2900	5.7	0.1	0.6	0.2	0.1	5.7	5.7
2925	2.5	0.1	0.1	5.7	0.1	5.7	5.5
2950	0.1	0.5	0.1	5.8	0.1	5.7	1.0
2975	0.1	5.7	0.1	0.1	0.1	5.4	0.1
3000	0.1	5.7	0.1	0.1	0.1	1.2	0.1
3025	0.1	0.1	0.1	4.1	0.1	0.1	0.1
3050	0.1	0.1	0.1	0.1	0.1	0.1	0.1
3075	0.1	0.1	0.1	0.1	0.1	0.1	0.1
3100	0.2	0.1	0.1	0.1	0.1	0.1	0.1
3125	0.2	0.1	0.1	0.1	0.1	0.1	0.1
3150	0.1	0.1	0.1	0.1	0.1	0.1	0.1
3175	0.2	0.1	0.1	0.1	0.1	0.1	0.1
3200	0.1	0.1	0.1	0.1	0.1	0.1	0.1
3225	0.2	0.1	0.1	0.1	0.1	0.1	0.1
3250	0.1	0.1	0.1	0.1	0.1	0.1	0.1
3275	0.1	0.1	0.1	0.1	0.1	0.1	0.1
3300	0.2	0.1	0.1	0.1	0.1	0.1	0.1
3325	0.1	0.1	0.1	0.1	0.1	0.1	0.1
3350	0.2	0.1	0.1	0.1	0.1	0.1	0.1
3375	0.1	0.1	0.1	0.1	0.1	0.1	0.1
3400	0.1	0.1	0.1	0.1	0.1	0.1	0.1
3425	0.1	0.1	0.1	0.1	0.1	0.1	0.1
3450	0.1	0.1	0.1	0.1	0.1	0.1	0.1
3475	0.2	0.1	0.1	0.1	0.1	0.1	0.1
3500	0.1	0.1	0.1	0.1	0.1	0.1	0.1
3525	0.2	0.1	0.1	0.1	0.1	0.1	0.1
3550	0.0	0.1	0.0	0.1	0.0	0.1	0.1
3575	0.0	0.0	0.0	0.1	0.0	0.1	0.0
3600	0.0	0.0	0.0	0.0	0.0	0.1	0.0

UNCERTAINTY ANALYSIS:

The uncertainty analysis for the power measurements were performed exactly as per the Fluke 1735 power logger user manual. The total uncertainty value calculated using the methods below is given in section 3.2.1.

Power uncertainties are calculated by adding the uncertainties of voltage and current. There were four types of uncertainties associated with the current measurements indicated below.

Current uncertainties

- Intrinsic uncertainty: $\pm$(0.5% of measured value + (10 x resolution))
- Operating uncertainty: $\pm$(1% of measured value + (10 x resolution))
- Flexi set measuring uncertainty: $\pm$(2% of measured value + (10 x resolution))
- Position influence: $\pm$(3% of measured value + (10 x resolution))

With a current resolution of 0.01 A.

The total current uncertainty was obtained using the sum of squares rule.

$$u_c = \sqrt{u_i^2 + u_{op}^2 + u_m^2 + u_{pi}^2}$$

Where,

u_c	=	Total uncertainty associated with current measurements
u_i	=	Intrinsic uncertainty
u_{op}	=	Operating uncertainty
u_m	=	Flexi set measuring uncertainty
u_{pi}	=	Uncertainty associated with position influence

There were two types of uncertainty associated with voltage measurements.

Voltage uncertainties

- Intrinsic uncertainty: $\pm$(0.2% of measured value + (5 x resolution))
- Operating uncertainty: $\pm$(0.5% of measured value + (10 x resolution))

With a voltage resolution of 0.1 V.

The total voltage uncertainty was obtained using the sum of squares rule.

$$u_v = \sqrt{u_i^2 + u_{op}^2}$$

Where,

u_v	=	Total uncertainty associated with current measurements
u_i	=	Intrinsic uncertainty

u_{op} =   Operating uncertainty

Ultimately, the total uncertainty associated with the power measurements was calculated by adding the current and voltage uncertainties as indicated by the user manual.

$$u_{tot} = u_c + u_v$$

Where,

u_{tot} =   Total uncertainty associated with power measurements

Appendix F: CAB TEMPERATURE MEASUREMENTS

The data from sample 7 corresponds to the plot seen in Figure 2.15. Note that for the compactness of this narrative, only every 20th data point is displayed in the following table. The complete data set is stored in the electronic data archive in the data folder titled "Gasser Thesis Data" in the Brazing Laboratory.

Samples 1-3

	Sample 1			Sample 2			Sample 3		
Time	Heater TC	Work 1 TC	Work 2 TC	Heater TC	Work 1 TC	Work 2 TC	Heater TC	Work 1 TC	Work 2 TC
(sec.)	(deg. F)	(deg. F)	(deg. F)	(deg. F)	(deg. F)	(deg. F)	(deg. F)	(deg. F)	(deg. F)
0	75.8	78	74.7	80.3	81.6	78.6	77.3	78.8	75.7
41	130.9	79.3	77.3	136	83	81.4	131.8	80.5	78.6
81	275.7	97.9	109	285.2	102.2	113.3	278.4	106.2	109.6
122	452.1	137.7	185.7	460.4	142.6	190.6	448.6	156.5	183.7
163	588.7	182.1	266.8	595.4	190	271.2	590.7	206.6	263.2
203	685	227.4	331.4	688.8	240	338.9	689.4	255.3	329.6
244	749.5	275.7	387.9	754.9	293.3	400.2	753.8	307.7	389.9
284	801	326.6	442.2	791.8	336	446.6	776.6	342.2	429.9
325	770.3	343.8	440.8	741.6	347.1	432.9	722.1	347.4	413.8
366	690	352.6	408.9	668.1	364.3	409.6	652	357.8	396.6
406	634.1	368.7	404.5	614.8	382.1	408.7	603	375.4	396.2
447	595.3	384.7	411.2	578.7	397.5	415.2	568.1	389.8	402.8
488	566.6	400.9	420.5	552.1	408.6	423	542.1	399.8	411
528	545.1	410.2	429	532.6	417.5	430.1	521.9	406.3	418.8
569	529.7	419.8	436.1	517.5	427.1	436.9	507.3	411.9	425.7
610	516.4	426.7	443.3	504.2	432.8	442	495	416.7	431.2
650	505.7	432.4	449.1	494.5	436.9	446.6	484.1	420.7	435.4
691	495.2	436.5	452.8	484.9	439.3	449.9	474.8	423.6	439
732	487.1	440.2	456.3	476.3	441.1	452.4	466	425.7	441.6
772	479.3	442.8	458.3	469.3	441.6	454	458.7	427.5	442.7
813	472.3	445	459.7	462.3	441.8	454	452.2	427.5	443.9
853	464.7	446	460.3	455.5	441.3	454.6	445	427.5	444.7
894	457.6	446.3	460.4	448.7	439.5	454	438.5	427.3	443.9
935	451.3	446.8	460	441.8	437.7	453.5	432.6	426.7	443.2
975	445	445.5	459	436.2	435.4	452	426.7	425.7	441.9
1016	438.8	444.5	457.3	430.5	433.6	450.5	420.6	424.2	440.6
1057	432.5	442.5	455.7	424.8	431	448.4	414.5	422	439.1
1097	427.2	441.1	453.9	419	428.3	445.9	409	420.1	436.7

1138	421.2	439.2	451.5	414.3	425.1	443.4	404.2	418.1	434.6
1179	415.8	437.1	448.6	408.8	422.8	440.8	398.8	415.8	431.8
1219	410.4	433.9	446.3	403.6	419.4	438.1	393.4	412.6	429.2
1260	404.6	431.7	443.8	398.8	416.5	434.6	388.6	410.4	427.1
1301	400.2	428.5	440.9	393.8	413	431.9	384.3	407.8	424.2
1341	395	425.9	437.8	388.7	409.9	429.4	378.7	404.6	421.1
1382	389.6	422.4	434.7	383.8	406.6	425.7	374.1	401.4	418.1
1423	385.3	419.6	431.6	378.9	403.6	422.7	369.8	398.5	415.5
1463	380.1	416.3	427.9	374.7	400.2	419.5	365.3	395.5	412
1504	375.2	412.9	425.2	370.1	397	415.9	360.7	392.3	409
1544	370.8	409.7	421.5	366	393.4	413.6	356.6	389.3	406.1
1585	366.7	406.5	418	361.9	389.8	409.5	352.3	386.2	402.4
1626	361.9	402.8	415	357.4	386.5	406.4	347.6	382.8	399.5
1666	358.2	399.8	411.6	353.2	383.5	403.4	344.2	380	396.8
1707	353.6	396.2	408.3	349.3	379.9	400.5	340.2	376.6	393.2
1748	348.8	392.8	404.7	345.5	377.2	396.7	336.2	373.2	390
1788	345.1	389.6	400.8	340.9	373.7	393.8	331.7	369.7	387.4
1829	341.4	385.9	397.7	337.1	370.2	390.6	328.8	367	383.1
1870	337.1	382.7	393.9	333.5	367.2	387	324.9	363.9	380.7
1910	340.8	380.1	392	340.6	364.8	385	330	362.1	378
1951	432.2	391.1	409.6	437.8	379.5	406.6	422.8	377.6	396.8
1992	578.9	429.1	470.4	588.2	422.3	471.2	573.6	424.6	456.6
2032	713.1	477.7	539.2	718.6	478.2	540.8	705.9	480.6	526
2073	804.7	525.3	598.7	807.3	531.5	600.9	801.3	535.6	586.9
2113	868.3	572.9	651.4	871	583.4	654.9	866.5	590.4	644.1
2154	917.2	620.7	701.4	919.5	633.5	706.6	916.2	646.9	695.3
2195	957.9	671.2	751.2	959.8	681.7	757.3	957.4	698.9	747
2235	996	720.4	800.9	996.3	735	808.1	993	753.3	798.1
2276	1030.6	772.8	850.1	1031	787.5	858.6	1028.6	800	847.5
2317	1033.3	811.8	877.4	1035	828.5	884.8	1032.4	847.6	875
2357	1074.9	866	926.6	1079	880.7	938.1	1075	899.4	927.6
2398	1114.3	920.8	974	1116.4	935.7	986.4	1111.9	947.3	976
2439	1147.5	970.9	1017.1	1148.8	991.7	1028.4	1144	994.5	1019.8
2479	1177.2	1017.3	1058.2	1178.9	1038.2	1069.2	1174.7	1038.4	1060.5
2520	1205.7	1061.3	1097.2	1206.7	1080	1105.5	1202.1	1083.6	1099.3
2561	1220.1	1095.7	1126.3	1199	1101.2	1117.7	1201.1	1102.3	1117.8
2601	1203.2	1110.5	1132.6	1189.3	1114.5	1125.5	1202.7	1115.4	1131.4
2642	1190.2	1120.7	1137.2	1179.6	1122.5	1130.9	1187.4	1123.2	1135.4
2683	1175.9	1126.4	1136.7	1172.6	1128	1134.6	1174	1127.6	1135.8

2723	1165.2	1129.9	1137	1167.5	1130.8	1136.7	1165.9	1130.4	1136.7
2764	1158	1132	1137.1	1163.3	1133	1138	1160.6	1132.2	1137.7
2804	1155	1132.3	1137.2	1161.3	1134.1	1138.8	1158.7	1134.4	1139.1
2845	1153.1	1132.8	1137.6	1159.1	1134.9	1139.8	1157.9	1134.9	1140.1
2886	1152.5	1133.6	1137.9	1158.3	1135.4	1140.4	1155.6	1134.8	1140.3
2926	1152.7	1134	1137.9	1157	1135.7	1140.3	1153.3	1134.3	1139
2967	1151.5	1133.7	1138	1155.8	1136	1140.7	1152	1134	1138.9
3008	1151.3	1098.5	1117.6	1156.2	1113.9	1131.7	1146.6	1101.4	1105.9
3048	1103	1019.2	1020.7	1111.1	1014.9	1043.8	1098.3	1042.7	1018.7
3089	1061	972.2	975.9	1068.4	985.5	996.5	1057.4	1000.7	977.7
3130	1024	928.7	938	1031.5	942.8	965	1021.3	955.9	936.8
3170	989.4	890.5	900.2	997.7	907.7	928.5	987.9	921.4	906.9
3211	957.7	855.6	868.5	966.8	869.7	894.2	956.3	884.2	872.8
3252	927.1	824.4	836.9	937	844.3	867.4	927	857.5	845.1
3292	897.9	797.9	805.9	909.1	819	840.4	898.7	833.8	817.5
3333	870.6	768.6	784.6	882.8	794.7	812	872.5	802.7	791.9
3373	843.6	740.3	756.6	856.5	765.9	786.3	845.9	777.2	763
3414	817.9	717.1	733.3	832.1	739.8	761.6	821.3	749.9	741.7
3455	793.6	698.6	702	808.3	721.7	740.1	797.1	728.5	719.5
3495	769.8	674.1	680.4	786	706.3	720.8	774.7	707.9	697.6
3536	746.7	696	680.1	763.9	676.1	699.9	752.6	692	673.8
3577	727.3	727	709.3	743.7	730.5	711.8			

Samples 4-6

	Sample 4			Sample 5			Sample 6		
	Heater TC	Work 1 TC	Work 2 TC	Heater TC	Work 1 TC	Work 2 TC	Heater TC	Work 1 TC	Work 2 TC
Time (sec.)	(deg. F)	(deg. F)	(deg. F)	(deg. F)	(deg. F)	(deg. F)	(deg. F)	(deg. F)	(deg. F)
0	75.8	77.1	73.7	76.6	78.1	76.7	81.3	82.1	79.1
41	131.8	79.3	77.6	130.3	80.5	77.9	137.3	84.7	81.6
81	278.4	105	108.6	275.1	106.2	111	287.3	115.4	115.6
122	451.2	155.9	187.4	446	156.1	190.6	457.3	170.7	194.7
163	588.6	208.9	271.3	589.5	206.1	274	593.2	221.5	275.9
203	689.5	260.7	339.4	683.3	256.5	340.8	686.2	267.4	339.6
244	756.4	310.6	403.5	752.9	308	400.9	750.5	312.4	392.4
284	769.9	339.3	436.8	774	337.7	434.8	787.5	340.3	426.4
325	717.6	347.4	419.1	736.1	347.6	424.1	759.7	345.7	416.3
366	649	358.9	399.7	667.7	354.4	401.1	701.5	346.8	395.7
406	599.1	372.2	398.1	615.6	369.5	398.8	645.1	358.7	387.2

447	563	384.3	402.2	578.1	384.8	404.4	603.6	369.8	391.9
488	537.9	395.5	409.1	550.9	398	413.1	574.4	385	401.3
528	518.6	405.3	415.7	530.8	408.2	421.7	552.1	393.1	410.8
569	502.8	413.4	422.9	514.8	416.7	429.5	535.3	399.4	419.9
610	490.1	417.3	428.1	502.5	423.2	435.7	521.4	407.1	427.6
650	479.8	421.3	432	491.6	427.5	440.2	510.9	414	434
691	470.6	423.6	435.3	481.5	431.5	444	500.6	419.9	439.1
732	462.3	424.7	437.3	473.2	434.1	446.4	491.7	423.8	443.4
772	454.8	425.7	439.5	465.6	435.5	448.3	483.8	426.8	446.4
813	447	425.7	440	458.9	435.8	449.4	476.1	429.6	449.1
853	441.1	425.2	440.1	451.4	436.4	449.4	469.6	430.7	450.5
894	434.8	424.2	439.9	445.4	435.7	449.2	462.2	431.6	451.3
935	428.3	422.4	439.3	438.9	434.7	448	456	431.8	451.4
975	422.2	421.1	438	432.5	432.9	447.8	449.6	431.7	450.9
1016	416.5	418.9	436.1	426.8	430.5	446.1	443.3	430.7	450.2
1057	411.1	416.3	434.2	421.1	428.5	443.4	437.8	429.9	449.3
1097	406.3	414.3	432	416	426.5	441.9	431.3	428.5	448
1138	400.4	411.7	429.7	410	423.4	439.3	425.3	426.5	446.1
1179	395.2	409.1	427.2	405.5	421	436.4	420.2	424.4	444.2
1219	390.3	407.4	424.4	399.4	418	434.1	415.1	423	441.8
1260	385	404	422.1	394.1	414.9	430.9	409.2	420.2	439.4
1301	380.3	401.3	418.9	388.8	411.6	428.3	404.7	418.2	437
1341	375.2	398.4	416.3	384.4	408.4	425.4	399.4	415.4	435
1382	370.4	395.2	413.1	379.7	405.6	422	394.4	412.5	431.9
1423	366.1	392.7	410.3	374.9	402.5	419.4	389.6	410.2	429.4
1463	361.7	389.2	407.6	370.7	399.3	415.8	384.8	407.5	427.1
1504	357.3	386.5	404	366.3	395.9	412.9	380	404.2	424
1544	353.4	383.4	401.3	361.7	392.6	409.5	375.9	401.8	420.5
1585	348.7	379.4	398.2	357.5	389.4	406.9	370.8	398.6	417.9
1626	344.2	376.8	395.2	353.3	386.2	403.3	366.9	395.4	414.3
1666	340.9	373.8	392.1	348.8	382.9	400.1	361.9	392.5	411.4
1707	337	370.8	388.5	344.7	379.4	397	357.9	389	408.8
1748	332.5	367.7	386	340.8	376.1	393.7	354.3	385.3	405.3
1788	329	364.5	382.8	336.5	373	390.3	350	382.9	401.7
1829	324.8	361.9	379.3	332.5	369.9	387.4	346.1	380	398.7
1870	321.2	358.2	376.6	329.1	366.8	384.3	342	377.1	395.6
1910	326.8	356.5	373.9	334	364.4	381.4	349	375.1	393.6
1951	419.1	372.4	393.7	428	380.6	402.3	446.6	395.5	417.1
1992	570.5	418	457.1	576.5	427.2	466.1	596.7	446.2	481.6

2032	704.3	478.6	529.9	709.3	486.7	538.1	727.3	502.3	550.3
2073	800.6	539	592.9	804.5	538.8	599.4	818.7	553	607.6
2113	865.2	593.9	649.1	867	589.5	654.3	879	598	656.7
2154	913.5	642.3	702.3	915.9	636.7	705.7	925.8	640.7	703.1
2195	954.6	695.1	752.9	956.5	688.4	756	967.2	687.4	747.6
2235	991.9	745.2	804.2	993.6	740.8	806.2	1004.1	734.6	793.6
2276	1026	799.4	854.4	1028.3	795.3	855.9	1038	783.2	840.2
2317	1033	836.4	881.8	1032.5	835.4	883.3	1044.6	817.9	865
2357	1074.9	890.2	934.1	1075.6	894.2	938	1087	873.3	917.4
2398	1111.7	941.3	980.9	1112.3	943.6	984	1124.2	922.5	965.3
2439	1144.2	1012.5	1023.3	1145.9	991.6	1025.9	1156	968.7	1007.6
2479	1173.6	1060.6	1062.9	1175.6	1039.4	1066.7	1185.3	1012.5	1046.8
2520	1193.9	1092.7	1093.4	1203.9	1080.3	1103.9	1212.2	1051.2	1086.5
2561	1184	1101.8	1104.7	1203.2	1099.9	1120.5	1237.1	1078.5	1123.6
2601	1177.3	1110.4	1115.7	1190.5	1111.9	1124	1219.3	1099.9	1129.1
2642	1175.1	1118.8	1123.2	1183.5	1120.7	1131.3	1199.6	1112.1	1126.7
2683	1171.3	1124.8	1129.2	1172.7	1124.9	1133.5	1195.3	1120.9	1134.7
2723	1169.5	1128.2	1133.6	1165.8	1128.1	1135.9	1186.9	1127.7	1139.3
2764	1168.5	1132.6	1137	1160.9	1131.5	1136.1	1177.2	1131.2	1141.2
2804	1166.2	1133.6	1139.9	1158.5	1133.3	1137.8	1169	1132.6	1141.8
2845	1163.9	1135.5	1140.8	1157.3	1135	1138.8	1162.5	1133.2	1141.2
2886	1161.7	1134.9	1141.1	1156.2	1135	1138.9	1160.1	1133.2	1141.1
2926	1160	1134.5	1141.4	1153.8	1134.6	1139	1159.1	1134.7	1141.3
2967	1157.9	1134.6	1141.4	1152	1134.7	1138.8	1159.2	1135.7	1141.9
3008	1157.5	1134.4	1142.2	1151.5	1134.8	1137.4	1159.5	1136.2	1143.3
3048	1141.4	1047.6	1073.5	1114.3	1049.2	1035.4	1159.5	1134.8	1142.1
3089	1094.3	992.7	1004	1070.2	996.1	983.5	1113.6	1043.8	1029.3
3130	1054.5	954.5	966.1	1032	962.9	954.2	1071.9	994.2	983.8
3170	1019.8	922.7	928.3	997	923.2	910.8	1035.6	958	946.3
3211	986.5	892.9	902.3	965.2	897.6	884.3	1002.2	916.6	907.2
3252	955.9	865	865	935.1	861.7	850.3	971	899.5	883.3
3292	926.5	829.8	836.2	905.8	824.8	814.1	941	862.5	855.8
3333	898.9	806.5	815.2	878.1	800.4	788.5	912.9	845.1	828.7
3373	871.6	783.6	782.1	851.6	774	770.3	886	813.8	804
3414	845.8	756.3	752.6	826.5	752.9	742.3	860.2	788.9	777.9
3455	820.4	732.1	733.4	801.8	728.3	715.1	835.8	767	757.2
3495	796.2	708.6	711.1	778.2	706.9	695.9	812.6	746.9	734.4
3536	774.2	689.9	685.1	756.8	690.9	678.4	789.5	726.4	715.8
3577	751.3	666.2	664.9	735.4	740.7	716.8	768.6	706.2	697.8

Sample 7

| Time | Sample 7 | | |
| | Heater TC | Work 1 TC | Work 2 TC |
(sec.)	(deg. F)	(deg. F)	(deg. F)
0	83.5	84.1	82.1
41	135	86.9	84.4
81	277.3	113.2	118.1
122	452.3	161.3	193.4
163	587.1	210.9	272.8
203	682.3	257.1	337.7
244	753.2	302.6	394
284	785.2	339.5	432.7
325	743.3	345.9	418.5
366	677.7	352.4	397.3
406	625.5	366.7	393.7
447	587.5	380.2	400.2
488	560.2	394.1	409.1
528	540.9	401.8	418.2
569	524.3	409.2	425.7
610	511.4	415.9	432.5
650	500.7	421.2	437.7
691	491.1	425.3	441.5
732	482.4	429	444.9
772	474.6	431.2	447.9
813	468.2	433.5	449.3
853	460.9	435.1	450.4
894	454.2	435.4	451
935	447.8	435.4	451
975	441.3	435.3	450.2
1016	435.9	434.9	449.3
1057	430.2	433.3	447.9
1097	424.8	432	446.1
1138	418.9	430	444.5
1179	413.8	427.8	442.6
1219	408.8	425.7	440.4
1260	403.5	423.6	438.6

1301	398.6	420.9	435.8
1341	393.8	417.9	433.5
1382	389.1	414.9	430.7
1423	384	411.9	427.8
1463	379.1	409.3	425.1
1504	375.3	406.6	422.1
1544	370.1	403.2	419.4
1585	366	400.2	416.9
1626	362.1	397.4	413.3
1666	358.1	394.2	410.4
1707	354	391	407.4
1748	350.3	388	404.2
1788	346.2	384.9	401.6
1829	341.6	382	398.2
1870	338.2	378.9	395.2
1910	348.1	377.3	393.5
1951	447.3	397.1	417.5
1992	594.4	443.1	480.7
2032	723.6	495	547.5
2073	811	544.4	605.1
2113	874.5	593.1	658.1
2154	924.6	638.2	707.2
2195	965.2	687.8	754.6
2235	1001.4	737.6	802.8
2276	1035.6	788.6	850.5
2317	1042	829.9	877.3
2357	1084.5	883.6	930.2
2398	1120.4	933.1	977
2439	1151.4	979.9	1019.5
2479	1181.9	1023.8	1059.1
2520	1209.1	1065.7	1095.7
2561	1226.5	1098.2	1124.3
2601	1217	1108.7	1133.5
2642	1205.7	1119.4	1136.6
2683	1189.4	1127	1139.4
2723	1175.5	1130	1139.8
2764	1165.4	1132.1	1140.1
2804	1162.8	1134.1	1141.4
2845	1162	1135.3	1143

2886	1159.3	1134.4	1142.7
2926	1159.2	1133.9	1142.8
2967	1158.5	1134.8	1143.5
3008	1159.9	1135	1142.9
3048	1118.2	1042.9	1040
3089	1076.4	1002.9	995.9
3130	1038.7	969.6	963.4
3170	1004.9	936.1	928.4
3211	973.5	909.6	891.8
3252	944.5	874.3	869.1
3292	915.6	842.8	841
3333	888.4	819.6	811.2
3373	862.4	792.1	790.7
3414	837.7	773.5	760.8
3455	813.1	742.1	742.7
3495	790.2	727.2	721.2
3536	768.2	701.4	696.9
3577	746.6	728.1	696.9

Appendix G: CAB CHAMBER DEW POINT MEASUREMENTS

Note that for the compactness of this narrative, only every 20th data point is displayed in the following table. The complete data set is stored in the electronic data archive in the data folder titled "Gasser Thesis Data" in the Brazing Laboratory.

Time (sec.)	Sample 1 Dewpoint (deg. F)	Sample 2 Dewpoint (deg. F)	Sample 3 Dewpoint (deg. F)	Sample 4 Dewpoint (deg. F)	Sample 5 Dewpoint (deg. F)	Sample 6 Dewpoint (deg. F)	Sample 7 Dewpoint (deg. F)
0	-41.8	-66.3	-12.9	-16.6	62	-9.2	-3.1
41	-36.7	-74.2	-14.5	-17.4	-15.9	-10.4	-6.9
81	-35.7	-75	-14.1	-16.5	-16.1	-11.1	-7.1
122	-35	-74.7	-14.8	-16.4	-15.8	-10.3	-6.7
163	-34.3	-73.9	-14.5	-16.5	-16.2	-9.3	-6.9
203	-29.9	-73.1	-14.2	-15.6	-16.1	-9.6	-6.8
244	-24.3	-73.4	-14.3	-15.2	-16.1	6.2	-6.3
284	-15.2	-69.2	-14.4	-14.3	-14.7	-3.1	-6.7
325	-5.5	-61.2	-13.7	-13.8	-15.2	-5.5	-6.6
366	9.3	-56.4	-13.8	-13.4	-16	-8.6	-7.2
406	20.4	-42	-13.7	-13.6	-15.7	-7.9	-6.8
447	30.4	-30.3	-14.5	-13.8	-16	-9	-6
488	38.9	-29.6	-15.1	-14.1	-16.3	-9	-6.6
528	47	-31.8	-15.3	-14.3	-16	-9	-6.4
569	50	-31.7	-14.9	-13.7	-16.8	-9	-6.7
610	51.4	-30.2	-15.2	-13.4	-16.3	-9.1	-7.2
650	51.9	-29.5	-14.9	-13.6	-17	-9.5	-7.3
691	52.5	-30	-15.2	-13.5	-16.4	-9.9	-7.4
732	53.5	-30.5	-15.5	-12.9	-16.9	-9.4	-7.7
772	53	-33.3	-15.8	-13.7	-16.9	-9.5	-7.5
813	53.4	-35.5	-15.3	-13.6	-16.9	-9.4	-8.2
853	53.6	-35.5	-15.4	-14.2	-17.2	-9.4	-8.1
894	53.3	-35.5	-15.5	-13.9	-16.8	-9.3	-8.2
935	53.1	-36.1	-15.1	-14	-17.2	-9.8	-8.2
975	53.7	-36.4	-14.9	-14	-17.4	-9.7	-8.1
1016	54.4	-35	-14.9	-14	-16.7	-9.3	-8.2
1057	54.9	-34.5	-15.4	-13.8	-17.1	-9.7	-8
1097	55.1	-35.6	-15.1	-14	-16.7	-9.6	-8.3
1138	56.4	-34.8	-15.3	-15.5	-16.9	-10	-8.1
1179	56.3	-36	-14.5	-14.3	-16.9	-9.5	-8.3
1219	57	-35.9	-15	-14.4	-16.5	-9.5	-7.8

1260	56.9	-36.4	-15.3	-14.6	-17.3	-9.3	-7.8
1301	57	-36.8	-14.4	-14.6	-16.7	-9	-7.3
1341	57.6	-37.1	-15	-14.6	-16.3	-9.5	-7.6
1382	58	-37.2	-14.4	-14.6	-16.9	-9.3	-7.1
1423	58.8	-37.5	-13.8	-14.3	-16.5	-8.7	-8.6
1463	59.1	-38.4	-14.3	-14.6	-16.7	-9.1	-8.5
1504	58.9	-38	-15.2	-14.4	-16.7	-9.2	-7.8
1544	59.4	-37.9	-14.7	-14.7	-16.5	-9.2	-7.6
1585	59.4	-38.8	-14.5	-14.6	-16.4	-9.5	-8.1
1626	59.1	-39.1	-14.7	-14.7	-16.9	-9.6	-7.8
1666	59.4	-39.2	-14.8	-14.6	-16.7	-9.4	-8.1
1707	59.7	-40.2	-15.2	-15	-16.5	-8.7	-8.1
1748	60.2	-40.1	-15.2	-14.9	-16.2	-9.4	-8.8
1788	60.9	-41	-14.8	-14.8	-16.7	-9	-8.1
1829	60.4	-41.2	-15.5	-15.4	-16.2	-8.6	-7.8
1870	60.5	-42.1	-15.1	-15.1	-16.2	-8.3	-8.2
1910	60.8	-42.1	-15.6	-15.3	-16.4	-9	-8.3
1951	60.3	-42.6	-15.6	-15.7	-16.2	-8.5	-7.5
1992	61.5	-42.4	-15.9	-14.8	-16	-8.4	-8.2
2032	60.6	-42.9	-15.6	-15	-16.3	-8.4	-9
2073	61.2	-43.1	-15.6	-15.8	-15.9	-8.4	-8.3
2113	61.4	-43.5	-15.1	-14.7	-15.5	-8.9	-9.2
2154	62.5	-43.8	-15.4	-14.5	-15.7	-9.1	-8
2195	63.9	-43.6	-15.5	-14.4	-15.4	-8.8	-7.8
2235	64.1	-42.2	-15.2	-14.2	-15.8	-8	-8.2
2276	64.5	-40.4	-15.8	-14.8	-15.4	-8.5	-8.4
2317	63.7	-37.6	-15.1	-14.2	-15.8	-8.9	-7.6
2357	64.2	-34.2	-15	-14.5	-15.6	-9.2	-8.3
2398	64.1	-33.7	-15.5	-14.1	-16.2	-8.6	-8.2
2439	64.1	-32.7	-15.1	-15	-15.8	-8.5	-8.3
2479	64.1	-32.9	-15.2	-15.2	-15.4	-8.8	-8.6
2520	64	-33.7	-15.5	-14.3	-16	-8.5	-8.5
2561	64.1	-35.3	-15.4	-14.5	-15.7	-8.1	-8.2
2601	63.7	-35.2	-14.1	-14.7	-15.8	-8.8	-8.7
2642	63.2	-36.2	-15.2	-14.3	-15.9	-8.1	-8.7
2683	63.9	-36.9	-15.4	-14.2	-15.9	-8.3	-9
2723	63.8	-38.2	-15.4	-14.2	-15.7	-8.6	-8.6
2764	63.6	-39.1	-15	-14.2	-15.6	-9.3	-8.9
2804	63.7	-39.4	-14.6	-14.3	-15.9	-8.3	-8.8

2845	63.9	-39.6	-15.1	-14.2	-15.7	-9	-8.4
2886	64.2	-40.8	-15.3	-14.4	-16.7	-8.9	-9.2
2926	64.2	-41.4	-15.3	-14.4	-16	-9.1	-8.6
2967	64.4	-42.6	-14.9	-14.3	-16	-8.9	-8.8
3008	64.9	-42.6	-15.1	-14.3	-16.1	-9.5	-9
3048	64.7	-43.1	-15.7	-14.2	-16.1	-9	-9.8
3089	64.6	-45	-15.7	-14.8	-16.8	-9.2	-10.2
3130	63.5	-47.6	-16	-15.2	-17.2	-9.7	-10.1
3170	62.9	-49.5	-15.8	-15.8	-17.3	-10.3	-10.4
3211	61.9	-50.7	-16.2	-16	-17	-10.4	-10.4
3252	61.6	-52.3	-15.4	-15.8	-17.2	-10.6	-10.3
3292	62	-53.5	-16.4	-15.8	-17.1	-10.8	-10.5
3333	62.4	-54.1	-16.1	-16.1	-16.9	-10.2	-10.3
3373	63.5	-54.7	-16.4	-16.1	-17	-10.8	-11
3414	63.6	-54.9	-16.2	-15.7	-17	-11.5	-10.2
3455	64.3	-54.9	-16.1	-15.8	-16.8	-11.1	-10.4
3495	63.6	-54.2	-16.2	-15.8	-17.1	-11.4	-10.8
3536	64.4	-54.8	-16.1	-15.8	-17.2	-10.3	-10.4
3577	64.3	-54.6	-16.1	-16.2	-16.9	-11.7	-10

Appendix H: CAB CHAMBER O₂ MEASUREMENTS

Note that for the compactness of this narrative, only every 20th data point is displayed in the following table. The complete data set is stored in the electronic data archive in the data folder titled "Gasser Thesis Data" in the Brazing Laboratory.

Time (sec.)	Sample 1 O2 Partial (ppm)	Sample 2 O2 Partial (ppm)	Sample 3 O2 Partial (ppm)	Sample 4 O2 Partial (ppm)	Sample 5 O2 Partial (ppm)	Sample 6 O2 Partial (ppm)	Sample 7 O2 Partial (ppm)
0	11	9	16	14	9	9	10
41	10	9	15	19	10	9	10
81	10	9	15	19	9	9	10
122	10	9	14	18	9	9	10
163	10	9	14	17	9	9	10
203	10	9	14	16	9	10	10
244	10	9	13	14	10	36	10
284	10	9	12	15	12	9	10
325	10	9	12	14	9	9	10
366	10	9	12	14	9	9	10
406	10	9	12	14	9	9	10
447	10	9	13	14	9	9	10
488	10	9	13	14	9	9	10
528	10	9	13	14	9	9	10
569	10	9	13	13	9	9	10
610	10	9	13	13	9	9	9
650	10	9	13	13	9	9	9
691	10	9	13	13	9	9	9
732	10	9	13	13	9	9	9
772	10	9	13	13	9	9	9
813	9	9	12	13	9	9	9
853	9	9	12	13	9	9	9
894	9	9	12	11	9	9	9
935	9	9	12	11	9	9	9
975	9	8	12	11	9	9	9
1016	9	8	12	11	9	9	9
1057	9	8	12	11	9	9	9
1097	9	8	12	11	9	9	9
1138	9	8	12	11	9	9	9
1179	9	8	12	11	9	9	9
1219	9	8	12	11	9	9	9

1260	9	8	12	11	9	9	9
1301	9	8	12	11	9	9	9
1341	9	8	11	11	9	9	9
1382	9	9	11	11	9	9	9
1423	9	8	11	10	9	9	9
1463	9	9	11	10	9	9	9
1504	9	9	11	10	9	9	9
1544	9	9	11	10	9	9	9
1585	9	9	11	10	9	9	9
1626	9	9	11	10	9	9	9
1666	9	9	11	10	9	9	9
1707	9	9	11	11	9	9	9
1748	9	9	11	11	9	9	9
1788	9	9	11	11	9	9	9
1829	9	9	11	11	9	9	9
1870	9	9	11	11	9	9	9
1910	9	9	11	11	9	9	9
1951	9	9	11	11	9	9	9
1992	9	9	11	10	9	9	9
2032	9	9	11	10	9	9	9
2073	9	9	11	10	9	9	9
2113	9	8	11	10	9	8	9
2154	9	8	10	10	8	8	9
2195	8	7	10	9	8	8	8
2235	7	6	10	9	7	7	7
2276	6	6	9	8	6	6	6
2317	5	5	9	7	6	5	5
2357	4	4	8	6	5	4	4
2398	3	3	7	5	4	3	3
2439	3	3	6	4	3	3	3
2479	2	2	5	4	3	2	2
2520	2	2	5	3	2	2	2
2561	2	2	4	3	2	2	2
2601	2	2	4	3	2	2	2
2642	2	2	4	2	2	2	2
2683	2	2	4	2	2	2	2
2723	2	2	4	2	2	1	2
2764	2	1	4	2	2	2	2
2804	2	2	4	2	2	2	2

2845	2	2	4	2	2	2	2
2886	2	2	3	2	2	2	2
2926	2	2	4	2	2	1	2
2967	2	2	3	2	2	2	2
3008	2	2	3	2	2	2	2
3048	5	11	7	2	29	1	70
3089	4	5	5	8	4	19	65
3130	4	5	5	4	3	4	66
3170	4	5	5	4	3	4	66
3211	4	5	5	4	3	4	66
3252	4	5	5	4	3	4	66
3292	4	5	5	4	3	4	67
3333	4	5	5	4	3	4	67
3373	4	5	5	4	3	4	67
3414	4	5	5	3	3	4	67
3455	4	5	5	3	3	5	67
3495	4	5	5	3	4	5	67
3536	5	6	5	3	4	65	67

Appendix I: THEORETICAL MINIMUM ENERGY CALCULATIONS

WELDED JOINT

$$E_{min} = m[c(T_m - T_0) + L_f]$$

Where,

E_{min}	=	Theoretical minimum energy required to complete the weld [kJ]
m	=	Mass of aluminum which experienced phase change, 1.91×10^{-3} [kg]
c	=	Specific heat, 1.05 [kJ/kg K] (NIST standard reference data, 2011)
T_m	=	Melting temperature, 933 [K] (NIST standard reference data, 2011)
T_0	=	Ambient temperature, 298 [K]
L_f	=	Latent heat of fusion, 388 [kJ/kg] (Buch, 2000)

$$E_{min} = 2.0 \ kJ$$

BRAZED JOINT

$$E_{min} = m[c(T_m - T_0) + L_f]$$

Where,

E_{min}	=	Theoretical minimum energy required to complete the brazed joint [kJ]
m	=	Mass of aluminum which experienced phase change, 3.54×10^{-4} [kg]
c	=	Specific heat, 1.04 [kJ/kg K] (NIST standard reference data, 2011)
T_m	=	Melting temperature, 850 [K] (NIST standard reference data, 2011)
T_0	=	Ambient temperature, 298 [K]
L_f	=	Latent heat of fusion, 388 [kJ/kg] (Buch, 2000)

$$E_{min} = 0.34 \ kJ$$

Appendix J: ENTHALPY CALCULATIONS

ALUMINUM SAMPLE

$$H = m\left(cT + \frac{v^2}{2} + gz\right)$$

Where,

H	=	Enthalpy of aluminum sample [kJ]
m	=	Mass of aluminum sample, 0.0279 [kg]
c	=	Specific heat, 0.897 [kJ/kg K] (NIST standard reference data, 2011)
T	=	Aluminum sample temperature, 298 [K]
v	=	Velocity of aluminum sample, 0 [m/s]
g	=	Acceleration due to gravity, 9.81 [m/s²]
z	=	Height, 0 [m]

$$H_{Al,in/out} = 0.0279[kg]\left(0.897\left[\frac{kJ}{kgK}\right] * 298[K] + 0 + 0\right) = 7.5\ kJ$$

ARGON GAS

$$H = m\left(c_pT + \frac{v^2}{2} + gz\right)$$

Where,

H	=	Enthalpy of argon gas [kJ]
m	=	Mass of argon gas, 0.00816 [kg]
c_p	=	Specific heat, 0.52 [kJ/kg K] (NIST standard reference data, 2011)
T	=	Argon gas temperature, 298 [K]
v	=	Velocity of argon gas [m/s]
g	=	Acceleration due to gravity, 9.81 [m/s²]
z	=	Height, 0 [m]

$$H_{Ar,in} = 0.00816[kg]\left(0.52\left[\frac{kJ}{kgK}\right] * 298[K] + \frac{\left(1.85\left[\frac{m}{s}\right]\right)^2}{2} * \frac{1}{1000}\left[\frac{kJ/kg}{m^2/s^2}\right] + 0\right)$$

$$= 1.3 \pm 0.1\ kJ$$

$$H_{Ar,out} = 0.00816[kg]\left(0.52\left[\frac{kJ}{kgK}\right] * 298[K] + 0 + 0\right) = 1.3 \pm 0.1 \ kJ$$

Note that the kinetic term of the enthalpy equation was included in the calculation for argon gas entering the system. The argon gas flow rate was set to 1.18×10^{-4} m^3/s using the flow meter on the storage tank. Under the assumption that volumetric flow rate is the product of velocity and cross-sectional area, the argon velocity from the orifice was found to be 1.85 m/s by dividing the volumetric flow rate by the orifice area of 6.36x10-5 m^2. It is assumed that the velocity of the argon gas is significantly less than entering the system due to the large ratio of cross-sectional areas. The kinetic term is ultimately deemed negligible compared to the c_pT term of the equation.

Appendix K: ALTERNATIVE METHODS FOR CALCULATING THERMAL LOSSES FROM SAMPLE

The validity of the integration method presented in the text was supported by showing that two other methods presented below yield similar results. Both methods described below utilize the following equation for calculating heat transfer using the lumped capacitance method (Incropera et al, 2007).

$$Q = (\rho v c)(T_i - T_\infty)\left[1 - exp\left(\frac{-t}{\tau_t}\right)\right]$$

Where,

Q = Heat transfer to the environment [kJ]
ρ = Density of sample [kg/m^3]
c = Specific heat [kJ/kg K]
T_i = Initial temperature of aluminum sample temperature [K]
T_∞ = Temperature of surrounding environment [K]
t = Time [s]

And,

$$\tau_t = \frac{\rho v c}{h A_s}$$

Where,

τ_t = Time constant [s]
h = Heat transfer coefficient [kW/m^{2}K]
A_s = Surface area of sample [m^2]

Method 1

The first method used a value for τ_t that was found experimentally. This was accomplished by collecting sample temperature vs. time data for 10 samples. The time constant was determined experimentally by identifying the time it takes for $\theta/\theta_i = {T - T_\infty}/{T_i - T_\infty} = 0.368$. The 10 experimental values of the time constant are presented in the table below. The average time constant 188s was used to calculate the heat loss from the sample.

Test	τ_t
1	168
2	192

3	217
4	168
5	184
6	211
7	187
8	185
9	182
10	189
Average	**188**
Standard Deviation	**16**

Method 2

The second method calculated τ_t using sample properties for ρ, v, c, and A_s instead of using experimental data as in the first method. The heat transfer coefficient, h, is given by h* which combines the convective and radiative heat transfer coefficients as seen below.

$$h^* = h_{conv} + \epsilon\sigma(T_s + T_\infty)(T_s^2 + T_\infty^2)$$

Where,

h_{conv} = Convective heat transfer coefficient, $0.0135[kW/m^2K]$ (taken as the average of typical values of the convection heat transfer coefficient of air for free convection from Incropera et al, 2007)

ϵ = Emissivity of aluminum sample, 0.4 (Touloukian, 1970)

σ = Stefan Boltzmann constant, 5.67×10^{-11} [kW/m²K]

T_s = Temperature of aluminum sample temperature [K] (The integral mean temperature of the sample)

The results for both methods are displayed in the table below with the results of the integration method presented in the text. It is apparent that the results given in the text are reasonable based on the corroboration of the other two methods presented in this appendix.

|	Thermal losses from sample to environment (kW)		
Sample	**Integration Method (presented in text)**	**Method 1**	**Method 2**
1	14.3	13.7	14.3
2	20.6	19.5	21.1
3	16.8	15.8	16.9
4	19.6	18.3	19.6
Average	**17.8**	**16.8**	**18.0**
Standard Deviation	**2.9**	**2.6**	**3.0**

Appendix L: SPECIFIC ENERGY STUDY CONSTANTS

The following constants were taken from the NIST database and used in Equation 1.7 to yield the theoretical minimum energy values displayed in Table 1.1 (NIST standard reference data, 2011).
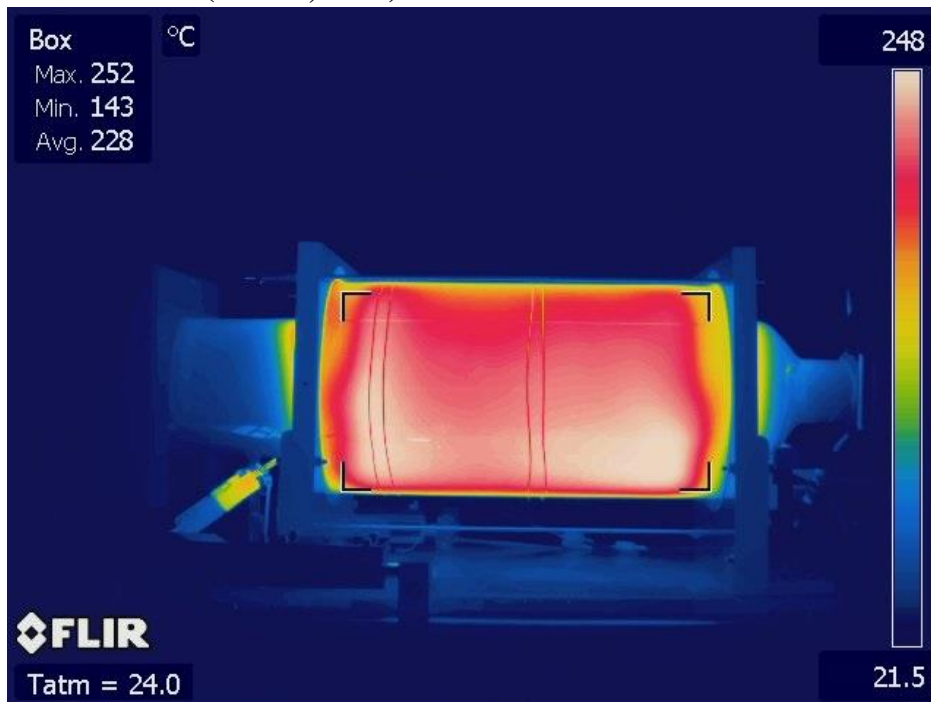
- MIG welding (Zhu et al, 2011): c (1.05 kJ/kg K), T_m (933 K), T_0 (298 K), L_f (398 kJ/kg)
- Spot resistance welding AC and DC (Li, 2004): c (0.59 kJ/kg K), T_m (1773 K), T_0 (298 K), L_f (270 kJ/kg)
- TIG welding (W.H. Giedt et al, 1989): c (0.50 kJ/kg K), T_m (1,672 K), T_0 (298 K), L_f (270 kJ/kg)
- Laser welding (E. Akman et al, 2008): c (0.62 kJ/kg K), T_m (1939 K), T_0 (298 K), L_f (365 kJ/kg)
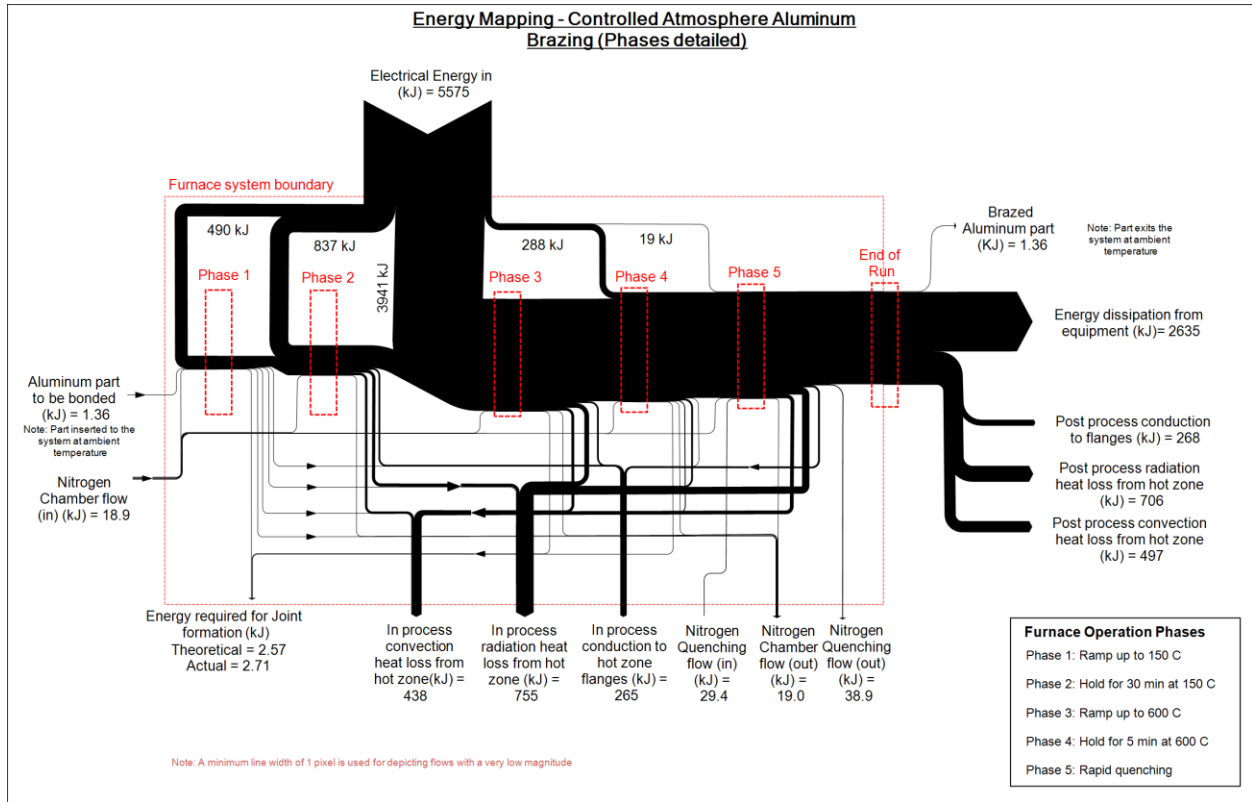
Appendix M: THERMAL IMAGES

TIG Welding
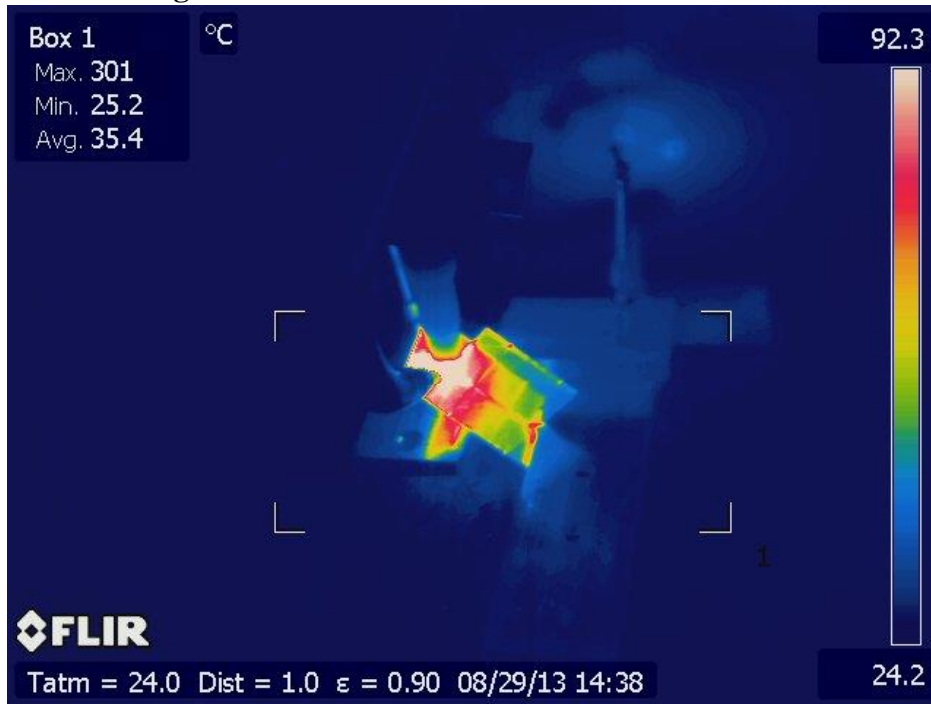
CAB Furnace (Nehete, 2013)

Appendix N: CONTROLLED ATMOSPHERE BRAZING SANKEY DIAGRAM

The following is a comprehensive Sankey diagram adapted from Nehete, 2013 which details the energy balance for the controlled atmosphere brazing process (Nehete, 2013).

Energy Sankey Diagram

References

Akman, E., Demir, A., Canel, T. and Sinmazcelik, T. 2009. *Laser welding of Ti6Al4V titanium alloys*. Journal of materials processing technology, 209 (8), pp. 3705--3713.

Alcotec Wire Corporation. 2013. *Technical Assistance Form*. Traverse City: Available through: www.alcotec.com http://www.alcotec.com/us/en/support/upload/a4043tds.pdf [Accessed: 21 Oct 2013].

Aremco Products. 2013. *High Temperature Ceramic-Metallic Pastes Technical Bulletin*. Valley Cottage: Aremco Products, Inc. Available through: www.aremco.com http://www.aremco.com/wp-content/uploads/2010/11/A03_12.pdf [Accessed: 2 Dec 2013].

Autoline® PM 200 Arc Welding Power Source Technical Manual. 2005.

Bakshi, B., Gutowski, T. and Sekulić, D. 2011. *Thermodynamics and the destruction of resources*. New York: Cambridge University Press.

Branham, M., Gutowski, T., Jones, A. and Sekulic, D. 2008. *A thermodynamic framework for analyzing and improving manufacturing processes*. pp. 1--6.

Buch, A. 2000. *Short handbook of metal elements properties*. Warsaw: "Krzysztof Biesaga".

Çengel, Y. and Boles, M. 2002.*Thermodynamics*. Boston: McGraw-Hill.

Chu, S. and Majumdar, A. 2012. Opportunities and challenges for a sustainable energy future. *Nature*, 488 (7411), pp. 294—303

Commission on Sustainable Development, 9th Session. Background Paper No. 3, 2001. *Indicators of Sustainable Development: Framework and Methodologies*. Available through: www.un.org/esa/sustdev/csd/csd9_indi_bp3.pdf [Accessed: 17 Dec 2013].

Environmental Performance Index. 2013. *Home*. Available at: http://epi.yale.edu/ [Accessed: 8 Dec 2013].

Fluke Corporation. 2006. *Fluke 115 C User Manual*. Everett: Fluke Corporation. Available through http://assets.fluke.com/manuals/115C117Cumeng0000.pdf [Accessed: 25 Oct 2013].

Fluke Corporation. 2006. *Power Logger 1735 User's Manual*.

Gasser, J. 2013. *TIG Welding Power Data*. [digital]. University of Kentucky, Brazing Laboratory, ISM, Lexington, KY.

General Eastern. 2006. *General Easter Dew Point Analyzer Operator's Manual*. Billerica: Available through: www.gesensing.com [Accessed: 27 Dec 2013].

Giedt, W., Tallerico, L. and Fuerschbach, P. 1989. *GTA welding efficiency: calorimetric and temperature field measurements*. Weld. J., 68 (1), p. 28.

Gutowski, T., Branahm, M., Dahmus, J., Jones, A. and Sekulic, D. 2009. *Thermodynamic Analysis of Resources Used in Manufacturing Processes*. Environ. Sci. Technol., 43 (5), p. 1584.

Heathcote, M. 2007. *J & P Transformer Book*. 13th ed. Elsevier Ltd..

Incropera, F., Dewitt, D., Bergman, T. and Lavine, A. 2007. *Introduction to Heat Transfer*. Danvers: John Wiley & Sons, Inc.

Moffat, R. 1988. Describing the uncertainties in experimental results. *Experimental thermal and fluid science*, 1 (1), pp. 3--17.

Li, W., Feng, E., Cerjanec, D. and Grzadzinski, G. 2004. *Energy consumption in AC and MFDC resistance spot welding*, paper presented at Sheet Metal Welding Conference XI, Sterling Heights, MI, May 11-14.

L&R Ultrasonics. 2013. *PC3 Ultrasonic Cleaning System*. Kearny: L&R Manufacturing Company. Available through http://www.lrultrasonics.com/pdf/PC3.pdf [Accessed: 17 Dec 2013].

National Instruments Corporation. 2008. *User Guide and Specifications NI cDAQ-9172*. Austin: Available through http://www.ni.com/pdf/manuals/371747f.pdf [Accessed: 3 Nov 2013].

National Instruments Corporation. 2010. *Operating Instructions and Specifications NI 9211, 4-Channel Thermocouple Input Module*. Austin: Available through http://www.ni.com/pdf/manuals/373466e.pdf [Accessed: 7 Nov 2013].

Nehete, R. 2013. *Energy Resource Use Metrics*. M.S.. University of Kentucky.

Nehete, R., Yu, C. and Sekulic, D. 2013. *Limits of Energy Resources use n Traditional Technological Processes A General Approach and Metal Bonding Case Study*, paper presented at Proceedings of the International Symposium on Sustainable Systems & Technologies, May 15 - 17. Lexington.

NOCOLOK® Flux. 2003. *Material Safety Data Sheet*. Solvay Fluorides, LLC. Available through http://www.ford-white-dust.com/MSDS-Nocolok.pdf [Accessed: 4 Dec 2013].

Omega. 2013. *Thermocouple Reference Tables*. Stamford: One Omega Drive. pp. Z-204. http://www.omega.com/temperature/Z/pdf/z204-206.pdf [Accessed: 7 Nov 2013].

Purity Plus. 2013. *Specialty Gases Specification Sheet*. Available through www.purityplusgas.com [Accessed: 4 Dec 2013].

Purslow, M. 2012. *Reducing the Ecological Impact of Arc Welding*. Welding Journal, December pp. 24-27.

Sekulic, D.P. 2013. *Advances in brazing*. Cambridge, UK: Woodhead Publishing.

117

Sekulic, D.P. 2013. Personal Communication, University of Kentucky, Lexington.

Teledyne Analytical Instruments. 1993. *Trace Oxygen Analyzer Instruction Manual*. Industry: [Accessed: 27 Dec 2013].

The Aluminum Association. 2009. International Alloy Designations and Chemical Composition Limits for Wrought Aluminum and Wrought Aluminum Alloys. Registration Record Series Teal Sheets, Arlington. www.aluminum.org.

Touloukian, Y. 1970. *Thermal radiative properties: metallic elements and alloys*. 7th ed. New York: IFI/Plenum.

(UNDP), H. 2013. *Indices & Data | Human Development Index | Human Development Reports (HDR) | United Nations Development Programme (UNDP)*. Available at: http://hdr.undp.org/en/statistics/hdi/ [Accessed: 8 Dec 2013].

Venetoulis, J. and Talberth, J. 2008. Refining the ecological footprint. *Environment, Development and Sustainability*, 10 (4), pp. 441--469.

Yang, C. and Lin, S. 2003. *The Fundamentals of Arc Welding*. Harbin Institute of Technology Press.

Yu, C., Hawksworth, D., Liu, W. and Sekulic, D. 2012. *Al brazing under severe alterations of the background atmosphere: A new vs. traditional brazing sheet*.

Zhang, Y-M. 2013. Personal Communication, University of Kentucky, Lexington.

Zhu, S., Wang, Q., Wang, X. and Han, G. 2011. *Analysis on Thermal Efficiency and Softening Behavior of MIG Welding with Longitudinal Magnetic Field. Advanced Materials Research*, 148 pp. 326--331.

<div align="center">**VITA**</div>

Name: Jonathan David Gasser

Place of Birth: Louisville, KY

Education

- B.S. in Mechanical Engineering, University of Kentucky, 2012

Professional positions held:

- Graduate Research Assistant, University of Kentucky, 2012-2014

Educational institutions attended:

- University of Kentucky, 2007-2014